Synthesis and Characterization of Crosslinked Chitosan/Polyvinylpyrrolidone and Sodium alginate/Chitosan Hybrid Hydrogels for Controlled Drug Release and Bactericidal Efficacy

Zerihun Feyissa Jebessa

A dissertation submitted in partial fulfillment of the requirements for the Degree of Doctor of Philosophy in Materials Chemistry

Department of Applied Chemistry
School of Applied Natural Science
Adama Science and Technology University

November, 2023
Adama, Ethiopia

Synthesis and Characterization of Crosslinked Chitosan/Polyvinylpyrrolidone and Sodium alginate/Chitosan Hybrid Hydrogels for Controlled Drug Release and Bactericidal Efficacy

Zerihun Feyissa Jebessa

Major Advisor: Professor Neeraj Kumar Gupta (PhD)

Co-advisor: Dr. Gemechu Deressa (Associate Professor)

A dissertation submitted in partial fulfillment of the requirements for the Degree of Doctor of Philosophy in Materials Chemistry

Department of Applied Chemistry

School of Applied Natural Science

Adama Science and Technology University

November, 2023

Adama, Ethiopia

Declaration

I declare that this Ph.D dissertation entitled "**Synthesis and Characterization of Crosslinked Chitosan/Polyvinylpyrrolidone and Sodium alginate/Chitosan Hybrid Hydrogels for Controlled Drug Release and Bactericidal Efficacy**" is my own work and has not been submitted to any university for similar purposes. The references used in this Dissertation are duly recognized by proper citations.

Zerihun Feyissa Jebessa	_____	_____
Name of student	Signature	Date

Recommendation of Advisors/ Supervisors

We, the major advisor and co-advisor of this dissertation, hereby certify that we have closely advised the student while developing this dissertation and read the draft of the dissertation entitled **"Synthesis and Characterization of Crosslinked Chitosan/Polyvinylpyrrolidone and Sodium alginate/Chitosan Hybrid Hydrogels for Controlled Drug Release and Bactericidal Efficacy"** prepared under our guidance by **Zerihun Feyissa Jebessa.** Therefore, we recommend the submission of the dissertation to the department.

Professor Neeraj Kumar Gupta (PhD) _____ _____
Major Advisor Signature Date

Dr. Gemechu Deressa (Associate Professor) _____ _____
Co-advisor Signature Date

SCHOOL OF GRADUATE STUDIES

ADAMA SCIENCE AND TECHNOLOGY UNIVERSITY

Approval sheet for PhD Dissertation

We hereby certify that the recommendation and suggestion given by the dissertation review committee are appropriately incorporated into the final dissertation entitled "Synthesis and Characterization of Crosslinked Chitosan/Polyvinylpyrrolidone and Sodium alginate/Chitosan Hybrid Hydrogels for Controlled Drug Release and Bactericidal Efficacy" by **Zerihun Feyissa Jebessa**. Therefore, we recommend the submission of the dissertation to the department.

Professor Neeraj Kumar Gupta _____ _____
Major Advisor Signature Date

Dr. Gemechu Deressa Edossa (PhD) _____ _____
Co-advisor Signature Date

Approval of Board of Reviewers

We, the undersigned, members of the Board of Reviewers of the dissertation open defense by Zerihun Feyissa Jebessa, have read and evaluated the dissertation entitled **"**Synthesis and Characterization of Crosslinked Chitosan/Polyvinylpyrrolidone and Sodium alginate/Chitosan Hybrid Hydrogels for Controlled Drug Release and Bactericidal Efficacy" and assessed the understanding of the candidate about the research. This is, therefore, to certify that the dissertation is accepted, and we recommend the implementation of the dissertation.

_____	_____	_____
Chairperson	Signature	Date
_____	_____	_____
Reviewer 1	Signature	Date
_____	_____	_____
Reviewer 2	Signature	Date
_____	_____	_____
Department Chair	Signature	Date
_____	_____	_____
School Dean	Signature	Date
_____	_____	_____
Postgraduate Dean	Signature	Date

ACKNOWLEDGEMENT

This PhD dissertation was made possible through the support of many individuals. Therefore; I would like to take this chance to appreciate and express my gratitude for all of their help. I would like to thank **Professor Neeraj Kumar Gupta**, the major advisor, for his guidance throughout the course of this research. My heartfelt gratitude goes to my co-supervisor, Dr. **Gemechu Deressa Edossa (**associate professor**)**. Thank you for your advice, suggestions, encouragement, and invaluable assistance, as well as the opportunity to work in your office. Your expert suggestions and ideas were quite helpful in completing this study endeavor. It was a great pleasure and honor to meet you.

I would like to extend my gratitude to **Dr. Defaru Negara** the head of applied chemistry department of Adama Science and Technology University (ASTU), this work would not have been possible without him.

I would like to express my heartfelt appreciation and gratitude to **Mr. Guta Amenu**, Applied Chemistry Laboratory staff member (ASTU), as well as **Mr. Leta Guta**, Applied Biology Laboratory staff member (ASTU), for their cooperation during my research work, for providing me with materials that were extremely important for lab work, and for creating such a comfortable working environment.

Dr. Takle Gemachu, Department of Applied Mathematics, Adama Science and Technology University, deserves special appreciation for his generous assistance and moral guidance. I would like to express my gratitude to my dearest friend **Tariku Bayisa** for having great time together guided under the same Advisors for the past five years in ASTU. I thank you for your sharing ideas and encouraging me to reach this level.

I sincerely appreciate **Dr. Enyew Amare** and **Dr. Endiries Yibru** for taking the necessary time and effort to thoroughly review this dissertation, as well as for all of their useful comments and recommendations that helped me to improve the quality of this dissertation.

Most importantly, I would like to offer sincere appreciation to my family, particularly **Meseret Dibaba, Jagama Zerihun, Damtew Feyissa, Dagne Feyissa, and Adanech Feyissa**, for their invaluable support and encouragement during this PhD study. This achievement would not have been achievable without their assistance.

Finally, I would like to thank **Bule Hora University** for financially and **Adama Science and Technology University (ASTU)** for supporting my PhD study.

TABLE OF CONTENTS

CONTENT **PAGE**

LIST OF TABLES

TABLE **PAGE**

LIST OF FIGURES

FIGURE **PAGE**

ABBREVIATIONS

ATCC	American type culture collection
AMX	Amoxicillin
CFU	Colony forming unit
CLSI	Clinical and laboratory standards
CMC	Carboxy methylcellulose
CS	Chitosan
DDA	Degree of deacetylation
DDSs	Drug release systems
DDW	Double distilled water
DEX	Dexamethasone
DNA	Deoxyribonucleic acid
DOX	Doxorubicin
FTIR	Fourier Transform Infrared spectroscopy
GI	Gastrointestinal
GPTMS	Glycidyloxypropyl trimethoxysilane
HPMC	Hydroxypropyl methylcellulose
ICDD	International Center for Diffraction Data
IPN	Interpenetrating polymer network
LCST	Lower critical solution temperature
MEC	Minimum effective concentration
MSC	Maximum safe concentration
MTZ	Metronidazole
MTC	Minimum toxic concentration
NSAID	Non-steroidal anti-inflammatory drugs
PAA	Poly (acrylic acid)
PEG	Poly (ethylene glycol)
PEO	Poly (Ethylene oxide)
PLGA	Poly (lactide-co-glycolide)
PMA	Poly (methacrylic acid)
PNIPAAm	Poly (N-isopropyl acrylamide)
PVA	Poly (vinyl alcohol)
PVP	Poly (vinyl pyrrolidone)

SALG	Sodium alginate
SCF	Simulated colon fluid
SEM	Scanning electron microscopy
SGF	Simulated gastric fluid
SIF	Simulated intestinal fluid
TGA	Thermo-gravimetric analysis
UCST	Upper critical solution temperature
UV–vis	Ultraviolet visible
XRD	X-Ray diffraction
WHO	World Health Organization

ABSTRACT

Hydrogels have received much consideration in controlled drug delivery systems for their exceptional characteristics such as swelling, biocompatibility, biodegradability, and sensetivity to external stimuli. pH-sensitive hydrogels swell in response to changes in pH and have been employed in controlled release applications. Despite all these attractive properties of stimuli-responsive hydrogels, mechanically fragile structures resulting in a rapid burst drug release, slow responsiveness and poor drug bioavailability due to failure of controlled drug delivery systems design are still challenging. By adjusting the compositions of the polymers and crosslinking agents, features like porosity, mechanical properties, swelling, and drug release behavior can all be controlled precisely. In this study, pH-sensitive hybrid hydrogels, including chitosan/polyvinylpyrrolidone by chemical crosslinking method using glutaraldehyde and double-crosslinked chitosan/sodium alginate by the ionotropic method using calcium chloride and glutaraldehyde as crosslinking agents were produced. The prepared hydrogels were applied in a controlled-release study of the model drugs (metronidazole and amoxicillin) incorporated into the optimal hydrogel system using in situ crosslinking method. To optimize the hydrogel compositions used for the controlled drug release study, important hydrogel physicochemical properties such as swelling ratio, porosity, and gel fraction with respect to polymer weight ratios and crosslinker concentration as well as biodegradation were evaluated. Based on their swelling behavior, chitosan/polyvinylpyrrolidone hydrogel (weight ratio of 60:40) crosslinked by 600 µL glutaraldehyde and a sodium alginate/chitosan hydrogel (weight ratio of 75:25) crosslinked with 2% calcium chloride soaked in enough glutaraldehyde (25%, w/v) were chosen for an in situ polymerization of 200 milligrams each drug. The functional groups of the polymers and presence of well defined polymer and drug interactions, improved thermal stabilities of the hydrogels than the polymers, amorphous and porous structures of the hydrogels were confirmed by fourier transform infrared spectroscopy, thermogravimetric analysis, X-ray diffraction, and scanning electron microscopy, respectively. The correlation coefficient ($p < 0.05$) showed a significant linear dependence of swelling ratio of the hydrogels and each drug release profile in all physiological fluids. The *in vitro* studies revealed that the hydrogels are pH-sensitive and have considerable biodegradability. The Korsmeyer-Peppas model is the best fit for the release of each drug following a diffusion- and swelling-controlled time-dependent non-Fickian process. The hydrogels demonstrated impressive antibacterial efficacy against the Bactria strains, indicating they are viable candidates for controlled drug release applications.

Key words: Chitosan, Polyvinylpyrrolidone, Sodium alginate, Glutaraldehyde, Hydrogel, Drug release

CHAPTER 1: INTRODUCTION

1.1. Background of the study

Hydrogels are cross-linked three-dimensional (3D) networks of hydrophilic polymeric materials capable of absorbing large amounts of physiological fluids leading to swelling and flexibility while preserving their structural integrity due to the crosslinking force that connects the polymer chains (Gull et al., 2020b). Depending on the aqueous medium's makeup and the hydrogel components, these materials can hold water more than 90% of their weight when swelled without dissolving (Rapp & DeForest, 2021). The hydrophilic groups, including CONH, OH, $CONH_2$, HSO_3, and COOH, in the polymer chain frameworks boost the hydrogels' affinity for water. In hydrogels, water either forms hydrogen bond with the hydrophilic groups (bond water) or fills the porous channels (free water) (Payne, 2018). A further key characteristic of hydrogels is their ability to show detectable size change in response to surrounding triggers (e.g., pH, temperature, ionic strength, light, and electric) without dissolving (Mohsen et al., 2017). These hydrogels are also known as smart materials as they display significant variations in their size in response to the changes in external stimuli (Kasiński et al., 2020).

pH-responsive hydrogels usually contain functional groups such as amino (NH_2), carboxylate (COO-), and hydroxyl (OH) that can be protonated or deprotonated in various physiological fluids (Ngwabebhoh et al., 2021). When the pH of the surrounding medium is higher than the pka of the functional group, it is deprotonated; when the pH of the surrounding media is lower than pka, the functional group is protonated, resulting in a change in the hydrophilicity of the hydrogel. Because of these amazing properties, pH-sensitive hydrogels exhibit swelling and biodegradablity in various medium, making them suitable for oral controlled drug release applications that aim to minimize swelling and drug release in the stomach while optimizing swelling and drug release in the intestinal tract, where drug absorption occurs (Ebrahimi & Salavaty, 2018).

Hydrogels are divided into two categories: physical and chemical hydrogels, based on the kind of crosslinking forces that exist in hydrogel systems (Zainal et al., 2021). The physical hydrogels have non-permanent links formed by interactions of weak intermolecular forces, including hydrogen bonds, crystallization, and ionic or hydrophobic interactions (Ganguly et al., 2020). The chemical hydrogels that are thought to be true or permanent gels are crosslinked by more powerful and persistent covalent bonds. Radical polymerization, radiation, chemical reactions

involving functional groups, and enzyme use can all be used to produce chemical hydrogels (Zainal et al., 2021).

Because of their compositional versatility, stimuli responsive nature, tunable structure, biocompatibility, biodegradability, and nontoxicity, and their resemblance with the natural extracellular matrix, hydrogels have been used in a variety of biomedical applications such as wound dressing, tissue engineering, soft contact lenses, and controlled drug delivery systems (Garg & Garg, 2016; Panahi et al., 2019). Controlled drug delivery systems (CDDSs) based on hydrogels offer substantial benefits over the conventional drug delivery systems.

The conventional method of drug administration is generally based on immediate drug release form in which the concentration of the drug in the blood increases immediately after administration and then drops over time (Mujtaba & Alotaibi, 2020). All drugs have therapeutic range which is a plasma drug concentration above which the drug is harmful and below which the drug is ineffective (Pal et al., 2018). Overdose, toxicities, side effects, premature death, emergence of antibiotic resistant bacteria, and treatment failure have all been linked to the repeated administration of conventional drug formulations, and patient drug misuse, particularly in low-income countries (Gebramariam et al., 2019). These effects are associated with a drug's uncontrolled release and nonspecific distribution in the body system, causing the initial concentration to exceed the toxicity limit and slowly becoming less effective over time (Oliveira et al., 2020).

Hydrogel based CDDSs are being researched to mitigate the problems associated with the immadiate release form of drugs in the conventional methods, to attain prolonged therapeutic effects via sustained drug release over a prolonged time following administration (Ngwabebhoh et al., 2021). The driving force behind such development is the sustain drug release at appropriate therapeutic levels without causing adverse side effects and improving patient safety. An effective CDDSs should generally display biocompatibility, non-toxicity, and biodegradability. They should also consider factors like high drug loading capacity, prolonged drug dispersion, appropriate drug-to-carrier binding affinity, controlled drug release kinetics, and adequate stability when combined with drug carrier materials (Heng, 2018).

A hydrogel matrix as CDDSs can be loaded with many components, including drugs, proteins, peptides, and genes, either by an absorption process or through the in-suit polymerization of a blend of a drug and a precursor polymer solution simultaneously (Ahmed & Aljaeid, 2016). The drug-loaded hydrogel materials can be administered to a patient through oral dose, nasal,

dressing, implantation, or parenteral routes (Jana & Jana, 2020). In hydrogels, controlled drug release is attained most prominently through diffusion and swelling processes. In swelling process, when the material is in contact with water or physiological fluids, it absorbs fluid and expands leading to macromolecular mobility allowing drug dissolution and diffusion (Wang et al., 2020).

Hydrogels can often be tailored for specific drug release rates and designed to degrade for easy bodily removal (Webber & Pashuck, 2021). Single-component hydrogels based explicitly on natural polymers exhibit reduced mechanical strength and fast biodegradability leading to limited performance as CDDSs (Zou et al., 2020). It is of considerable interest to develop hydrogel systems with multi-polymer components (natural, or synthetic) crosslinked to form a stable polymeric network to achieve more effective performance superior to that of their individual components. When multiple hydrophilic polymers are crosslinked, the resulting crosslinked hydrogel exhibits synergistic features (such as mechanical qualities) and improved drug-releasing capability (Das & Subuddhi, 2019).

Many biocompatible natural or synthetic polymeric materials can be used for producing hydrogels. Chitosan, silk, gelatin, alginate, pectin, agar, xanthan gum, and starch are just a few examples of natural, biocompatible polymer materials that can be crosslinked to prepare hydrogels easily and affordably (Ganguly et al., 2020) and the synthetic polymers for example polyvinyl alcohol, polyethylene oxide, polyvinylpyrrolidone, and polyacrylamide (Jeong et al., 2020) have been used to develop for applications in CDDSs. Some of those relevant to this research are described below.

Chitosan (CS) is a natural unbranched carbohydrate polymer, produced from chitin by alkaline deacetylation. It primarily consists of N-acetyl-D-glucosamine linked β-(1→4) D-glucosamine units. Owing to its mucoadhesiveness, biodegradability, biocompatibility, nontoxicity, and inexpensive cost, CS and its derivatives have been employed in several biomedical applications such as wound dressing, bioerodible implants, tissue engeenering and controlled drug delivery systems. Functional features in the CS polymer chains, like the primary amine ($-NH_2$) and hydroxyl (-OH) groups that can act as electron donors, make it easier to change the structure of the polymer. Because its amine groups have protonated, CS is hydrophilic and soluble in an acidic solution (Pellá et al., 2018).

Despite its benefits, CS has a relatively weak mechanical strength. Concern over their low mechanical strength and disintegration in an acidic environment has necessitated their

modification by reacting with other biocompatible natural (like alginate) or synthetic (like PVP) polymers to produce stable networked material for use in controlled drug release systems (Garakani et al., 2020).

The synthetic polymer polyvinylpyrrolidone (PVP), which is water-soluble, inert, non-toxic, unaffected by body temperature, steady pH, biocompatible, and bio-degradable, can be interacted with naturally occurring carbohydrate polymers including CS to prepare hydrogel systems having enhanced properties for different biomedical applications such as soft implants, bone tissue engeenering and drug delivery systems (Kurakula & Rao, 2020). Due to these advantages, PVP is essential to control the porosity and inhibit crystal formation of crosslinked systems hence used to manage the drug-releasing pattern of hydrogels (Pereira et al., 2020).

Sodium alginate (SALG), which has a linear structure comprising varying proportions of ὰ-(1→4)-linked Ḷ-guluronic acid (G) and β-(1→4)-linked β-mannuronic acid (M) with a carboxyl group (COO^-). SALG is a natural polysaccharide, anionic and water-soluble polymer derived from brown algae (A. Sharma et al., 2020). SALG has also been employed in several biomedical applications such as wound healing, tissue engeenering and drug delivery, owing to its excellent biocompatiblity, non-toxicity, mucoadhesive nature, and biodegradablilty (Nalini et al., 2019). Similar to CS, pure SALG has some drawbacks when used as CDDSs. The significant limitations include poor drug encapsulation efficiency and quick release of the incorporated drug moieties, which are related to high water solubility, poor mechanical strength, and substantial gel porosity, which causes the loaded drug molecule to leak out of the gel network into the solution (Tahtat et al., 2013). Hydroxyl functional groups (-OH) along the SALG backbone helps crosslink with other polymers like CS to modify its properties.

Many previous studies of CDDSs utilizing CS in combination with other biocompatible polymers, including PVP and SALG, involve the development of blends or inter-penetrating polymer networks (IPN). Perea et al. (2023) recently reported the drug release and antimicrobial activities of cloxacillin-loaded CS/PVP material. Grant et al. (2021) prepared 5-Fluorouracil loaded CS/PVP blend and studied its controlled release profile. Ata et al. (2020) prepared CS/PVP hydrogels using silane as a crosslinker for a controlled-release study of cefixime. Gull et al. (2020a) fabricated a povidone-iodine loaded CS/PVP hydrogel system using a varied amount of 3-glycidyloxypropyl trimethoxysilane (GPTMS) crosslinker, for in vitro release studies. Gull et al. (2019) prepared crosslinked CS/PVP hydrogels by varying concentrations of the crosslinker tetraethyl orthosilicate to regulate lidocaine release. Zamani et al. (2023)

described the drug release profile of 5-fluorouracil-loaded CS/SALG polyelectrolyte particles. Frent et al. (2022) prepared CS/PVP microspheres loaded with quercetin. Khan et al. (2021) prepared CS/SALG hydrogel systems using $CaCl_2$ as a crosslinker intended for concurrent and prolonged release of antibiotics such as ciprofloxacin, amoxicillin, and vancomycin for combination treatment. They also prepared dual crosslinked CS/SALG hydrogel beads using $CaCl_2$ and glutaraldehyde crosslinkers for control release of a colon-targeting doxorubicin hydrochloride drug. Hydrogels have become essential to drug delivery systems, and efforts will continue to produce advanced drug carrier materials, ultimately providing the intended therapeutic effect. The effects of crosslinker concentrations and polymer ratio resulting from crosslinked polymer networks and the subsequent controlled-release behavior still need further investigation. Moreover, to our knowledge, no research on crosslinked CS/PVP and CS/SALG hydrogels loaded with AMX or MTZ for controlled release and antibacterial efficacy has been published.

The main focus of the present study was the synthesis and characterization of crosslinked hybrid hydrogels based on CS/PVP using glutaraldehyde as the crosslinking agent and double-crosslinked CS/SALG using $CaCl_2$ and glutaraldehyde as crosslinking agents for the controlled release studies of the most widely prescribed antibiotics amoxicillin as well as metronidazole and investigated their antibacterial activities.

1.2. Statement of the problem

Hydrogels are appealing polymeric materials for CDDSs due to their ease of processing and easily adjustable physicochemical properties such as biocompatibility, bioadhesiveness, outstanding hydrophilic nature, and swelling capability (Chai et al., 2017). CS, SALG, and PVP are biocompatible and biodegradable polymers that have been widely used for producing hydrogels for controlled drug release applications. Despite their numerous advantages, they have some limitations in controlled drug release applications, which vary depending on the nature and content of the polymers and crosslinkers used.

The rapid dissolving of CS matrices in stomach (acidic medium) in oral drug delivery systems, resulting in rapid burst drug release following swelling (Ngwabebhoh et al., 2021). Because of their high hydrophilicity, SALG-based hydrogels have a high water content and wide pore sizes, resulting in relatively rapid drug release within a few hours (Niu et al., 2019). Due to its highly hydrophilic nature PVP also exhibits poor mechanical strength (Gerami et al., 2021). These limitations are challenging in various controlled drug release applications as they affect the

quantity and uniformity of drug loading into hydrogels and may induce drugs side effects. Furthermore, failure of the CDDSs design due to inappropriate polymer ratio and crosslinker concentrations may result in slow stimuli responsiveness of hydrogels, difficulty in dosage adjustment (drug loading), rapid burst drug release, and poor drug bioavailability (Gull et al., 2020).

Different ways can be used to overcome the limitations of CS, SALG and PVP polymers as CDDSs. Hybridization of CS, SALG, and PVP structures with one other or with other biocompatible and biodegradable polymers utilizing appropriate crosslinking agents via covalent or physical crosslinking methods aids in improving their characteristics (Alnaief et al., 2020). Hybrid hydrogels have several synergistic properties including controllable porosity, improved drug loading capacity, excellent bio-adhesion, biodegradability, controlled drug release rate, and improved mechanical properties that are affordable for applications in CDDSs (Garakani et al., 2020). The crosslinking of a drug to the hybrid systems prior to hydrogel formation (in situ method) also allows to overcome the rapid dissolution and fast drug release problems. In particular, CS/PVP and double crosslinked SALG/CS hydrogel formulations that maintain therapeutic plasma concentration, providing slow and prolong drug release through a highly controlled mechanism for most commonly adminsterd model antibiotic drugs (AMX and MTZ) were desirable.

AMX is the most commonly prescribed broad-spectrum antibiotic to treat various bacterial infections worldwide (Segura-Egea et al., 2017), including chest (bronchitis or pneumonia), skin, tonsils, ears (otitis media), bone, teeth, sinusitis, heart, kidneys, blood, bladder, and intra-abdominal infections. WHO suggests AMX as a first-line prescription for pneumonia (Hanning et al., 2020). MTZ, a potent antiprotozoal and antibiotic drug, is on the list of essential drugs by the WHO (Rahman et al., 2020) and Ethiopian (Demoz et al., 2020). It is effective against anaerobic bacteria and certain protozoan illnesses, such as giardiasis, trichomoniasis, and amebiasis. Both AMX and MTZ for oral administration are available in immediate-release form as capsules and tablets in 250 mg and 500 mg doses in capsules and tablets formats. Each drug reachs the maximum blood plasma concentrations occur within 1-2 hours. About 60% of the AMX and MTZ dosages taken orally are metabolized by the liver and is primarily eliminated unaltered in the urine within 6 to 8 hours. For this reason, the 500 mg dosage form of AMX and MTZ are commonly administered regularly every 8 hours per day due to their short elimination half-life.

Furthermore, in developing countries like Ethiopia, people, particularly in the low and middle-income groups, use antibiotics such as AMX and MTZ irrationally, which can lead to dose accumulation in the body, a risk of higher drug plasma concentration, and development of antibiotic-resistant bacteria. Various cross sectional assessment reports in Ethiopia showed wide misuse of these antibiotics across the country's healthcare centers (Adane et al., 2020; Gebeyehu & Ararsie, 2023; Kassie Netere & Sendekie, 2022). Overdose of AMX can cause severe damage to the kidney and lead to renal failure (Couto et al., 2017) and MTZ reaction with alcohol causes neurotoxicity and brain damage. The repetitive AMX and MTZ administrations, as well as their irrational consumption may result in their accumulation in the body, undesirable side effects, the emergence of antibiotic-resistant bacteria, and a reduction in their therapeutic effect. As a result, controlled and sustained release mechanisms are desirable for AMX and MTZ.

In this study, we developed cross-linked CS/PVP hydrogel using glutaraldehyde and double crosslinked SALG/CS hydrogels using $CaCl_2$ and glutaraldehyde crosslinking agents by varying the polymers ratio and crosslinker concentrations. AMX and MTZ were loaded to the optimal hydrogels using in situ crosslinking method for in vitro controlled release study.

1.3. Objective of the study

1.3.1. General objective

The main objective of this study was to synthesize and characterize crosslinked hybrid hydrogels based on CS, PVP, and SALG polymers for controlled release of AMX and MTZ and antibacterial activity.

1.3.2. Specific objectives

- To synthesis of crosslinked CS/PVP hydrogels using glutaraldehyde as the crosslinking agent with and without AMX and MTZ loading.
- To synthesis of double crosslinked SALG/CS hydrogels using $CaCl_2$ and glutaraldehyde as the crosslinkers with and without AMX and MTZ loading.
- To characterize the synthesized hydrogel systems with and without drug loading for their physical, chemical, morphological, and in vitro drug release kinetics in simulated physiological fluids.

- To establish inter-property correlations beteween the hydrogels swelling ratios and the *in vitro* drug release profiles.

- To evaluate the antibacterial activity of the crosslinked hybrid hydrogel with and without drug loading.

1.4. Significance of the study

This study aimed to develop crosslinked hybrid hydrogels incorporating AMX and MTZ for their controlled *in vitro* release study and antibacterial activitity. Two types of hydrogels were developed; the first, crosslinked CS/PVP hydrogels, and the second, double crosslinked SALG/CS hydrogels. During synthesis, efforts were made to improve the properties of the hydrogels for optimum drug-release to address the challenges of oral AMX and MTZ delivery. The major significances of the developed controlled-release systems are expected to have substantial implications for reducing the duration (frequency) of drug intake, maintaining drug plasma concentrations in the therapeutic range, avoiding overdose, and minimizing drug adverse effects. The hydrogels synthesized in this study could be of interest to the pharmaceutical sector due to their ease of preparation and low cost, and the synthesis techniques can be scaled up for bulk manufacturing in the industry.

This research also contributed significantly to knowledge and information built on hydrogel preparation methods, properties, and applications. Furthermore, the results of this work serve as a baseline for future research for developing more effective hydrogels for oral drug delivery.

CHAPTER 2: REVIEW OF LITERATURE

2.1. Controlled drug delivery systems

Sustained CDDSs deliver drugs for prolonged periods at predetermined release rates without generating adverse side effects (Bhupathyraaj & Pole, 2020). When a drug is administered conventionally, drug blood levels increase after each administration until the upper dosage limit is reached. However, it then falls below the effective dosage until the next administration. In contrast, controlled-release systems are designed for an extended-release period so that the drug's blood level remains constant within the required minimum and maximum limits during the release period (Oliveira et al., 2020). In sustained drug release systems, drug dosage is maintained for an extended time, and the drug release rate is not determinable. However, drug release is highly definite in controlled release forms per unit of time, as shown in Figure 2.1 (Gopikrishna et al., 2016). Generally, CDDSs regulate drug delivery at a predetermined rate, keep drug concentration within optimal and effective range, increase the efficacy of the drug, minimize side effects, fewer dosing frequency, improve patient compliance, enhance the solubility of lipophilic drugs, increase bioavailability, and decrease the wastage of highly water-soluble drugs which need slower and extended time of release (Bhatt et al., 2021).

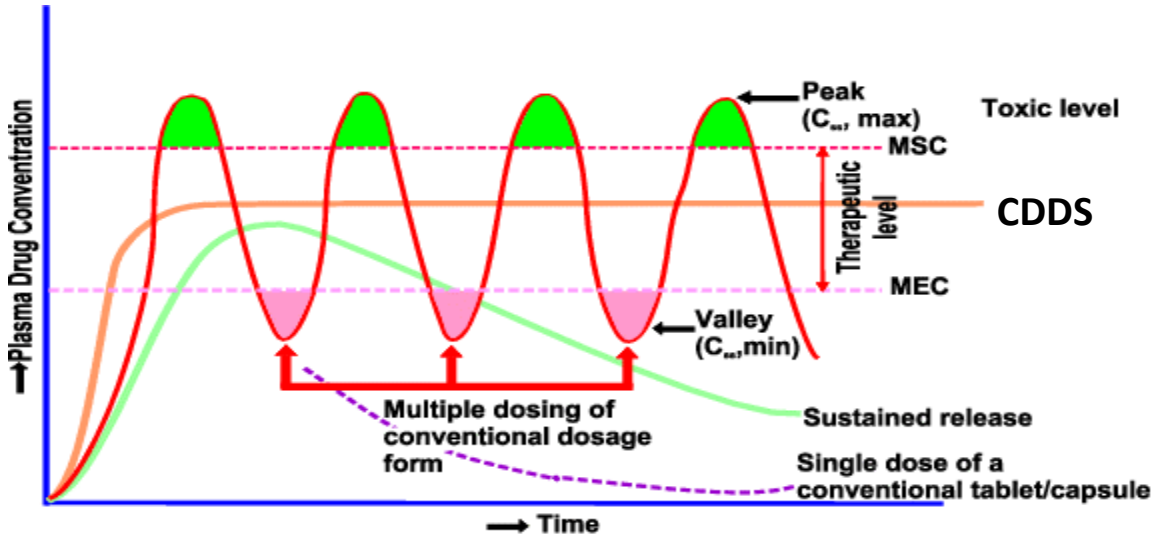

Figure 2. 1 Plasma concentration versus time profiles of drug release dosage forms. Reprinted from Gopikrishna et al., 2016.

In hydrogel-based systems, the controlled release of a drug is obtained by several release mechanisms, the most prominent of which being diffusion and swelling processes (Wang et al., 2020). The two types of diffusion-CDDSs, reservoir and matrix systems, are distinguished in their importance for prolonged drug release. Drug diffusion in reservoir systems adheres to the

first law of Fickian diffusion because drug molecules are contained in the drug carrier (Ghasemiyeh & Mohammadi-Samani, 2019). In the matrix type diffusion-CDDSs, the drugs are homogeneously disseminated in a porous carrier matrix, and drug release mostly follows the Higuchi diffusion equation (Nogami et al., 2021). In swelling-CDDSs, the drug cannot diffuse through the highly densified matrix. However, when the system is in contact with water or physiological fluids, it absorbs liquids to increase plasticity, volume, and macromolecular mobility permitting drug dissolution and diffusion, obeying the first law of Fickian diffusion (Wang et al., 2020).

Osmosis is the natural passage of water through a semi-membrane into a medium. In osmosis-based CDDSs, when a substance interacts with the aqueous environment, water enters into the substance to balance the variation in the amounts of the solute (Wang et al., 2020). In this instance, the pressure created within the system, aid in the drug's expulsion, via, widely spaced openings within the semi-membrane. Since only water may diffuse through the semi-membrane (constant water flow) but not solute, the process achieves zero-order kinetics, resulting in constant drug concentration (Kaur et al., 2018). As a result, the release rate dependens solely on the flow of water through the holes and is independent of concentration or surroundings.

Generally, CDDSs in hydrogel-based systems involving swelling and diffusion, are influenced by a variety of external factors like ionic strength, pH, and temperature (Franco & De Marco, 2020). In a diffusion-controlled release mechanism, the mass flow of a drug follows the Fickian rules of diffusion, moving from high-concentration regions to low-content areas. For porous hydrogel, the rate of drug diffusion will increase if the volume of the pores is greater than the size of the drug particles. A hydrogel is used as either a reservoir or matrix in a diffusion controlled-release mechanism. For reservoir drug release systems, drugs are coated with polymeric hydrogels, and the drug release mechanism generally obeys the first law of Fickian diffusion (Ghasemiyeh & Mohammadi-Samani, 2019). According to this law, the amount of drug moving through a unit area of a membrane is proportional to the concentration difference along the plane's dimension, as shown in the equation below.

$$J = -\frac{DdC}{dX} \tag{2.1}$$

J is the change in diffusion (flux) in g/cm^{2}s, D is coefficient of diffusion in m^2/s, C is the substance (drug) amount in unit volume, and X is diffusion flow distance (m).

The Higuchi law of diffusion is frequently applied in the matrix drug release system, where drugs are equally dispersed in polymeric hydrogels and drug release occurs at a consistent rate.

Wathoni et al. (2019) reported α-mangostin loaded CS/SALG based hydrogel film for aphthous stomatitis treatment. People have traditionally utilized the α-mangostin found in mangosteen peel as a conventional drug to treat diarrhea, infected wounds, and stomachaches. According to the in vitro release investigation, the drug's release from a hydrogel made of CS/SALG demonstrated a release mechanism with a matrix based on the Higuchi law of diffusion.

In designing CDDSs, several factors must be considered, such as drug administration route, physicochemical properties, and biological effects of a drug and polymer-related effects . Drugs have been administered by various methods, including oral, rectal, intravenous, nasal, implanted under the skin, ophthalmic, and vaginal. The oral drug delivery route has been the utmost favored and convenient among the other routes owing to its high suitability for patients, easy administration, lower cost, the flexibility of drug formulations and large surface area lined with viscous mucosal for drug absorption (Spizzirri & Cirillo, 2017). In an oral delivery route, a drug is taken through the oral cavity and conveyed to GI segments (stomach, intestine, and colon). This route has multipurpose for treating specific diseases such as bacterial infections, stomatitis, viral infections, oral cavity cancer, and fungi. Despite of its advantages, the oral drug delivery route is associated with some drawbacks; for instance, colon-targeted drugs like protein and peptides are affected by the acidic nature of the upper GI tract (Dubey et al., 2021).

After a drug leaves the mouth cavity, it moves directly into the stomach through the esophagus within 10 seconds (viswanathan et al., 2017). In the GI tract, the factors that influence the absorption and efficacy of the drugs depend on the average length of the tract, the chemical stability of the drug, the presence of food, surface area, pH, residence time, and mucus layer thickness (Kaur et al., 2018). In the stomach, gastric mucus secreted by goblets cells, acidic pH of gastric due to HCl, and small surface area of stomach cells block effective drug absorption. Gastric enzymes such as gelatinase and pepsin can degrade and remove drugs, lowering drug efficacy (viswanathan et al., 2017). The influence of acids in the stomach is often protected by coating the drug with polymeric coating materials to release the drug at a lower portion of the GI tract. Enzyme degradation is prevented by modification of the chemical structure of the drug by connecting with specialized functional groups (pro-drug) that will be eliminated from the body once the drug has been released (Gârea et al., 2017). Chen et al. (2014) fabricated an endosomal pH-activated pro-drug via doxorubicin-CS conjugation using a hydrazone link that is acid-

cleavable. The outcome demonstrated that, under neutral pH conditions, the conjugates self-assembled into nanoparticles that were extremely stable and did not burst release of doxorubicin. Because the villi are crucial in the absorption of drugs, the small intestine has a considerably higher surface area for drug absorption. However, the epithelial layer and mucus surface generated by goblet cells act as an efficient barrier to medicines in the intestinal lumen. Most drugs pass through the cellular barriers through diffusion process (Dubey et al., 2021). Hydrophilic active ingredients because of the hydrophobic nature of the outmost coating of the mucus, exhibit fewer interactions enabling the absorption of particles through the mucus. Due to mucus' protective and sticky properties, the dispersed drug components are impeded and take longer to move along the GI system (Homayun et al., 2019). The colon is mainly used to absorb water and electrolytes. Relative to the small intestine, the colon has a small surface area; however, some drugs are significantly absorbed owing to the more extended residence period in the colon (20–50 h). The most essential application of drug delivery to a colon is the distribution of vaccination drugs comprising protein and peptides.

The drug release rate and amount in the GI tract can be affected by the physico-chemical properties of drugs such as drug solubility, stability, and lipophilicity. Due to insufficiently dissolution, drugs with very low solubility in physiological fluid (aqueous) have lower bioavailability. A weaker acidic drug is protonated in an acidic environment (stomach) and becomes unionized, but in an alkaline environment, it remains ionized. Compared to ionized drugs, unionized drugs diffuse through the cellular barrier and enter the bloodstream (absorbed) (Akhtar et al., 2020). In general, drugs that are weaker acids are absorbed more in the acidic environment (stomach). In contrast weaker base drugs are absorbed more in the alkaline environment (small intestines) (Kaur et al., 2018).

Food intake may also influence the absorption of drugs in the stomach, which can enhance or hinder drug absorption by forming insoluble complexes. However, while being acidic, the stomach's tiny surface area and thick mucus layer make it unsuitable for drug absorption, even for basic drugs. Thus, rather than being a site for drug absorption, the stomach is a storage area (Dubey et al., 2021). In the intravenous drug prescription route, the drugs are injected into the bloodstream, and absorption is not an issue (Kaur et al., 2018).

Currently, different CDDSs including microcapsules, liposomes, nanoparticles, and hydrogels, are being actively researched and are also under advancement (Das & Subuddhi, 2019). Microcapsule is a micrometric size uniform wall coating encapsulating bioactive moieties. Microencapsulation is used to reduce dosing frequency and avoid the degradation of drugs.

Polymers such as SALG and lipids are commonly used as encapsulating materials of interest. Liposomes are small spherical forms of phospholipid molecules that can carry drugs or nutrients in CDDSs such as DNA vaccines. However, some challenges of attaining a required release for a pre-determined duration and stability are still associated with the microcapsules and liposomes. CDDSs based on nanoparticles are among the novel methods of targeted and controlled drugs to reduce various side effects related to drug dose and dosage frequency. While nanoparticle drug delivery systems are effective, they are associated with challenges such as particle stability, concerns about toxicity, and effective bio-distribution of particles (Kupnik et al., 2020).

2.2. Hydrogels for controlled drug release systems

Hydrogels as polymeric materials are promising for drug release applications because of their simplicity of processing, easily tuneable chemical as well as physical characteristics like high biocompatibility, bioadhesiveness, hydrophilic nature, and swelling capability (Thakur & Thakur, 2018). They are crosslinked hydrophilic polymers having 3D network structures that can engross significant amounts of water and physiological fluids without disintegrating, forming swollen state. When exposed to numerous environmental stimuli, such as temperature, pH, ionic strength, and glucose concentration, hydrogels' volume can alter dramatically (Narayanaswamy &Torchilin, 2019). They can retain large amounts of drug and deliver through various means, including diffusion, swelling, or osmosis. Hydrogels can often be tailored for specific drug release rates and designed to degrade for easy bodily removal. Because of their high water content, hydrogels have advantages, for instance, being stimuli-responsive and having the potential to alter drug-release mechanisms (Webber & Pashuck, 2021).

The key elements that impact the swelling nature of hydrogels are their hydrophilic and hydrophobic characteristics, as well as the extent of crosslinking (Thakur & Thakur, 2018). In general, high hydrophilicity and low crosslinking density of polymer cause ample water or physiological fluids to enter into the 3D networked hydrogel system producing large swelling ratios, which is a suitable condition for the diffusion of drugs through hydrogels (Shoukat et al., 2020). Hydrogels with higher swelling rates release more quantity of drugs. The kinetic concept of swelling-controlled drug release is generally a relaxation-controlled process.

Jin et al. (2016) developed a novel hydrogel incorporated sodium fusidate drug for applications in wound treatment. They reported zero-order dissolution kinetics of the drug-loaded hydrogel system (swelling-controlled drug release). Hydrogel coated capsules, known as gel caps, composed of dispersed solid or liquid drugs are commonly used for oral drug administration. The

gel allows easy swallowing owing to its lubrication effect, controls drug release through diffusion over time, and slows the degradation of the capsule (Majcher & Hoare, 2019). Long-term drug adhesion to hydrogel is necessary to achieve extended release by minimizing drug loss due to uncontrolled swallowing and excessive salivary flow, which rinses the oral cavity mucosa (Onnainty & Granero, 2019). Mucoadhesive polymers such as CS are considered advantageous in avoiding immediate elimination of the drug by saliva actions, which is the fundamental limitation of oral route drug administration (Uzunoğlu et al., 2021).

2.3. Types of hydrogels

Depending on their response to the different environmental triggers, hydrogels are classified as pH, temperature, chemical (glucose and enzyme) responsive and other stimuli such as light, electric, and sound responsive hydrogels. Hydrogels responsive to environmental stimuli exhibit substantial volume change and are termed smart or intelligent materials with a broad range of applications (Nawaz et al., 2018). This section describes the pH, temperature, and glucose-sensitive types of hydrogels.

2.3.1. pH-sensitive hydrogels

pH-sensitive smart hydrogels have 3D polymer network structure containing acidic (e.g., -COOH, $-HSO_3$) and basic (e.g., $-NH_2$) functional groups that ionize in a medium with lower (cationic) or higher pH value (Irfan et al., 2019). Consequently, they change their volume, network structure, or mechanical strength as the pH of the surroundings has just slightly changed. When the pH of the surrounding media is altered, the reactive ends of the hydrogel are either protonated or deprotonated (ionized). Consequently, it undergoes degradation and releases drugs (Komatsu et al., 2021) as indicated in figure 2.2. The pH-sensitive hydrogels are potentially employed for oral drugs intended to reduce drug release in the stomach (minimize swelling) but maximize swelling in the intestinal tract promoting higher amounts of drug passing to the intestine (Ebrahimi & Salavaty, 2018).

Natural polymers such as SALG containing an anionic carboxylic functional group and cationic CS have been widely investigated to produce pH-sensitive hydrogels (İnal et al., 2017). At higher pH, SALG ionizes to COO- (deprotonated) in response to a medium's pH change. Consequently, H^+ concentration in the solution increases, hydrogen bonding in the polymer network decreases, repulsion between the anions (carboxylates) increases leading to relaxation and drug release (Bialik-Wąs et al., 2021).

CS consists of amino functional groups (–NH_2), which can be protonated when dissolved in aqueous acetic acid medium (lower pH) to form NH_3^+ species. As the alkaline deacetylation of chitin forms CS, the degree of deacetylation determines how easily it can be dissolved in acetic acid. CS can network with anionic components (drugs) because of its positive nature. It is hydrophobic and suitable for regulating drug release in gastric (low pH) conditions. pH-responsive hydrogels are used for loading and deliver different drugs. For example, pH-responsive CS/PVP hydrogel for cefixime delivery (Ata et al., 2020), CS/hydroxypropyl methylcellulose hydrogel for melatonin deliverying (Jafari et al., 2021), and SALG/PVP-co-vinyl acetate hydrogel for curcumin delivery (Jithendra et al., 2020) were reported. Hydrogel beads made of a pH-sensitive alginate-g-PVP/gelatin mixture were developed and evaluated for CDDSs. The outcomes demonstrated that the beads had comparatively high drug loading efficiency, ranging from 78 to 92% (İnal et al., 2017).

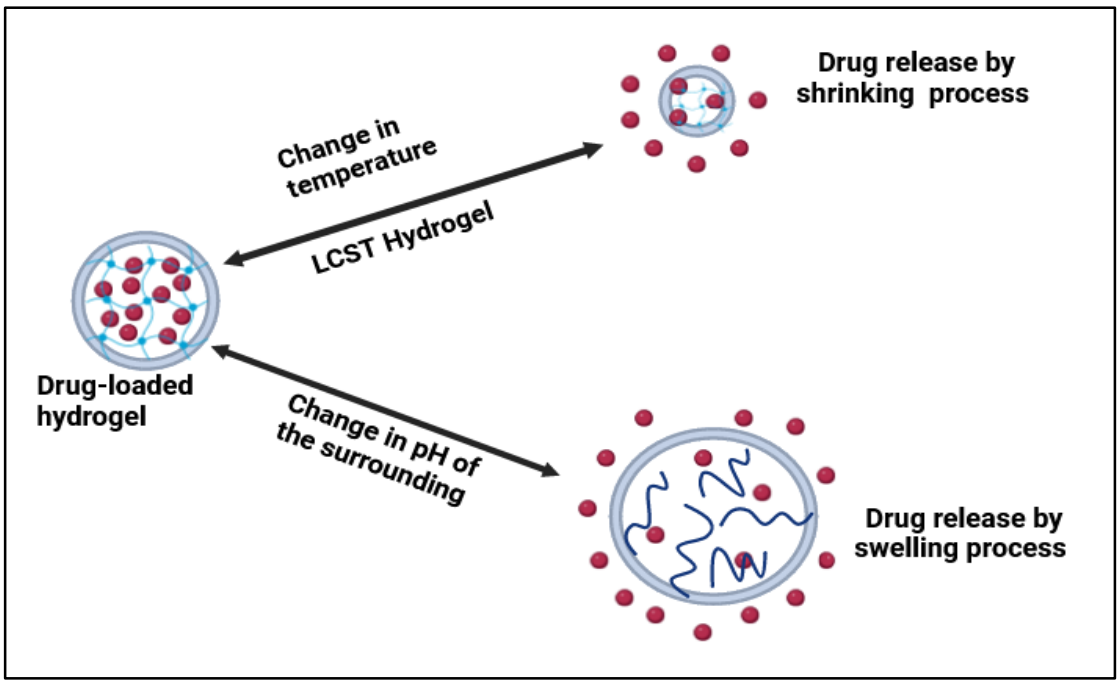

Figure 2. 2 Drug release patterns from temperature and pH sensitive hydrogels.

2.3.2. Thermosensitive hydrogels

In CDDSs, thermosensitive hydrogels are the most extensively studied stimuli-sensitive polymeric materials. They can change volume (swell/shrink) due to temperature variations in their surroundings. Thermosensitive hydrogels have critical solution temperatures (lower or upper) based on which they undergo swelling/shrinking phase transition, which can be either positive or negative. The presence of hydrophobic units, for example, methyl, ethyl, and propyl

groups, which are responsible for temperature transitions, is a common feature of thermosensitive hydrogels (Nayak et al., 2020).

Hydrogels that show positive temperature response have upper critical solution temperatures (UCST) above which the hydrogel is relaxed in volume and contracts below the UCST values. Their solubility in water increases upon heating (Spizzirri & Cirillo, 2017). In contrast, negative thermosensitive hydrogels have lower critical solution temperatures (LCST), below which they exhibit swelling and above which they shrink (loss in water affinity). Their solubility in water decreases upon heating (Alvarez-Lorenzo et al., 2020). The reversible swelling-shrinkage nature of temperature-sensitive hydrogels is essential for CDDSs. For instance, for the negative type hydrogels which relax at room temperature but shrink at 37 ℃ (body temperature), increasing temperature above the LCST value leads to shrinking and subsequently releasing the drug (Thakur & Thakur, 2018) as indicated in figure 2.2. The swelling below the LSCT value permits diffusion of the encapsulated drugs within the hydrogel network system, whereas shrinking above the LSCT value (~ 37 ℃) hinders drug diffusion. Thus, the hydrogel ensures sustained drug release over an extended in the targeted site (Alvarez-Lorenzo et al., 2020). Poly(N-isopropylacrylamide) is an example of the most widely used thermosensitive polymer in CDDSs, owing to its LCST value (32 ℃) which is approximately close to 37 ℃ (body temperature) (Guo et al., 2020).

Eskandari et al. (2020) prepared hydrogel incorporating silica nanoparticle core (etched out by hydrofluoric acid) and crosslinked poly(N-isopropylacrylamide) shell loaded with the drug doxorubicin. The result demonstrated that hydrogel with greater gel content relaxed above the LCST of the polymer. In contrast, the hollow the hydrogel having lower gel content relaxed below LCST. The authors showed that raising the temperature from 25 - 40 °C lowered the concentration of doxorubicin released. Ilić-Stojanović et al. (2021) suggested that hydrogels made of poly(N-isopropylacrylamide-co-2-hydroxypropyl methacrylate) could be an effective and sustained release system for naproxen when body temperature rises.

2.3.3. Glucose-sensitive hydrogels

Glucose-sensitive hydrogels display responses to particular glucose contents and are widely used to regulate blood glucose levels in diabetes patients (Thakur & Thakur, 2018). Insulin must be administered precisely and on time, as excessive insulin might result in a hypoglycemia coma or hyperglycemia if insufficient insulin is administered to the patient. Because of their swelling nature, glucose-sensitive hydrogels are promising tools for developing insulin delivery systems. When glucose levels rise, the crosslinking density of the hydrogel decreases, instigating the gel

to swell and release insulin. The glucose-responsive method also involves pH-sensitive hydrogels that respond to changes pH due to enzyme-substrate reactions in the body. When glucose interacts with the enzyme glucose oxidase, gluconic acid is produced, lowering the pH of the medium. In response to pH changes, the hydrogels either swell or shrink, depending on the polymeric materials' properties that promote insulin release. There are several reports on the investigation of glucose-sensitive hydrogels.

Chen et al. (2020) prepared glucose-responsive microneedle patches by copolymerizing N-vinyl-2-pyrrolidone, 3-acrylamidephenylboronic acid, and N-isopropyl acrylamide. In the basic medium (pH 9.0) and 27 ℃, the optimized microneedle hydrogel showed significant swelling capacity. Approximately 43.2% of the whole insulin could be dispersed into the network (loaded). The result indicated that within 12 hours, insulin release was greater (1.6 times) at a glucose content of 4 g/L than at 1 g/L. Holz & Rajagopal (2020) the reported in situ formation of a hyaluronic acid tailored with a boronic acid-derived hydrogel that responds to glucose. They concluded that the hydrogel has potential utility for sustained drug release applications.

2.4. Hydrogel synthesis methods

As previously indicated, chemical processes or physical interactions can be utilized to produce crosslinked hydrogels. An interpenetrated network (IPN) hydrogel is formed when two homo- or hetro-crosslinked polymeric chains are crosslinked, whereas a semi-IPN hydrogel is formed when only one polymer chain participates in crosslinking but the other polymer component remains uncrosslinked (Zou et al., 2020) as shown in figure 2.3.

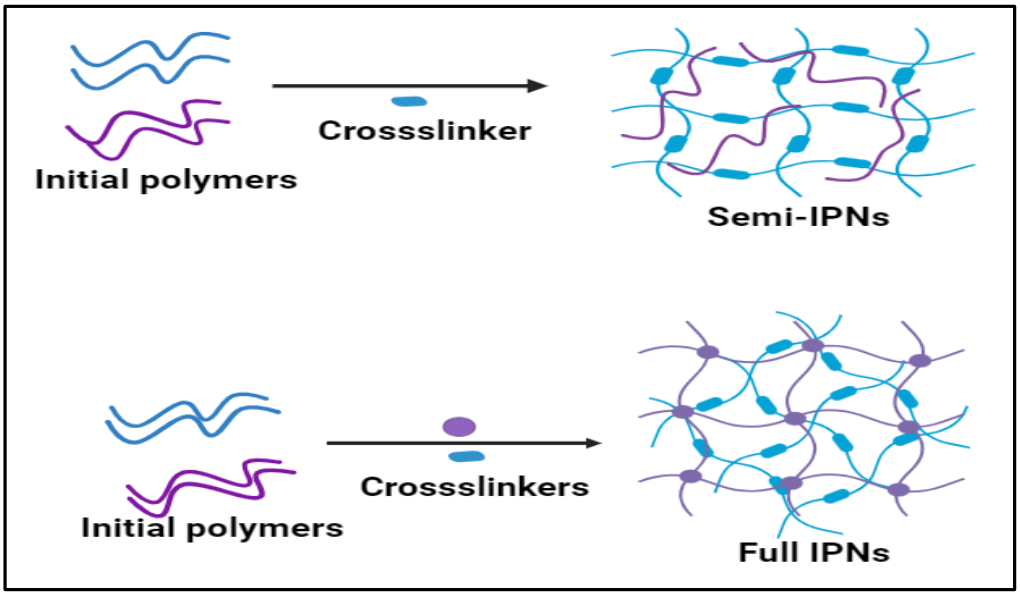

Figure 2. 3 Formation of full and semi- interpenetrating polymer networks (IPNs).

As hydrogels are primarily utilized for CDDSs, they have to form non-toxic products in the body to ensure their biocompatibility. Therefore, properly selecting raw materials and crosslinking agents is vital to designing biocompatible hydrogels. The common crosslinking techniques for preparing hydrogels are illustrated in Figure 2.4 and briefly explained.

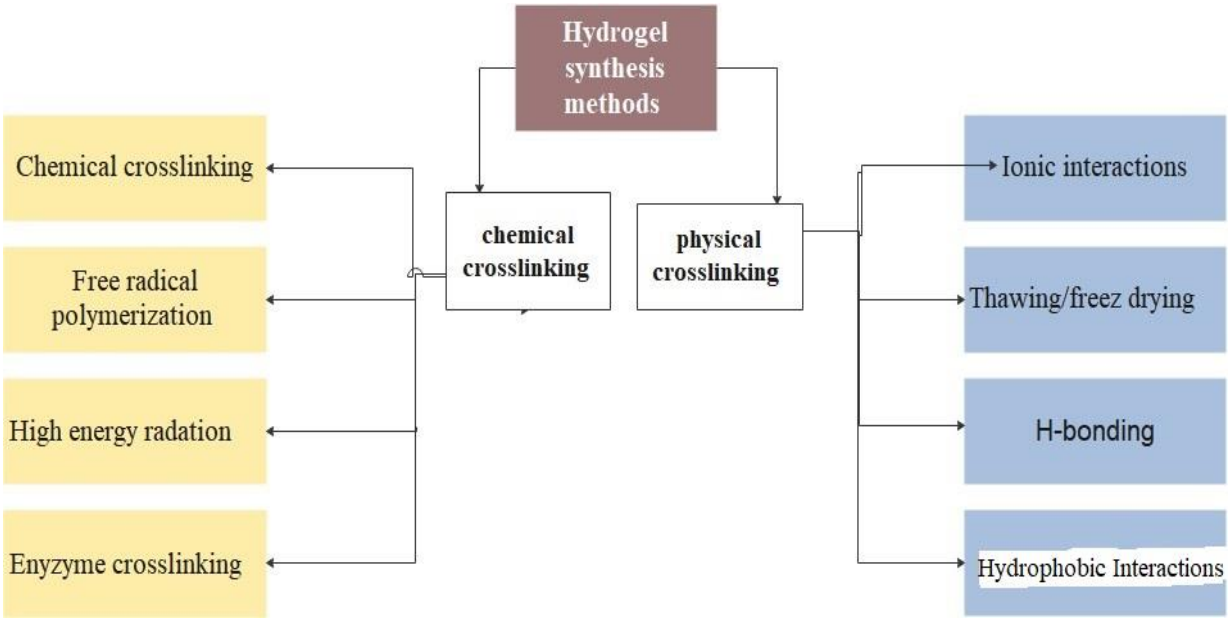

Figure 2. 4 Hydrogel synthesis methods.

2.4.1 Chemical crosslinking

2.4.1.1 Crosslinking using chemical reagents

The chemical reaction method of crosslinking polymers leads to the development of covalent links between raw hydrophilic polymer components. The chemically crosslinked hydrogel products are also known as permanent hydrogels (Ahmed, 2015). The standard chemical reaction methods for crosslinking polymers include functional chemicals (crosslinking agents), free radical polymerization, enzymes, and high-energy ionizing radiation to form 3D crosslinked polymer structure. During the synthesis of hydrogels utilizing chemical crosslinkers, chemical bonds (covalent) are formed between the hydrophilic polymer ends and the functional ends of the crosslinker.

The crosslinking agent is usually mixed with a diluted polymer solution of appropriate functionality to form a product with a crosslinked structure (Saini, 2017). The covalent connections are produced from polymer chains' hydrophilic functional ends, including amine (NH_2), hydroxyl (OH), isocyanate (OH/NH_2), and carboxylic acid (COOH) (Khan et al., 2016).

Adipic acid dihydrazide, epichlorohydrin, and glutaraldehyde are examples of chemical crosslinkers that may be used to crosslink hydroxyl-containing polymers (like PVA). Hydrogels produced by this method are primarily for slow drug release in sustained conditions. Ribeiro et al. (2019) utilized glutaraldehyde as a crosslinker to prepare three different ratios of CS/PVP (1:1, 7:3, and 3:7) hydrogels by the chemical crosslinking method. It was found that CS/PVP hydrogel with a ratio of 7:3 was the most interesting, showing more rigidity than others, ease of handling, and higher sensitivity to pH.

Garakani et al. (2020) synthesized crosslinked CS/PVP hydrogels containing poly (lactide-co-glycolide) particles employing glutaraldehyde as the crosslinking agent, loaded with 30 mg of dexamethasone (DEX) using in situ polymerization for biomedical applications. FTIR spectrum revealed that the interaction between DEX and PLGA was via hydrogen bonding. The SEM images showed that increased PVP content resulted in a denser microstructure and smaller pore size. Gull et al. (2020b) prepared a CS/PVP (60/40, w.t %) hydrogel loaded with diclofenac sodium using epichlorohydrin crosslinking agent. The produced hydrogel was analyzed for swelling ratio in phosphate buffer solutions. The result indicated that the hydrogel system with a crosslinker amount of 150 µL exhibited the maximum swelling degree than the other hydrogels at lower pH (acidic) as a result of the protonation of amine ($-NH_2$) of CS.

2.4.1.2. Free radical polymerization

Low molecular mass monomers, or branched homopolymers, are crosslinked using crosslinking agents in the free radical polymerization synthesis method. It is commonly carried out in aqueous solution. The basic steps of free radical polymerization crosslinking are initiation, propagation, and termination (Thakur & Thakur, 2018). In the initiation step, the polymer networks are initiated by chemical crosslinker or radiation to generate free radicals, followed by a reaction with a vinyl monomer. Propagation involves the monomers to the developing polymer chains with active the center remaining constant. In the termination step, radicals of two polymer chains are combined or coupled (Elsayed, 2019). A molecule or solvent transfer may also occur as part of the chain rearrangement process, which involves moving the active growth center to the passive center. Most hydrophilic polymers that have pendant hydroxyl groups, such as polyethylene oxide, polypropylene oxide, polyacrylic acid, and methacrylic acid, are used in free radical polymerization (Chatterjee et al., 2020). Free radical reaction initiators like azobisisobutyronitrile, benzoyl peroxide, and benzoyl alcohol have been used (Melnyk et al., 2020). This crosslinking technique has the benefits of being quick and inexpensive, and the product separation and purification processes are simple. However, the main drawback of the

free radical polymerization method is that further copolymerization is impossible due to the termination process (Misiak et al., 2020). Some of the commonly used crosslinking agents include N, N'-Methylenebisacrylamide, GA, acetaldehyde, epichlorohydrin, formaldehyde, maleic acid, and dimethylurea (Zainal et al., 2021). In general, for the preparation of hydrogels, a modest amount of a crosslinking agent is often used, while a higher concentration of monomers increases the polymerization rate. Ilić-Stojanović et al. (2021) synthesized crosslinked hydrogel poly(N-isopropylacrylamide-co-2-hydroxypropyl methacrylate) loaded with naproxen drug employing free radical polymerization method. 2, 2'-azobis (2-methyl propionitrile) was used as an initiator and ethylene glycol dimethylacrylate as cross-linking agent. A thermo-responsive composition was evaluated for prolonged drug release. The result showed that prolonged naproxen release was enhanced when the body temperature increased.

2.4.1.3. Crosslinking by enzymes

Enzyme-catalyzed polymer crosslinking is an emerging and attractive method for the preparation of covalently crosslinked hydrogels. The widely used enzymes in crosslinking polymers include microbial transglutaminase (TG), mushroom tyrosinase, and transferases (C. K. Sun et al., 2021). Enzyme crosslinking reactions occur mainly at mild conditions such as at ambient temperature and an aqueous solution with a neutral pH. Hence, they are suitable for in situ formation of hydrogels. Moreover, unlike other chemical methods, undesired side reactions (toxicity) and the likely loss of bioactivity do not occur (Khan et al., 2016). Covalently crosslinked gelatin/alginate hydrogel was prepared using transglutaminase (TG) enzyme for a controlled and effective gentamicin drug release profile (C. K. Sun et al., 2021).

2.4.1.4. Crosslinking by radiation

This method produces crosslinked hydrogels employing radiation (gamma, electron beam, or microwaves). The primary reaction is the formation of short-lived radicals that interact with the polymer chains. For instance, irradiation of an aqueous polymer solution involves water radiolysis generating reactive free radicals such as •OH and •H. As the •OH radical is a powerful oxidizing agent, it reacts with polymer chains in the aqueous solution to form polymer chain radicals, which subsequently couple with each other yielding crosslinked polymer (Zainal et al., 2021). The advantages of radiation-assisted polymer crosslinking over other techniques are no requirement for toxic chemical initiators, no further purification of the final product, gives higher yield, easy scale-up, and simultaneous sterilization of the hydrogels produced (Yang et al., 2021). E-beam radiation was used to crosslink highly elastic, superabsorbent collagen/PVP/polyacrylic acid/polyethylene oxide hydrogel (Demeter et al., 2020). The authors showed hydrogel formation

having a permanent network exhibited very high swelling ratio of 1600% in pure water and 4000% in simulated buffer solution. Gamma radiation was used to prepare ketoprofen-loaded PVP/crotonic acid novel hydrogel for a controlled release study (Ajji et al., 2020).

2.4.2. Physical-crosslinking method

Hydrogel formation via physical crosslinking approach requires non-covalent interactions such as ionic interaction, hydrogen bonds, and crystallization. This crosslinking method does not require multifunctional crosslinkers, nor is associate with toxicity, so further purification not required. The physical crosslinks are not permanent and yield reversible hydrogel products (Maitra & Shukla, 2019).

2.4.2.1. Crosslinking by ionic interactions

This method involves the interactions of oppositely charged polyelectrolytes to form an ionically crosslinked hydrogel in an aqueous medium through electrostatic attraction. Unlike chemical crosslinking, the ionic crosslinking approach does not need multifunctional crosslinking agents; nevertheless, it requires multivalent (commonly di- or trivalent) metal cations as crosslinkers of the polymer chains (Saini, 2017). Among the various polymers that can be crosslinked through ionic interactions, CS and alginate are well known. The divalent metal cations used as crosslinkers include Ca^{2+}, Zn^{2+}, Ba^{2+}, and Cu^{2+}. For example, a sericin/alginate hydrogel matrix was developed ionic crosslinking using $CaCl_2$ as the crosslinking agent (Bezerra et al., 2021). A physically crosslinked CS/SALG/Ca^{2+} ion bilayer hydrogel was prepared for heavy metal cation absorption (Tang et al., 2020). X.Wu et al. (2020) prepared SALG/CS bilayer hydrogel beads via the physical interaction method using $CaCl_2$ as the crosslinking agent for controlled release study of doxorubicin in a medium with varied pH (1.0, 6.5, and 7.4). Their analysis showed an increased drug release rate with an increasing SALG weight ratio due to the protonation of the SALG, leading to the disintegration of the hydrogel beads.

2.4.2.2. Crosslinking by crystallization

Crystallization involves crosslinking of polymers by repeatedly cooling and thawing their aqueous mixture, forming strong and elastic gels (Khan et al., 2016). The momers' molecular mass, their proportions in the aqueous mixture, temperature, and the duration and frequency of the cooling process all affect the nature of the produced gels. The polymer crystallites (lamellas) are generally joined through hydrogen bonding, which acts as a physical crosslinking site in the chains (Zainal et al., 2021). The advantages of the freeze-thaw method include improved biocompatibility, biodegradability, and non-toxicity of the polymer gels. It was reported that

ibuprofen-loaded PVA/PVP bilayer hydrogels were made using the crystallization process and had outstanding antibacterial wound-healing activity (Oustadi et al., 2020).

2.4.2.3. Crosslinking by hydrogen bonding

The crosslinking of polymer chains by the hydrogen bonding intermolecular forces is typically utilized to synthesize gelatin-based hydrogels involving interactions between H^+ and high electronegative functional ends (Saini, 2017). Such hydrogels are formed when carboxylate groups are protonated; consequently, the pH of the polymer mixture decreases (Nia et al., 2020). Different factors influencing hydrogel formation by hydrogen bonding include solvent type, temperature, polymer concentrations, and the molar ratio of each polymer. Song et al. (2016) investigated PVP/polyacrylamide hydrogels prepared via hydrogen bonding crosslinking method. The monomer ratios were shown to impact the hydrogels' characteristics significantly. Ibuprofen has been successfully encapsulated in CS/polyvinyl alcohol blend with the introduction of genipin, forming hydrogen bonds that link the amine ($-NH_2$) and hydroxyl (-OH) groups of CS and polyvinyl alcohol (Aycan et al., 2020).

2.5. Polymers for oral drug release systems

Polymers play an essential part in the preparation of drug delivery systems. They are used as either bioactive molecules (polymeric drugs) or inert carriers for drug delivery, like hydrogels. Polymeric materials for preparing hydrogels for CDDSs must satisfy numerous physiological and physical design standards, including biocompatibility, inert, non-toxic, and biodegradability (Nayak et al., 2020). Some hydrogels resemble the characteristics of the extracellular matrix (Noshadi et al., 2017). Because of this superior biocompatibility, hydrogels are considered ideal drug carriers. Hydrogels for CDDSs have been developed using natural polymers (for example, sodium alginate, guar gum, CS, collagen and cellulose) and synthetic polymers (for example, polyvinyl pyrrolidone, polyvinyl alcohol, polyethylene oxide, and polymethyl acrylate) (Batista et al., 2019). Some of those relevant to this research are described below.

2.5.1. Chitosan

CS is a carbohydrate polymer comprising of β (1→ 4) connection of 2-amino-2-deoxy-D-glucose and 2-acetamido-2-deoxy-D-glucose repeating structural units (Figure 2.5) (Nayak et al., 2020). CS is a derivative of alkaline deacetylation of chitin, being the only cationic (amino group) water-insoluble natural polysaccharide with amino ($-NH_2$) functional groups (pka ~ 6.3), and is used in pH-sensitive hydrogels in CDDSs. In acidic medium CS is protonated and exists as cationic form

($R\text{-}NH_3^+$) as shown in figure 2.6. Therefore; CS-based hydrogels swell (soluble) in dilute acidic media (e.g., in acetic or citric), whereas it deprotonated and shirnks in basic media. CS is biodegradable and is often crosslinked with other polymers to form pH-sensitive hydrogels (Garakani et al., 2020). Generally, it has a low molecular weight ranging from 3,800-20,000 Da on average, with different degrees of deacetylation (Ahmed & Aljaeid, 2016). Due to the electrostatic attractions between the cations and the anions on the surface, CS has mucoadhesive nature.

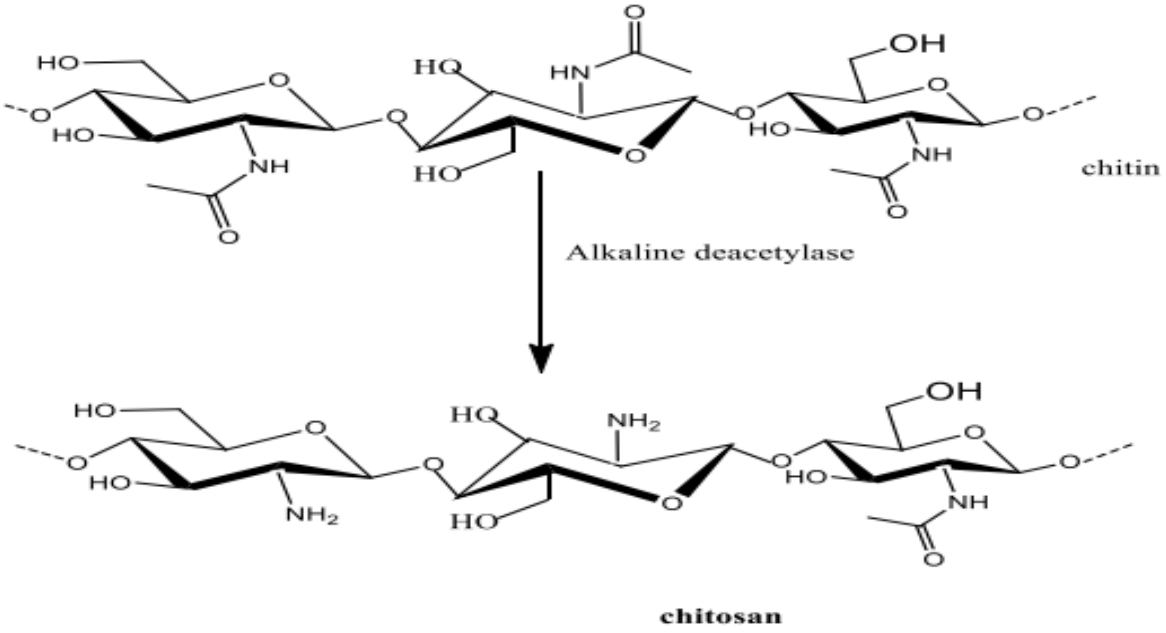

Figure 2. 5 Structure of chitin and CS. Reprinted from El Nokab and van der Wel, 2020.

It offers advantages including chain flexibility, the ability to form hydrogen bonding, ease of structural modification, biocompatibility, and low toxicity, with high potential use in various applications, especially for oral, topical, and nasal CDDSs (Nayak et al., 2020). The mucoadhesive nature of CS helps for extending at the drug's designated site of absorption or bioavailability, making it easier to the control drug release rate. In general, the availability of amino groups ($R\text{-}NH_3^+$) for crosslinking, easy control of drug release, and simplicity of hydrogel preparation make this polysaccharide the choice for synthesizing different hydrogel compositions.

Since CS displays relatively low mechanical strength, it is usually crosslinked with other polymers, such as PVP and SALG, for better performance in CDDSs. Table 2.1 illustrates some examples of previous works concerning CS/PVP based hydrogels employing different crosslinking agents for drug release applications. The table shows that CS/PVP with a weight

ratio of 60/40 is frequently used, indicating an optimal weight ratio for crosslinked CS/PVP hydrogels displaying optimal drug loading effiiency plus maximum drug release efficiency.

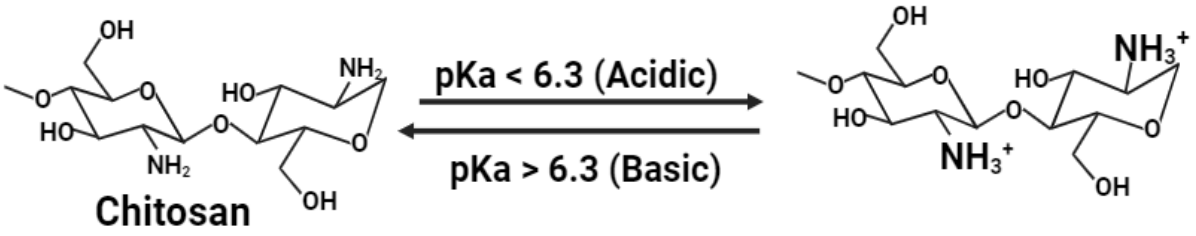

Figure 2. 6 pH-dependent protonation and deprotonation of CS.

Furthermore, CS/PVP crosslinked hydrogels have been used to load different drugs in different amounts, including painkillers, antibiotics, and antiseptics, with efficiencies ranging from 51% to 100 %. This variation in efficiency depends on the pH, time, porosity, and composition of constituents.

Table 2.2 depicts examples of the previous works concerning CS/SALG based hydrogel systems employing different crosslinking agents for drug release applications. It can be seen from the table that in the hydrogels, the CS to SALG polymer ratios used vary in each work, and $CaCl_2$ is commonly used as a crosslinking agent. In these hydrogels, ionic interactions occur between the amino ends (-NH_2) of CS, which display cationic nature, and the anionic group (COO-) of SALG. The drug loading efficiency and drug release properties of CS/SALG hydrogels vary due to similar factors as that of CS/PVP hydrogel systems.

2.6.2. Poly (vinyl pyrrolidone)

PVP, also known as povidone, is a water-soluble and biocompatible polymer made by polymerizing N-vinylpyrrolidone monomers (Contardi et al., 2021). A non-toxic, inert polymer is pH stable, temperature resistant, and biodegradable. It is used to load hydrophilic as well as hydrophobic drugs in CDDSs (Kurakula & Rao, 2020). PVP has been utilized in a wide range of biomedical applications for drug release due to its particular features, including transdermal, oral, and ocular administration. The polymer can be conjugated with less soluble drugs to increase bioavailability and enhance the desired swelling for their controlled-release (Kurakula & Rao, 2020). It is available in molecular weights identified by several K-values, like K12 (3100–5700 Da), K17 (7900–10,800 Da), K25 (23,000–32,000 Da), K30 (35,000–51,000 Da), and K90 (900,000 –1,300,000 Da) (Franco & De Marco, 2020). The structure of PVP is shown in figure 2.7 below.

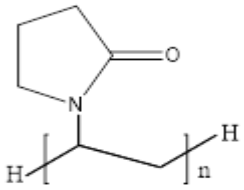

Figure 2. 7 Poly (vinyl pyrrolidone) structure. Reprinted from Zhang et al., 2020.

Ajji et al. (2020) studied a PVP/crotonic acid pH sensitive hydrogel for the controlled release of ketoprofen. The result indicated minimum drug release at lower pH (acidic medium) but a higher and prolong drug release at neutral pH, implying the feasibility of employing the hydrogel as a viable drug delivery material in the intestine. Ata et al. (2020) prepared CS/PVP hydrogels crosslinked with (3-aminopropyl) triethoxysilane and studied for controlled-release of cefixime release. The authors observed maximum swelling in an acidic medium (pH 2), which was reduced in basic medium. A drug release of 81.6% in 12 h was obtained in simulated gastric fluid (SGF). Gull et al. (2020a) synthesized CS/PVP (60/40, wt.%) based hydrogels using various amounts of glycidyloxypropyl trimethoxysilane crosslinker from 50 µL to 250 µL. The thermogravimetric analysis of the hydrogel samples showed three stages of consecutive decomposition. The thermal stages were observed at temperature ranges of 25 °C to 180 °C, followed by a second step extended to 425 °C with a mass loss of 55%, and the final stage was detected from 425 °C to 600 °C with a final residue of 32%. The author concluded that the optimum crosslinker concentration that showed better thermal stability was 200 µL.

2.6.3. Alginates

Alginates are unbranched carbohydrate polymers comprising of 1- 4-linked β-mannuronic acid and α-L-guluronic acid residues (Figure 2.8). They are available in a broad molecular mass range, 50 to 10,000 kDa. Alginates are often produced from brown seaweeds (algae), via dilute alkaline extraction or microbial fermentation (El Nokab & Van der Wel, 2020). Alginates exist in three structural forms, which are a homopolymeric form of guluronic acid (G) (rigid) with axil-axil linked, a homopolymeric form of mannuronic acid (M) (less rigid) with di-equatorial links, and the third is the mixture of equal proportion of the above two forms (G/M). Physical features of this mixture, including toughness and viscosity, depend on the proportion of the two components (M/G) (Hao et al., 2020). When crosslinked with divalent metal cations, alginates with a higher fraction of G blocks generate stiff structures. A higher fraction of M blocks, on the other hand, forms less sticky hydrogels and exhibits immune-stimulatory characteristics. The polymer can be crosslinked using divalent (Ca^{2+}, Ba^{2+}, Zn^{2+}, or Cu^{2+} ions) to enhance network of the polysaccharide units (Chowdhury et al., 2020).

Crosslinked SALG is formed through ionotropic interactions (physical crosslinking) in which the Na^+ ions of SALG are replaced by the bivalent or trivalent metal ions that substitute the Na^+ of SALG subsequently, the polymer chains become networked (El Nokab & van der Wel, 2020). Consequently, the H^+ ions concentration solution increases, hydrogen bonding in the polymer network decreases, and repulsion between the anions (carboxylates) increases, leading to swelling and, thus, drug release (El Nokab & van der Wel, 2020).

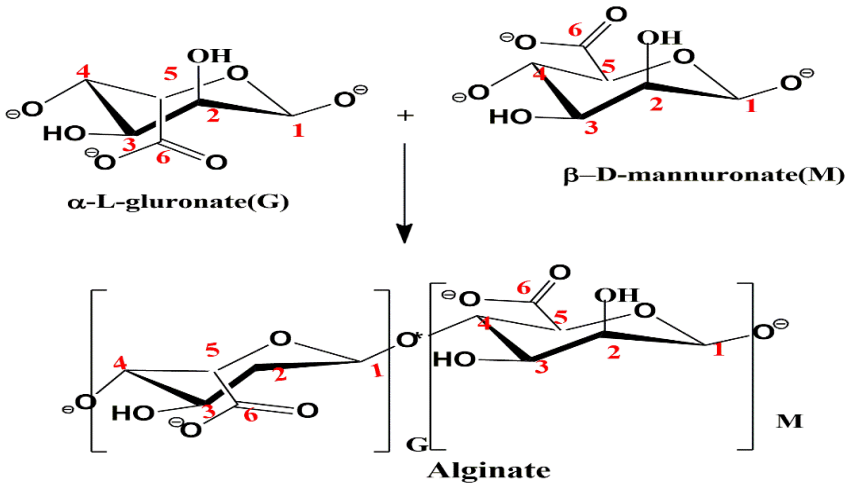

Figure 2. 8 Structure of alginate chain. Reprinted from El Nokab & van der Wel, 2020.

Alginates are widely utilized to prepare pH sensitive hydrogels for drug release applications because of their essential characteristics, including excellent biocompatibility, bioadhesive, bioinert, biodegradability, and high resemblance with extracellular matrix (Bezerra et al., 2021). However, the dissolution of alginate-based hydrogels at neutral pH causes the removal of the crosslinking divalent metal ion, which leads to the complexion and uncontrollable degradation kinetics.

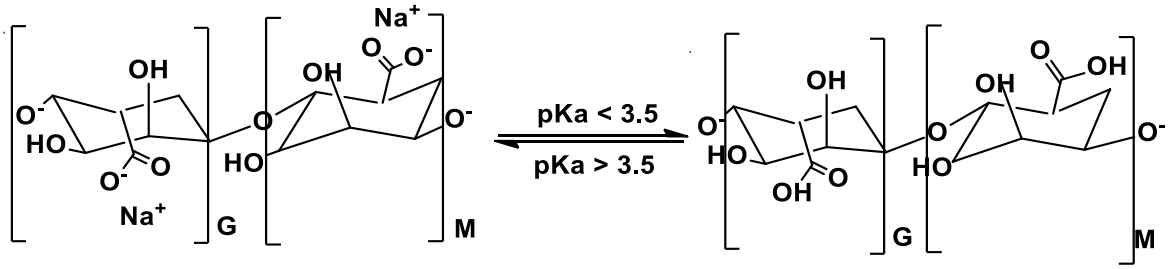

Figure 2. 9 pH-dependent protonation and deprotonation of SALG.

To overcome this problem, different modification methods of the alginate, such as crosslinking alginate with other polymers, e.g., CS and oxidation of the alginate, are used to develop different hydrogel systems of improved properties for drug delivery systems (Segale et al., 2016). SALG

(pka ~ 3.5 - 4.4), ionize to carboxylate ions (COO-) in basic medium and in acidic medium SALG is protonated and exists as alginic acid (Figure 2.9).

2.7. Biodegradation of hydrogels

Hydrogel degradation pertains to any chemical, physical, or biological process that entails breaking covalent bonds in the polymer's backbone, leading to an irreversible change in its characteristics due to changes in its chemical makeup and a decrease in its molecular mass forming smaller monpmors (Wilson, 2014). The breakage of fundamental chemical bonds in the primary or side chain produces reactive substances, which are accountable for promoting the breakdown process of the polymeric material. The in vitro degradation of hydrogels is critical for their use as biomaterials because their degradation nature decides important in vivo characteristics such as biological materials stability in a living organism and effectiveness in the release of various active ingredient. The *In vitro* biodegradation of polymers occur in the presence of abiotic variables, such as heat, light, radiation, humidity, pH of the environment, mechanical strain, and chemical exposure, stimulate the start of the polymer decomposition process. These types of commencement necessitate activation energy to rupture chemical bonds in the polymer, with the binding energy varied depending on the atoms' crosslinking, i.e., ionic, coordinate, or covalent primary bonds. Organic polymer bonds are typically covalent and entail short lengths and high energy (100 K/mol).

Polymer biodegradation can occur in the presence of numerous energy sources required for bond disintegration, such as water (hydrolysis), heat (thermolysis), oxygen (oxidation), light (photolysis), radiation (radiolysis), or shear (mechanical), among others. Hydrolysis process is a chemical degradation mechanism in which bonds are broken by interacting with water molecules (Pacheco et al., 2020). It is critical for starting the biodegradation of hydrogels. The rate of hydrolytic disintegration vary from several hours to years, based mostly on the materials crystallinity nature, functional group type, molecular mass, backbone structure, morphology, temperature, and pH of the environment (Mandal & Shunmugam, 2020). Hydrogel in vitro hydrolysis can occur through surface erosion or bulk erosion. During surface erosion, the outermost layer of the polymer dissolves first, followed by the inner material. Bulk erosion, on the other hand, takes place when water molecules rapidly diffuse into the polymer's amorphous regions, triggering a swift degradation of strength and structural integrity (Mandal & Shunmugam, 2020). Gull et al., (2020) showed the in vitro biodegradation of CS/PVP hydrogels in SCF (pH 7.4). The study demonstrated that an increase in GPTMS (crosslinking agent) concentration has improved the stability of CS/PVP hydrogels slowing its degradation rate.

Thermal decomposition (thermolysis), occurs when a hydrogel is heated and disintegrates into more than two new components. The thermal degradation of hydrogels produces molecules that differ from the source without the assistance of other chemicals. Thermal degradation is generally an endothermic process because the heat absorbed fractures the bonds of the hydrogels (L. Sun et al., 2022). Thermogravimetric analysis is used to investigate the decomposition of polymers into smaller molecules, constituent atoms, and/or the release of gases such as CO_2, CH_4, CO, and so on. Due to most the characteristics and purposes of hydrogels are thermosensitive, and some properties rely on intermolecular forces that break at low temperatures. TGA detects mass loss, and describes the event as thermal decomposition because it requires breaking of fundamental bonds, confirming the occurrence of hydrogels thermolysis.

2.8. Other biomedical applications of hydrogels

Hydrogels are attractive for a variety of biomedical applications due to their amazing features such as structural flexibility, high water content, softness, biodegradability, biocompatibility, and non-toxicity. In addition to the controlled drug delivery application stated above, hydrogels are widely used for wound healing, soft contact lenses, tissue engineering etc.

2.8.1. Wound healing

The skin, as the most important organ, may retain its original structural integrity after injury; nevertheless, various factors such as temperature, tissue oxygenation, stress, medication etc. may interfere with the wound healing process. To improve wound healing, many dressings and pharmacological therapies have been developed. The wound dressing is supposed to produce a moist environment, prevent the wound area from infections, and enhance the healing process (Chalitangkoon et al., 2020). Because of their high water content, flexible shape, and ability to resemble biological tissues, hydrogels provide ideal wound healing qualities.

Hydrogels are versatile biomaterial that possesses flexible mechanical properties, ability to reduce pain by promoting moisture and cooling the wound area, as well as maintain the wound area close and clean by eliminating infectious tissue via autolysis (Duceac et al., 2020). Hydrogels do not cause skin irritation, when administered to the wound area, they do not stick to the wound site, allowing metabolites to circulate easily and promoting wound re-epithelialization (skin tissue growth). Furthermore, hydrogels are used to load with medications that promote wound healing (Chalitangkoon et al., 2020). L.Wang et al. (2022) developed N-carboxymethyl CS/SALG hydrogel incorporating plasmid DNA for wound healing application. SALG/CS hydrogel loaded with gentamicin was also reported in literature (Bakhsheshi-Rad et al., 2020).

2.8.2. Soft contact lenses

Hydrogels due to their high water content and flexible shape have been widely used in the development of ultra-thin, flexible soft contact lenses (Chatterjee et al., 2020). Hydrogel based contact lenses are biocompatible and comfortable because they adapt to the ocular curvature. Such soft contact lenses allow ambient oxygen to enter the cornea via the water in the lenses (Oucif et al., 2022). Hydrogel-based contact lenses can also be loaded with drugs for ocular drug delivery. Because of the dimensional barrier that contact lenses offer to the drug as it dissipates out of the gel matrix, they allow for slow and extended drug release in the pre-corneal area (Ahmadi et al., 2015). Because of their excellent biocompatibility and flexible characteristics, polymers such as hydroxyethyl methacrylate (HEMA), polyacrylamide, and PVP have been widely used in the development of soft contact lenses. N-vinyl-2-pyrrolidone's effects on the curing properties of poly(2-hydroxyethyl methacrylate)-based hydrogel employed as contact lenses were examined (Lee et al., 2020). Oucif et al. (2022) developed Poly (hydroxyethyl methacrylate-co-hydroxyethyl acrylate) hydrogel based soft contact lenses for controlled release of acetazolamide.

2.8.3. Tissue engineering

Hydrogels have gained high attraction for tissue engineering applications, owing to their unique characteristics, such as their capacity to hold high water, preserve porous structure, adapt structural flexibility, excellent biocompatibility, operate as scaffold, and resemble extracellular matrix (Moshayedi et al., 2021). These structural properties enable hydrogels to be employed as tissue scaffolds in the body by allowing cell metabolite inflow, eliminate waste, nutrient transfer via their pores. By integrating cells into their framework and gradually decompose thereby leaving only healthy tissue behind (Jariya et al., 2021). Chen et al.(2022) fabricated SALG/polyacrylamide/CS/gelatin hydrogel scaffolds for tissue engineering applications. X.Wang et al. (2022) developed gelatin/Carboxymethyl CS/SALG scaffolds for in vivo and in vitro tissue engineering study.

2.9. Amoxicillin

AMX [6-D-(-)-alpha-amino-4-hydroxyphenyl-acetamido] is a penicillanic acid drug and is a family of β-lactam antibiotics used for the treatment of various kinds of bacterial infections (Nia et al., 2020). AMX is effective against various gram-positive bacteria strains, including *Streptococcus aureus, Streptococcus pneumonia*, *Enterococcus faecalis,* and gram-negative bacteria strains, including *Haemophilus influenza*, *Escherichia coli,* and *Neisseria gonorrhea.*

AMX is often combined with clavulanic acid to enhance its activity against drug-resistant bacteria like β-lactamase producing bacteria which can degrade AMX (Fazulbhoy et al., 2021). It has an empirical formula of $C_{16}H_9N_3O_5S.3H_2O$ with the structure shown in figure 2.10 and a molecular weight of 419.5 g/mol. It is a white to pale yellow color, crystalline powder that is hardly soluble in hydrophillic solvents (e.g., water or methanol). However, it cannot be dissolved in hydrophobic solvents (e.g., benzenes, chloroform, or ether).

Action mechanism: AMX works by attaching to penicillin-binding proteins, which prevent transpeptidation (a growing step in cell wall building), activating autolytic enzymes in the bacterial cell wall (Fazulbhoy et al., 2021). The lysis of the cell wall that results from this activation kills the bacterial cell and causes it to be destroyed. In the absence of β-lactam antibiotics, the bacteria grow and reproduce through crosslinking of their cell wall derived from developing peptidoglycan layer-enhanced transpeptidase, often referred to as penicillin-binding proteins. In the presence of the β-lactam antibiotics, this transpeptidase component of the cell wall binds to the antibiotics.

Consequently, enhance the activation of autolytic cell wall hydrolases and inhibition of bacterial cell wall crosslinking without forming a new peptidoglycan layer (destruction of the cell wall) (Fazulbhoy et al., 2021). Further, drug administration can be used alongside a beta lactamase blocker such as clavulanic acid or sulbactam, which forms an irreversible link with the beta-lactamase enzyme's catalytic site. This leads the enzyme to hydrolyze the beta-lactam ring's amide bond, which is resistant to the original beta-lactam ring of AMX (Rodríguez-villodres et al., 2020). Beta-lactamase blockers do not naturally kill bacteria, but when coupled with AMX, they might increase the drug's effectiveness against bacteria strains that generate beta-lactamase enzyme.

Pharmacokinetics: AMX is a penicillin derivative with a structure similar to ampicillin. However, when orally administered, it has better absorption than ampicillin and hence has higher bioavailability in blood. Currently, AMX is present in the conventional capsule form for oral administration. AMX administration depends more on time than concentration., i.e., time is taken for its concentration in the blood to reach a minimum concentration unable to inhibit bacterial actions (Van Donge et al., 2021). Therefore, the drug is prescribed more repeatedly, for instance, thrice daily (Malcolm et al., 2020).

Table 2. 1: Crosslinked CS/PVP hydrogels for drug controlled-release applications

CS/PVP (molecular weight, g/mol)	**CS/PVP (weight ratio)**	**Crosslinking agent**	**Model drug**	**Drug amount**	**Drug loading efficiency**	**Drug release profile (maximum)**	**Antibacterial activity test**	**Reference**
497K/360K	20/80%	-	Cloxacillin	0.7g	-	90% in 30 minutes pH 7.4	Diffusion method against *Staphylococcus aureus*	Perea et al.(2023)
190K/1300K	40/60%	-	5-Fluorouracil	10 mg	-	120 µg/mL in 24 hours pH 7.4	-	Grant et al. (2021)
90K/40K	60/40%	3-Glycidyloxy propyl trimethoxysila-ne(GPTMS) (50 µL)	Povidone-iodine:	50 mg	86%	85.24% in 190 min pH 7.4	Diffusion method against *Escherichia coli*	Gull et al.(2020a)
90K/40K	60/40%	Tetraethyl orthosilicate (150 µL)	Lidocaine	50 mg	-	*In SGF (pH 1.2),100% in 30 minuteS *In SCF (pH 7.4), 96.37% in 110 minuteS	Optical density (OD) against *Escherichia coli*	Gull et al. (2019)
90K/40K	60/40%	Epichlorohydrin	diclofenac sodium	50 mg	84%	87.56% in130 minutes pH 7.4	Optical density (OD) against *Escherichia coli*	Gull et al. (2020b)
DDA≥ 75%,density 0.15-0.3 g/cm^3)/4k	0.5/0.5g	Aminopropyletrie thoxy silane	Cefixime	25mg	-	*In SGF (pH 2), 81.6% in 12 h	Disc diffusion against *Escherichia coli*	Ata et al. (2020)
DDA 75-86%/40k	- 40/60% - 60/40%	GA (5 mL, 25% solution)	Metformin hydrochloride	5, 10, 15 wt.%	61.5% 70.9%	98% and 77% in 8 hours pH 7.4	-	Reddy et al. (2012)

* DDA: Degree of deacetylation

Table 2. 2: Crosslinked CS/SALG hydrogels for drug controlled-release applications

CS/SALG (molecular weight g/mol)	**CS/SALG (weight ratio)**	Crosslinking agent	**Model drug**	**Drug amount**	**Drug loading efficiency**	**Drug release profile (maximum)**	**Antibacterial activity test**	**Reference**
50/80-120 KDa	1.5/3% (w/v)	$CaCl_2$ 10% (w/v)	Cefixime	4.4mg	0-47.4%	3.5 and 13.9 mg/mL after 5 min and 120 min, respect. pH 7.4	Colony forming unit count method against *Escherichia coli*	Maestrelli et al. (2018)
120K/750K	0.2g/0.015g	-	5-Fluorouracil	0.0035 g	84%	61.45%, 36.75%, and 40% in pH 7.4, 6.8, and 5 respect. 8 h	-	Zamani et al. (2023)
190KDa/200K	25/75%	0.1 N $CaCl_2$	Gentamicin	0.05g	-	80% in 24 pH 7.4	Diffusion method against *Escherichia coli* and *Streptococcus mutans*	Beads et al. (2022)
190KDa/ 216.12	0.5g/0.5g	Glutaraldehyde and $CaCl_2$	Rifaximin	0.5g	92%	80% achieved at pH (7.2) in 24 h	Diffusion method against *Escherichia coli*	D. Kumar et al. (2021)
190-300K/ 300K g/mol	1/0.5 % (w/v)	Sodium tripolyphosph-ate 0.67% and $CaCl_2$ (0.6% w/v)	Quercetin,	5, 7.5 and 10 mg/mL	46.5% - 82.4%	1% in 1 h,78 % in 24 h, pH 7.4	-	Nalini et al. (2019)
190-300K/ 100K g/mol	0.3/0.6 mg/mL	0.51 mg/mL	Endolysin	3.5 mg	62 %	81% in 36 h pH 7.4	Diffusion method against *Staphylococcus aureus*	Kaur et al. (2020)

AMX is stable in the gastric fluid with acidic pH and can easily diffuse into the body tissues, fluids, and in small amounts into breast milk having about 1.4 hours half-life duration in adults. The liver metabolizes it, and nearly 60% to 80% dosage of the drug is defecated unchanged via the urine. AMX's pharmacokinetics and absorption are not significantly affected by whether it is taken after eating or without food (Veeraraghavan et al., 2021). However, it is quickly absorbed after oral administration in fasting states, with improved bioavailability than in fed states. In other words, the time to reach peak concentration is more significant in the fed state.

Adverse effects: The common side effects of orally administered AMX include nausea, vomiting, diarrhea, and skin rash with intense itching. Rare severe side effects may also occur, including confusion, anxiety, mental changes (unclear thinking), and insomnia (Fazulbhoy et al., 2021). Anaphylaxis is the most severe reaction due to the parenteral dosage form of AMX.

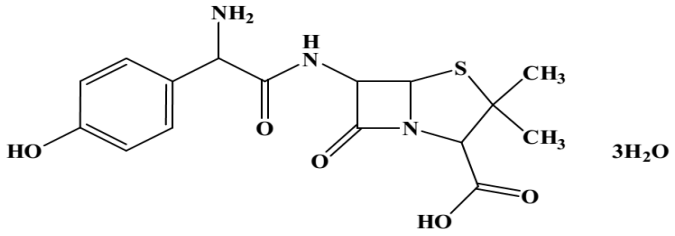

Figure 2. 10 Structure of AMX. Reprinted from Qader and Fakhre, 2015.

2.10. Metronidazole

MTZ, commonly called Flagyl ($C_6H_9N_3O_3$, molecular weight, 171.154 g/mol) and with the structure shown in figure 2.11, is a broad-spectrum antiprotozoal and antibacterial drug used to treat various inflammatory diseases. It is active against gram-negative bacteria such as *Bacteroides fragilis*, *Helicobacter pylori*, and gram-positive anaerobic bacteria such as *Clostridium difficile Bacteroides fragilis* causes extra-intestinal infections such as diabetic foot infections and brain, lung, abdominal, and surgical site infections (Ghotaslou et al., 2018). MTZ is also used in conjunction with additional antibiotics like AMX and tetracycline, which is highly effective against *H. pylori* eradication (Hernández et al., 2019). MTZ is available as an oral tablet, a cream (for oral and skin infections), and a solution for intravenous injection (Giske et al., 2017). The administration of MTZ for bacterial infection is administered thrice daily for seven days.

Mechanism of action: MTZ is among the nitroimidazole drugs that can diffuse into the microorganisms and inhibit protein synthesis (nucleic acid synthesis). It interacts with DNA to produce nitroso radicals and hydroxylamine groups, causing the microbial cells' DNA to lose its

helical forms. Therefore, it causes cell death in susceptible organisms (Arslan et al., 2017). MTZ undergoes reduction, during anaerobic bacteria and protozoans treatment (Suhail et al., 2021).

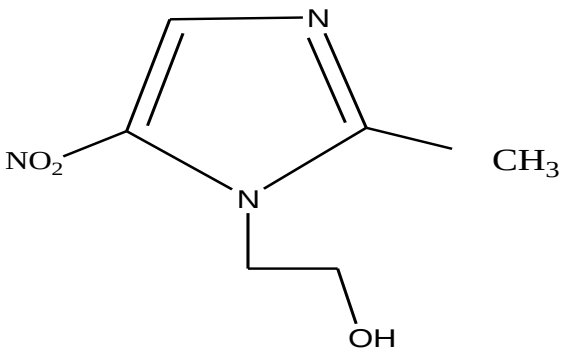

Figure 2. 11 MTZ structure [2-(2-methyl-5-nitroimidazol-1-yl) ethanol]. Reprinted from Katual, 2017.

Pharmacokinetics: For orally administered MTZ, nearly 80% bioavailable through the GI tract, and high blood plasma concentrations occur after 1-2 hours. Nearly 20% of the delivered dosage may form a plasma protein-bound state (Noor et al., 2018). It distributes well in tissues, cerebrospinal fluid, and breast milk. Approximately 60% of MTZ is metabolized through oxidation to MTZ, a major metabolite, and carboxylic acid derivative, all displaying antibacterial and antiprotozoal activities (Noor et al., 2018). About 77% of MTZ and hydroxyl MTZ are excreted through the urine (kidneys) and about 14% through the feces (Mimura et al., 2020). In healthy adults and children, the half-life of MTZ in cerebral fluid is 8 hours and approximately 24 hours, respectively.

Adverse effects: Adverse side effects of intravenous delivery are usually related to thrombophlebitis and rarely hypersensitivity reactions (e.g., fever, flushing), metallic after taste, stomach upset, dark urine, or damage of peripheral nerves (paraesthesia). Topically administered MTZ side effects commonly include local redness, dryness and skin irritation, temporary hearing loss, and possibly human carcinogenicity. Drinking alcohol while taking MTZ causes disulfiram-like side reactions leading to skin redness, nausea, vomiting, abnormal rapid heart rate, dizziness, and shortness of breath (Hernández et al., 2019).

CHAPTER 3: MATERIALS AND METHODS

The materials, methods, and characterization used in this study are presented in this chapter.

3.1. Materials

CS (having density 0.15 - 0.3 g/mL, deacetylated to ≥ 75%, viscosity > 200 centipoises, and medium molecular mass) and PVP-30, having molecular mass of 40,000 g/mol were purchased from Sisco Research Laboratory (SRL) Pvt. Ltd. India. Food grade SALG (purity, 91% and), calcium chloride ($CaCl_2$, 99%, AR), hydrochloric acid (HCl, 37 %, AR), 25% (v/v) glutaraldehyde aqueous solution, sodium hydroxide (NaOH, 99%, AR), anhydrous acetic acid ($C_2H_4CO_2$, purity 99.75%, AR), and ethanol (C_2H_6O, 97.6%, AR), and were all bought from Loba Chemie Pvt. Ltd in India. Sodium chloride (NaCl, 99%, AR), potassium chloride (KCl, 99%, AR), dibasic sodium phosphate (Na_2HPO_4, 99%, AR), potassium phosphate monobasic (KH_2PO_4, 99%, AR), and Mueller Hinton Agar (MHA) [OXOID CM0337] were acquired from Sigma-Aldrich. Pristine AMX and MTZ model drugs were donated by Ethiopian Pharmaceuticals Manufacturing Sh Co. (EPHARM) Ethiopia. During the course of the study, the chemicals were utilized as obtained, along with double distilled water (DDW). Different capacity borosilicate volumetric flasks, beakers, measuring cylinders, micropipettes, magnetic stirrers, analytical balance, desiccator, Petri dishes, thermometers, rulers, Whatman quantitative filter paper (ashless and grade 42), and double-function thermostatic shaking incubator were used during the experiments.

3.2. Instrumentation

Instruments used for characterization included FTIR spectrometer (Alpha-T, Bruker, Germany), X-ray diffraction (XRD-7000, SHIMADZU, Japan), thermogravimetric analyzer (TGA, BJ HENVEN, ATAT2012, China), field emission scanning electron microscopy (ApreoS, Thermo Fisher Scientific, Singapore), and UV-visible spectrophotometer (Maalab Scientific Equipment Ltd., India). Section 3.10 explains the details of these instruments and how these techniques were used.

3.3. Synthesis of crosslinked CS/PVP hydrogels

The chemical crosslinking method was utilized for the synthesis of CS/PVP hydrogels as previously described (Gull et al., 2020a). A precisely weighed amount of CS (Table 3.1) was added to 200 mL of DDW, along with 2 drops of a 2% acetic acid aqueous solution, and stirred with an overhead stirrer at 50 °C and 500 rpm until a clear solution was formed. The required

amount of PVP (Table 3.1), was dissolved in 200 mL of DDW separately and added to the CS solution. The solution mixture was stirred for 2 hours using an overhead stirrer at 50 °C and 500 revolutions per minute (rpm). 200 µL of glutaraldehyde solution in water (25%, v/v) was added while stirring at 50 °C and 50 rpm until a crosslinked structure (gel) formed. The working mass was transferred to glass Petri-dishes and dried at 40 °C in a shaking incubator (LFZ-TSI series, China). Finally, the prepared hydrogels were placed in a desiccator to prevent moisture adsorption and to preserve the hydrogels for subsequent study. The schematic of the CS/PVP hydrogel synthesis experimental setup is shown in figure 3.1.

Table 3. 1: Composition of CS/PVP hydrogels

Hydrogel system code	**CS/PVP Wt. % ratio**	Glutaraldehyde **Volume**
H1	70/30	200 µL
H2	60/40	200 µL
H3	50/50	200 µL
H4	40/60	200 µL
H5	30/70	200 µL

To evaluate the effect of crosslinker concentration, the hydrogel formulation determined optimal (H2) depending on its degree of swelling in simulated physiological solutions was utilized by varying the volume of glutaraldehyde (Table 3.2) using the procedure mentioned above.

Table 3. 2: Hydrogel H2 modified by varying amounts of glutaraldehyde

Hydrogel system code	**CS/PVP Wt. % ratio (Total polymer mass 8 g)**	**Glutaraldehyde Volume**
H2-G1	60/40	200 µL
H2-G2	60/40	400 µL
H2-G3	60/40	600 µL
H2-G4	60/40	800 µL
H2-G5	60/40	1000 µL

3.4. In situ, synthesis of AMX loaded CS/PVP hydrogels

AMX (200 mg) was incorporated into the hydrogel H2-G3 (60/40 wt. % and 600 µL of the crosslinker), which was identified as the optimal composition for drug loading based on swelling behavior in the simulated physiological solutions. 4.8 g of CS was transferred to 200 mL of DDW containing 2 drops of glacial acetic acid solution (2%) and stirred with an overheaded stirrer at 50 °C and 500 revolution per minute until a clear solution was formed. 3.2 g of PVP was dissolved separately in 200 mL of DDW and added to the CS solution. The solution mixture was blended using a motor stirrer at 500 rpm for 2 h at 50 °C. Then, AMX (200 mg) dissolved in 100 mL of a

dilute aqueous solution of hydrochloric acid (0.1M) and was added slowly to the polymer blend and stirred further for 1 h. Following that, the optimal amount of 25% (v/v) glutaraldehyde (600 µL) was added dropwise to the reaction mixture and stirred further for 4 h at the same temperature (50 ℃) until gel was formed. This reaction mass was then poured into Petri dishes and dried at 40 °C in a thermostatic shaking incubator (LFZ-TSI series, China). The dried drug-loaded hydrogel film (AMX-H2-G3) was preserved in a desiccator to avoid moisture adsorption for subsequent study.

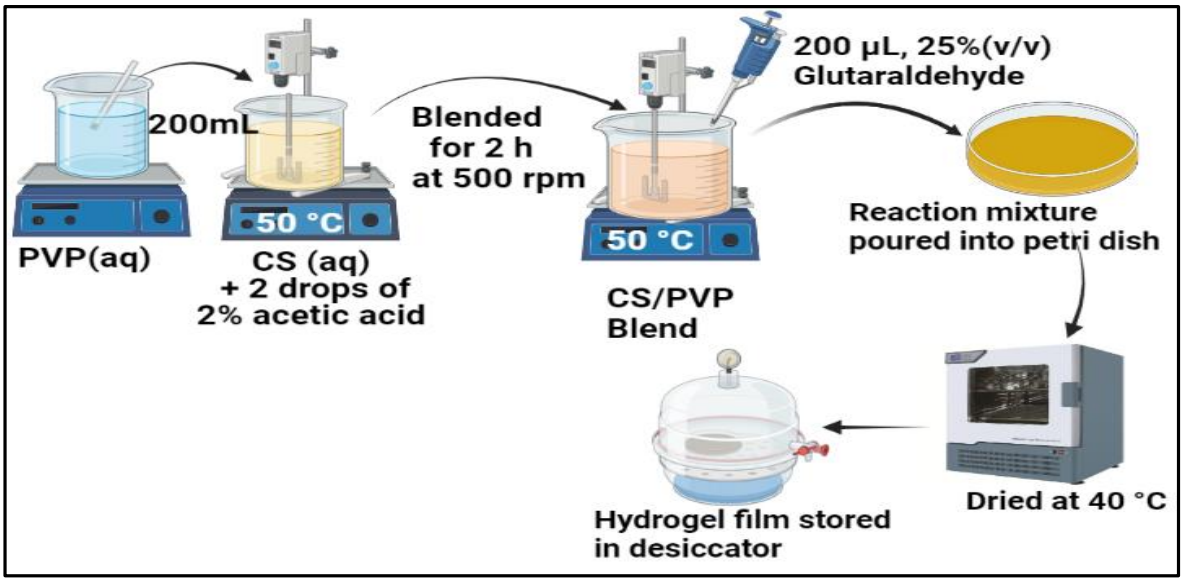

Figure 3. 1 Schematic of the experimental setup for CS/PVP hydrogel synthesis.

3.5. In situ, synthesis of MTZ loaded CS/PVP hydrogels

The hydrogel H2-G3, which was shown to have an optimum degree of swelling in the simulated physiological fluids, was loaded with 200 mg of MTZ. 4.8 g of CS was added to 200 mL of DDW containing 2 drops of 2% glacial acetic acid solution and stirred with an overhead stirrer at 50 °C and 500 revolutions per minute until a clear solution was formed. 3.2 g of PVP was dissolved separately in 200 mL of DDW and added to the CS solution. Then, the solutions were combined and blended using an overhead stirrer at 500 revolution per minute for 2 h at 50 °C. MTZ powder (200 mg) was dissolved in 100 mL of dilute aqueous hydrochloric acid (0.1M) added slowly to the polymer blend, and stirred further for 1 h. Following that, the optimal amount of 25% (v/v) glutaraldehyde (600 µL) was added dropwise to the reaction mixture and stirred for about 10 minutes at the same temperature (50 ℃) until the gel was formed. This reaction mass was then poured into Petri dishes and dried at 40 °C in a shaking incubator (LFZ-TSI series, China). The dried drug-loaded hydrogel film (MTZ-H2-G3) was preserved in a desiccator to avoid water adsorption for subsequent study.

3.6. Synthesis of SALG/CS hydrogels

The physical iono-tropic interaction method was utilized for the synthesis of SALG/CS hydrogels as previously described (T.Wu et al., 2020). A precisely weighed amount of CS (Table 3.3) was added to 200 mL of DDW, along with 2 drops of a 2% acetic acid aqueous solution, and stirred with an overhead stirrer at 50 °C and 500 rpm until a clear solution was formed. The required amount of SALG (Table 3.3) was dissolved in 200 mL DDW separately and transferred to the CS solution. After that, the polymer mixture was mixed at room temperature for 1.5 hours at 700 rpm using an overhead stirrer. The pH of the reaction mass was adjusted to 5.0 using a 1.0 M aqueous solution of sodium hydroxide (NaOH) while stirring. This polymer blend was added into 200 mL of 2% (w/v) aqueous solution of calcium chloride ($CaCl_2$) at a rate of 60 drops per minute while stirring at 700 rpm. After standing for 4 hours, the reaction mass was rinsed with DDW, filtered, and immersed into enough 25%(w/v) glutaraldehyde for 48 hours. This reaction mixture was then poured into Petri dishes and dried at 40 °C in a shaking incubator (LFZ-TSI series, China). The dried hydrogel beads were preserved in a desiccator to avoid moisture adsorption for subsequent study. The schematic of SALG/CS hydrogel synthesis experimental setup is shown in Figure 3.2.

Table 3. 3: Composition of SALG/CS hydrogel beads

Hydrogel system code	SALG/CS Wt. % ratio (Total polymer mass 8 g)	$CaCl_2$ concentration
B1	75/25	2%
B2	67/33	2%
B3	50/50	2%
B4	33/67	2%
B5	25/75	2%

To evaluate the influence of the crosslinking agent content, the hydrogel formulation determined optimum (B1) depending on its degree of swelling in simulated physiological fluids was used by varying $CaCl_2$ content (Table 3-4) employing the procedure mentioned above.

Table 3. 4: Hydrogel B1 modified by varying the concentration of $CaCl_2$

Hydrogel system code	SALG/CS Wt. % ratio (Total polymer mass 8 g)	$CaCl_2$ concentration
B1-C1	75/25	2%
B1-C2	75/25	4%
B1-C3	75/25	6%
B1-C4	75/25	8%
B1-C5	75/25	10%

3.7. Synthesis of AMX loaded SALG/CS hydrogels

The hydrogel formulation B1-C1 (SALG/CS, 75/25 wt.% with 2% $CaCl_2$ solution), which was shown to have an optimal swelling capacity, was loaded with 200 mg of AMX. 200 mL aqueous solution containing 2 drops of 2% glacial acetic acid was used to dissolve 2 g of CS while stirring with an overhead mixer at ambient temperature till a clear solution was attained. AMX (200 mg) dissolved in 100 mL of diluted hydrochloric acid (0.1M) aqueous solution was slowly mixed with the clear solution CS (2g/100 mL) using an overhead mixer at ambient temperature. Then, a 200 mL aqueous solution of the appropriate amount of SALG (6 g of SALG in 200 mL DDW) was mixed with the CS-drug solution mixture under stirring with an overhead stirrer at 700 rpm. Then, the same steps were repeated as for the preparation of SALG/CS hydrogel beads.

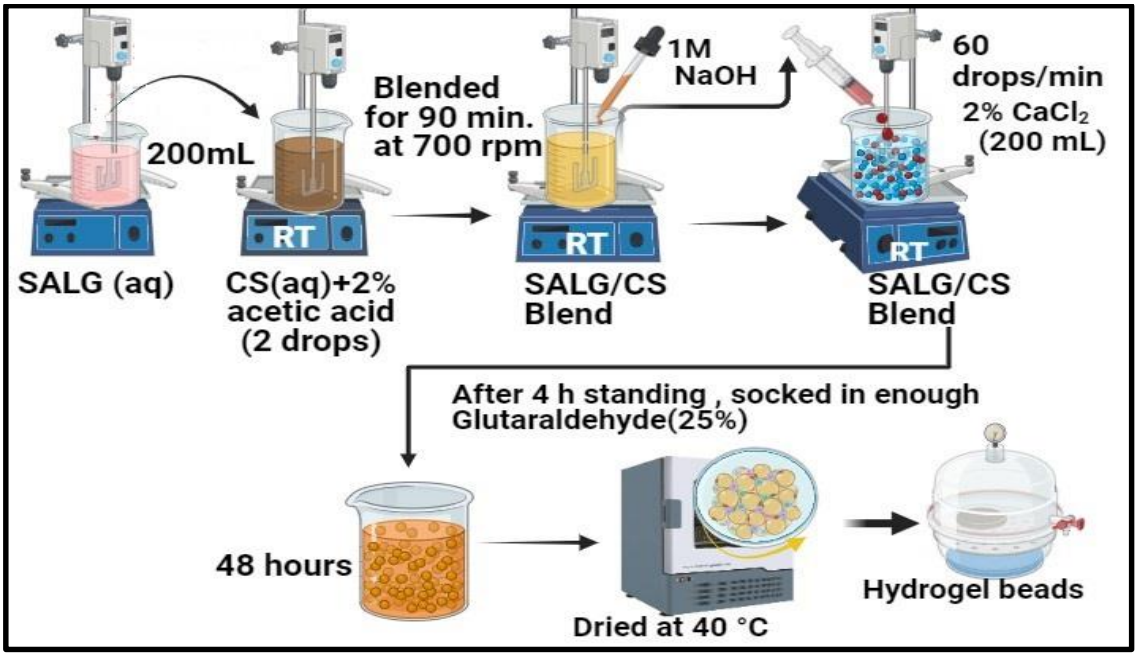

Figure 3. 2 Schematic of the experimental setup for SALG/CS hydrogel synthesis.

3.8. Synthesis of MTZ-loaded SALG/CS hydrogels

The hydrogel formulation B1-C1 (SALG/CS, 75/25 wt.% with 2% $CaCl_2$ solution), which was shown to have an optimal swelling capacity, was loaded with 200 mg of MTZ. 200 mL aqueous solution containing 2 drops of 2% glacial acetic acid was used to dissolve 2 g of CS while stirring with an overhead mixer at ambient temperature till a clear solution was obtained. MTZ (200 mg) dissolved in 100 mL of diluted hydrochloric acid (0.1M) aqueous solution was slowly mixed with the clear solution CS (2g/100 mL) using an overhead stirrer at room temperature. Then, a 200 mL aqueous solution of the appropriate amount of SALG (6 g of SALG in 200 mL DDW) was mixed with the CS-drug solution mixture under stirring with an overhead stirrer at 700 rpm. Then, the same steps were repeated as for the preparation of SALG/CS hydrogel beads.

3.9.Preparation of simulated physiological fluids

The simulated physiological fluids were made using a method previously reported (Marques et al., 2011) comprising gastric fluid (SGF), intestinal fluid (SIF), and colon fluid (SCF). SGF was made by combining 2 g of NaCl and 7 mL of 0.2 N HCl in 1 L DDW. The pH of the solution was brought to 1.2 ± 0.1. 6.8 g of KH_2PO_4 and 0.94 g of NaOH were combined and dissolved 1 L DDW to make SIF, and the pH was then adjusted to 6.8. The SCF was produced by combining 8 g of NaCl, 0.2 g of KCl, 1.15 g of Na_2HPO_4, and 0.2 g of KH_2PO_4 in 1L DDW. The pH was subsequently adjusted to 7.4 using 1 M HCl/1M NaOH (Lehner et al., 2021).

3.10. Characterization

3.10.1. Swelling behavior

To evaluate the influence of polymer composition and amount of crosslinking agent on the stimuli-sensitivity (pH-sensitivity) of the synthesized hydrogels, the swelling behavior was performed gravimetrically by submerging pre-weighed (Wi) hydrogels in 50 mL of each of SGF, SIF, and SCF, incubating at 37.2 °C under stirring at 100 revolutions min^{-1} in triplicates (Kiti & Suwantong, 2020). After time intervals of 10, 30, 60, 90, 120, 150, 180, 210, and 240 minutes, the hydrogels were taken out of the simulated physiological fluids, carefully cleaned by filter papers, and weighed (Wt). The hydrogel sample's constant mass was attained by repeating this operation several times. Equation (3.1) was used to compute the swelling ratio.

$$\text{Swelling ratio (\%)} = \frac{Wt - Wi}{Wi} \times 100 \quad (3.1)$$

3.10.2. Porosity

Porosity is an essential parameter of hydrogels in biomedical and pharmaceutical fields as controlled drug release applications. It is associated with the swelling capacity of hydrogels that allow the diffusion of physiological fluids in the network chain and subsequently enhance the release of drugs through the hydrogel matrix. To evaluate the influence of the polymer ratio and the concentration of crosslinking agent on the synthesized hydrogels porosity, ethanol solvent replacement method previously reported was used (Garakani et al., 2020). The porosity of the hydrogels was measured using 25 mL sealed beaker. First, the empty sealed beakers weighed (W_1). Then, 20 mL of absolute ethanol (inert solvent) and pre-weighed hydrogel sample (W_h) were added to the beaker, and the total weight was obtained (W_2). The hydrogel samples were taken out after 24 hours, and the remaining portions were weighed (W3). The pore volume of the hydrogels can be determined by measuring the ethanol-filled hydrogel pores. Equation (3. 2),

where ρe represents the density of the ethanol (g/mL), was used to determine the porosity of the hydrogels.

$$\text{Porosity (\%)} = \frac{W2 - W3 - Wh}{W1 - W3 + 20\rho e} \times 100 \quad (3.2)$$

3.10.3. Functional group analysis

FTIR measurements were utilized to investigate the presence of polymer-polymer and polymer-drug interactions, as well as to identify the functional groups of the polymer components in crosslinked hydrogel systems. An FTIR spectrometer (Alpha-T, Bruker, Germany) was used to obtain FTIR spectra of the polymers (CS, PVP, and SALG), the drugs (AMX and MTZ), the synthesised unloaded hydrogels, and drug-loaded hydrogels. The samples were ground with KBr and pressed into pellets. The analysis was carried out at a scanning rate of 50 scans per minute in the wavelength range of 4000-500 cm^{-1} with a resolution of 4 cm^{-1}.

3.10.4. Phase structure

X-ray diffraction (XRD) is a worthwhile characterization technique to describe changes in the crystalline structure of hydrogels during their synthesis process due to polymer interactions. XRD analysis was used to identify the phase nature of the polymers, pristine drugs, hydrogels, and drug-loaded hydrogels. The diffractograms were obtained using an XRD instrument (XRD-7000, SHIMADZU, Japan). The XRD measurements were performed by using CuKα (1.5406° A) radiation source, in the 2θ range of 5°- 40° at a scanning rate of 0.02 s^{-1}, 40 kV applied voltage and current of 30 mA at room temperature.

3.10.5. Thermal stability

The thermal stability of the polymers (CS, SALG, and PVP), drugs (AMX and MTZ), and synthesized hydrogels (unloaded and drug-loaded) was investigated using a thermogravimetric analysis (TGA) instrument (BJ HENVEN, ATAT2012, China), at a heating speed of 15 °$Cmin^{-1}$ in a temperature range of 25-700 °C and a nitrogen flow rate of 20 mL min^{-1}.

3.10.6. Gel fraction

Gel fraction, which indicates the insoluble (crosslinked) component of the polymer chains, is an important measure for characterizing hydrogels utilized for controlled drug release applications. When a hydrogel is submerged in physiological fluids or water, its non-crosslinked component dissolves, resulting in weight loss. The mass ratio of the dried hydrogel after and before submersion is referred to as gel fraction or crosslinking density, and it is inversely proportional

to the stiffness of a crosslinked polymer (Gower & Shanks, 2004; Mondal et al., 2018). The gel fraction of the synthesized hydrogels was investigated by immersing a determined weight (Wi) of the sample in DDW for two days (48 hours) at ambient temperature to release out non-crosslinked polymer parts (Ngwabebhoh et al., 2021). The separated hydrogel parts were filtered, gently rinsed with DDW, and dried to fixed weight (Wf) at 60 °C. Eq. (3.3) was used to determine the percentage of gel fraction.

$$\text{Gel fraction (\%)} = \frac{Wf}{Wi} \times 100 \quad (3.3)$$

3.10.7. In vitro biodegradation assay

The in vitro biodegradation was performed to evaluate the degradation of hydrogels (stability) in simulated physiological fluids. The biodegradation of the unloaded hydrogels was examined gravimetrically by immersing the hydrogels in the prepared SCF (pH 7.4) for 24 hours in order to totally swell and wieghed (Wi) and incubating at 37.2 °C under shaking at 80 rpm. After time gaps of 2-3 days for 30 days, the hydrogels were taken out from the simulated physiological fluid (SCF), which was then properly cleaned using ashless Whatman®filter paper (Grade II) to eliminate the surface water, and weighed (W_t). Fresh SCF was used to replace the immersion solution, which was then incubated at the same temperature. Eq. (3.4) was used to compute the mass loss percentage (Garakani et al., 2020).

$$\text{Weight loss (\%)} = \frac{Wi - Wt}{Wi} \times 100 \quad (3.4)$$

3.10.8. Morphology

Field emission scanning electron microscopy (FESEM) micrographs were acquired to analyze the morphology of the unloaded and drug-loaded hydrogels in terms of pore structure distribution and incorporation using an electron-scanning microscope (ApreoS, Thermo Fisher Scientific, Singapore). The hydrogels were sputter-coated with a tiny layer of gold before imaging.

3.10.9. Drug release profile

The AMX and MTZ loaded hydrogels were tested for drug release in vitro by immersing them in 50 mL of each of SGF, SIF, and SCF with pH values of 1.2, 6.8, and 7.4, respectively. The simulated fluid containing the hydrogels was incubated at 37.2 °C in a thermostatic shaking incubator (LFZ-TSI series, China) with continual shaking at 100 rpm. At defined time intervals of 1, 2, 3, 4, 5, 6, 7, 8, 9, 10, 11, 12, 13, 14, 15, 24, and 25 hours, the supernatant from each incubated sample was extracted. Then the absorbance of each drug was obtained using a UV-visible spectrophotometer (Maalab Scientific Equipment Ltd., India) at a wavelength of 272 nm

for AMX while MTZ absorbance was measured at a wavelength of 322 nm. Fresh simulated physiological fluids were added to each sample container to keep the volume consistent. The concentration of the released drug was measured in triplicate using a calibration curve constructed from standard solutions of each pure drug (0.5, 2, 4, 6, 8, 10, 12 g/mL). Eq. (3.5) was employed to determine the cumulative percentage concentration of the released drug, Wi represents the initial amount of a drug incorporated into the hydrogel, and Ct and Ct-1 represent the concentration of drug released at time t and t-1 (Su et al., 2020).

$$\text{Cumulative drug release (\%)} = \frac{\mathbf{50Ct + \sum 5Ct_{\underline{1}}}}{\mathbf{Wi}} \text{ x } 100 \quad (3.5)$$

3.10.10. Drug release kinetics

By incorporating the release data into the zero order, first order, Higuchi, and Korsmeyer-Peppas kinetic models, the kinetics and mechanisms of the in vitro drug release AMX and MTZ were established.

Zero-order model: The model addresses a system involving slow drug release with constant drug concentration and is expressed by the equation (Jain & Jain, 2016).

$$Qt = Q_0 + k_0t \quad (3.6)$$

Qt denotes the released drug concentration at time t, Q_o the amount of drug loaded into the hydrogel, and k_o the zero order constant.

First order Model: This model addresses the release kinetics of drug release that depends on the amounts of the drug initially loaded to the hydrogel and expressed by Eq. 3.7 (Nematollahi et al., 2021).

$$\ln Qt = \ln Q_0 + k_0t \quad (3.7)$$

Qt denotes the released drug concentration at time t, Q_o the amount of drug loaded into the hydrogel, and K_o the first order constant.

Higuchi model: Addresses the drug release rate from a polymer matrix, where the loading of the drug exceeds its solubility in the matrix into a surrounding fluid and is expressed by Eq. 3.8 (Ata et al., 2020).

$$Qt = k_Ht^{1/2} \quad (3.8)$$

Qt denotes the drug's concentration released at time t, and K_H denotes Higuchi constant.

Korsmeyer-Peppas model: Addresses the release kinetics of a drug from hydrogels when there is no known mechanism or when more than a drug release mechanism is involved (Korsmeyer et al., 1983)**.** Eq. 3.9 expresses Korsmeyer-Peppas model.

$$\frac{Mt}{M\infty} = kt^n \quad (3.9)$$

where, Mt/M∞ denotes the fraction of the released drug at time t, k is the Korsmeyer-Peppas constant, and n is the release exponent. When the value of $n \leq 0.45$, Fickian diffusion is the release mechanism and the release rate depends on solvent mobility. When $0.45 < n < 0.89$, the polymer relaxing (swelling) process or a non-Fickian (anomalous) mechanism controls the release rate (S. Kumar et al., 2021). To choose the most appropriate mathematical model that matches the drug's release profile, the most significant coefficient of correlation (R^2) was considered.

3.10.11. Antimicrobial efficacy test

The antimicrobial efficacy of the drug-loaded hydrogels was assessed utilizing the Kirby-Bauer disc diffusion technique (Patil, 2012) at Adama Public Health Research and Referral Laboratory Center as well as at Adama Science and Technology University, applied biology microbiological Lab (Ethiopia). The antibacterial activity of AMX-loaded hydrogels was tested against *Streptococcus pyogenes* (ATCC19615) and *Escherichia coli* (ATCC25922). At the same time, the antibacterial activity of and MTZ-loaded hydrogels were tested against *Staphylococcus aureus* (ATCC25923) and *Escherichia coli* (ATCC25922). The unloaded hydrogels (H2-G3 and B1-C1) were used as the negative control, and the pure form of AMX and MTZ were used as positive controls. The antibacterial activity test was done in a medium of solid agar in Petri dish according to the Kirby-Bauer disk diffusion susceptibility test protocol. First, the nutrient (agar media) was poured into the Petri-dishes. A 100 µL of each bacterial stock with an estimated $1x10^8$ CFU/mL concentration was uniformly dispersed on the Petri-dishes containing agar media. Then, the drug-loaded hydrogels of appropriate sizes were UV sterilized for two hours and placed on the agar plates' surface. 20 µL control samples of AMX and MTZ, each comprising 1 mg/mL of the drug stock solution, were poured onto a 6 mm-diameter filter paper that had undergone UV sterilization. The dishes were incubated upside down at 37°C for 24 hours. The inhibition zone was assessed by determining the diameter of the zone of inhibition. The measurements were done in triplicate for each bacterial strain.

3.11. Statistical analysis

The statistical data analysis and figures were done using Origin 2021b version software (Origin Lab Corporation, USA). The experiments were performed in triplicate, and the data are reported as means ± standard deviation (SD). Correlations between different parameters were determined using the Pearson correlation coefficient at $p < 0.05$ significance level.

CHAPTER 4: RESULTS AND DISCUSSION

4.1. Synthesis of CS/PVP hydrogels

The chemical method of polymer crosslinking with glutaraldehyde as a crosslinker was used to synthesize the CS/PVP hydrogels effectively. The CS/PVP polymer blend prepared during the preliminary experiment to determine the starting concentration of glutaraldehyde was highly viscous and fragile with 150 µL of glutaraldehyde due to the CS chains were insufficiently crosslinked. A stable CS/PVP hydrogel film was produced with 200 µL of glutaraldehyde. The images of the synthesized hydrogels H1 to H5 (Table 3.1) are illustrated in Figure 4.1. The illustration shows that as the PVP amount increased, the thickness of the hydrogels reduced and turned light brown.

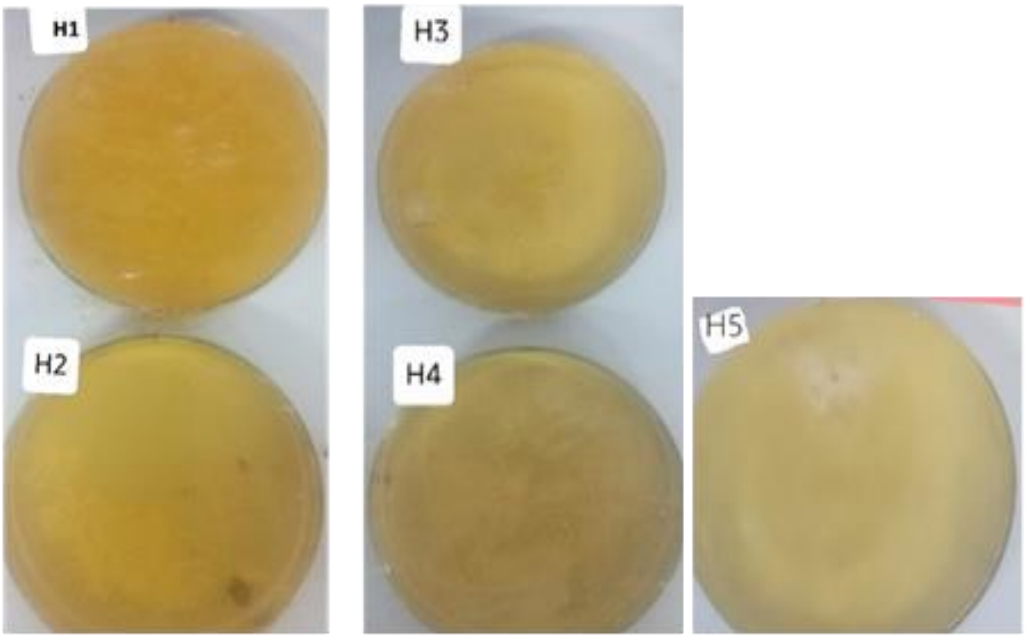

Figure 4. 1 Images of hydrogel H1 to H5 (CS/PV, 70/30, 60/40, 50/50, 40/60 and 30/70 wt.%).

Figure 4.2 illustrates the crosslinking mechanisms that entail the covalent binding and intermolecular interactions among the polymer constituents and the drugs. In the crosslinked hydrogels, the NH_2 and OH functional ends of the CS are crosslinked by glutaraldehyde. PVP, a water-loving polymer, is linked to the hydrogel system by inter-molecular interactions for example hydrogen bonding. Glutaraldehyde participate in the crosslinking processes with the NH_2 and OH ends of the CS chains through Schiff base or aldol reactions (S. Sharma et al., 2020), and the ring structure PVP chains enter into the CS networks through physical entanglement via physical interactions such as electrostatic interactions of the carbonyl groups of PVP with the NH_2 and OH ends of the CS chains (El Achaby et al., 2014). The inter-crosslinking of the CS

chains, as well as the physically entangled PVP segments within the CS networks, result in dense semi-interpenetrating polymer networks (semi-IPNs) (Reddy et al., 2012).

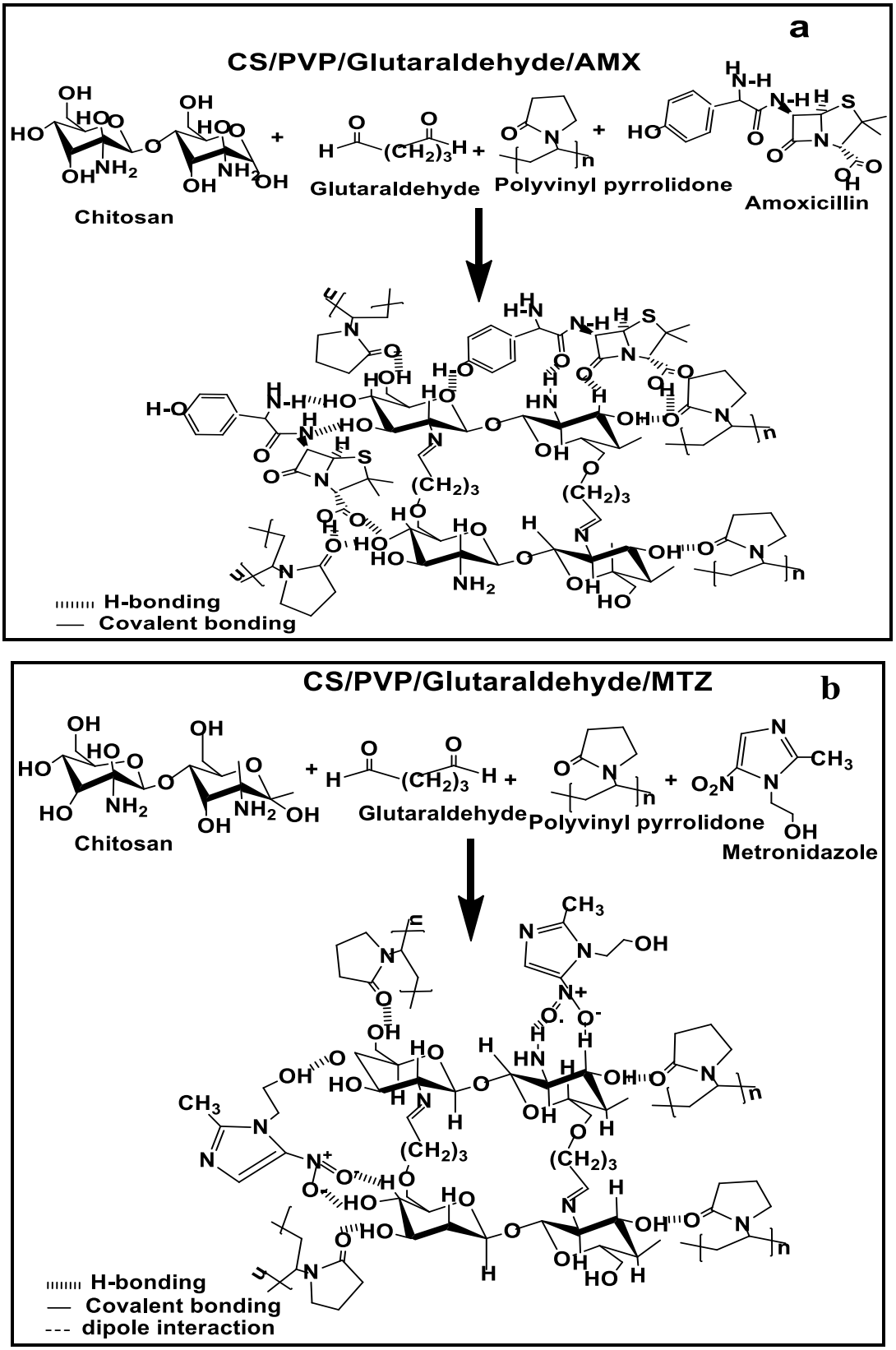

Figure 4. 2 Schematic showing the interaction of (a) CS, PVP, and AMX (b) CS, PVP, and MTZ using glutaraldehyde as the crosslinker.

In the polymer matrix interactions, due to the crosslinked hydrogel network's random arrangements, the ring-like structures of PVP form void spaces inside the hydrogel systems. Likewise, AMX and MTZ, both of which are hydrophilic, are integrated into the semi-interpenetrating polymer networks via various intermolecular interactions such as dipole-dipole interactions and hydrogen bonding among functional groups of the polymer components and the drug. The schematic showing interaction mechanisms of CS, PVP, AMX, and MTZ are presented in Figure 4.2 as previously reported in the literature (Nematollahi et al., 2021).

4. 2. Synthesis of double crosslinked SALG/CS hydrogels

The SALG/CS double crosslinked hydrogels with varied polymer compositions were effectively synthesized using $CaCl_2$ and glutaraldehyde as crosslinking agents. The images of the hydrogel samples are shown in Figure 4.3, and the possible polymer-polymer and polymer-drug crosslinking mechanisms are shown in Figure 4.4 (a, b, c). As discussed above, the NH_2 and OH ends of CS chains are interconnected by glutaraldehyde crosslinker via covalent bonds (Garakani et al., 2020).

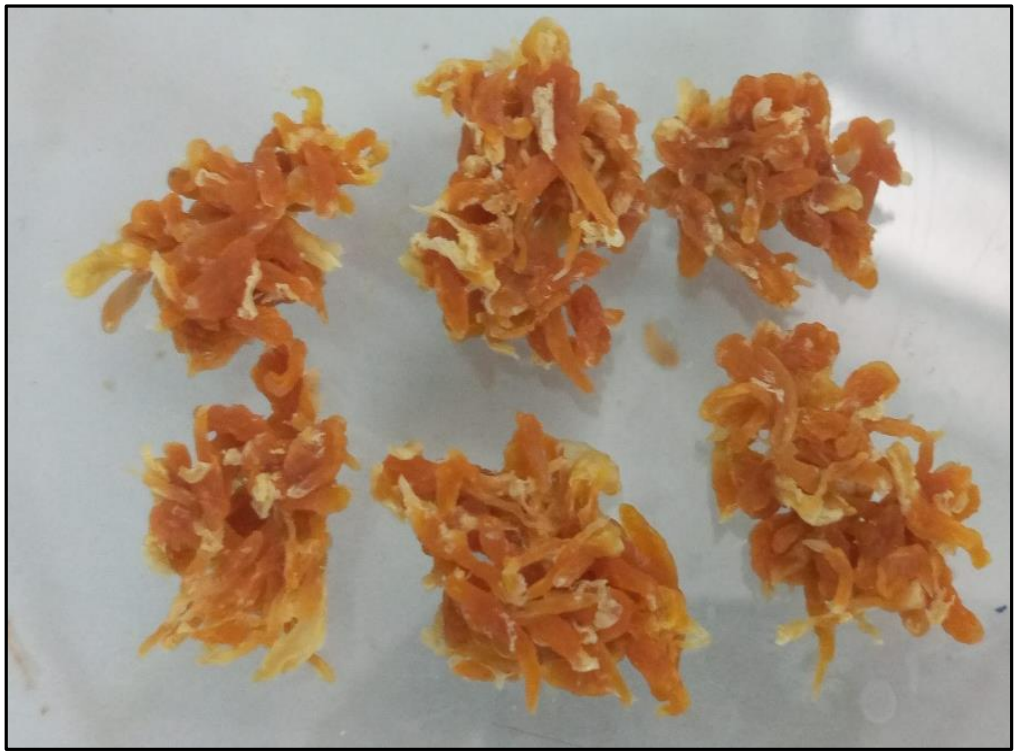

Figure 4. 3 Images of SALG/CS hydrogel B1 beads (SALG, 75/25 wt.%).

The SALG chains are interconnected through an ionic-crosslinking between the bivalent cation (Ca^{2+} ions) and the anionic carbonyl ends of SALG (COO-), resulting in "egg-box" copolymer chains substituting the Na^+ ions (Khajuria et al., 2020). The anionic carbonyl (COO-) ends of SALG also interacts with the cationic CS chains (NH_3^+) via electrostatic interactions (Baysal et

al., 2013). The established interchain connections among the polymers resulted in compacted bilayer interpenetrated network hydrogel beads (Figure 4.4a).

Likewise, the hydrophilic drugs AMX and MTZ are integrated into the interpenetrated channels of the hydrogels via various interactions, such as dipole-dipole and hydrogen bonding that occur among the drugs' polar functional groups and the polymer components, as shown in (Figure 4.4b) and (Figure 4.4c) respectively. In this study, the possible polymer-polymer and polymer-drug interactions for the CS/PVP and SALG/CS hydrogel systems and the drugs being studied (AMX and MTZ) were validated by FTIR characterizations.

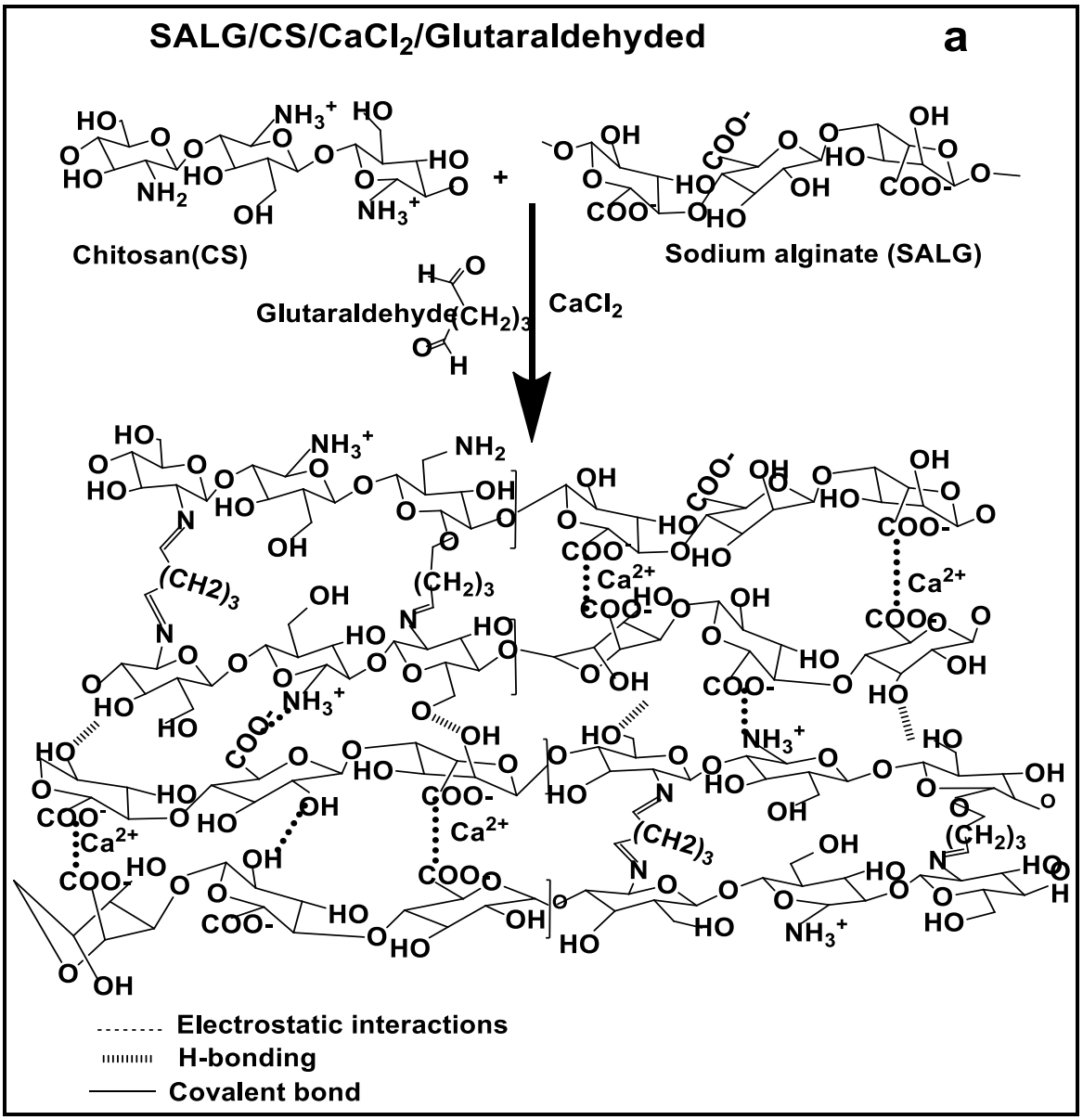

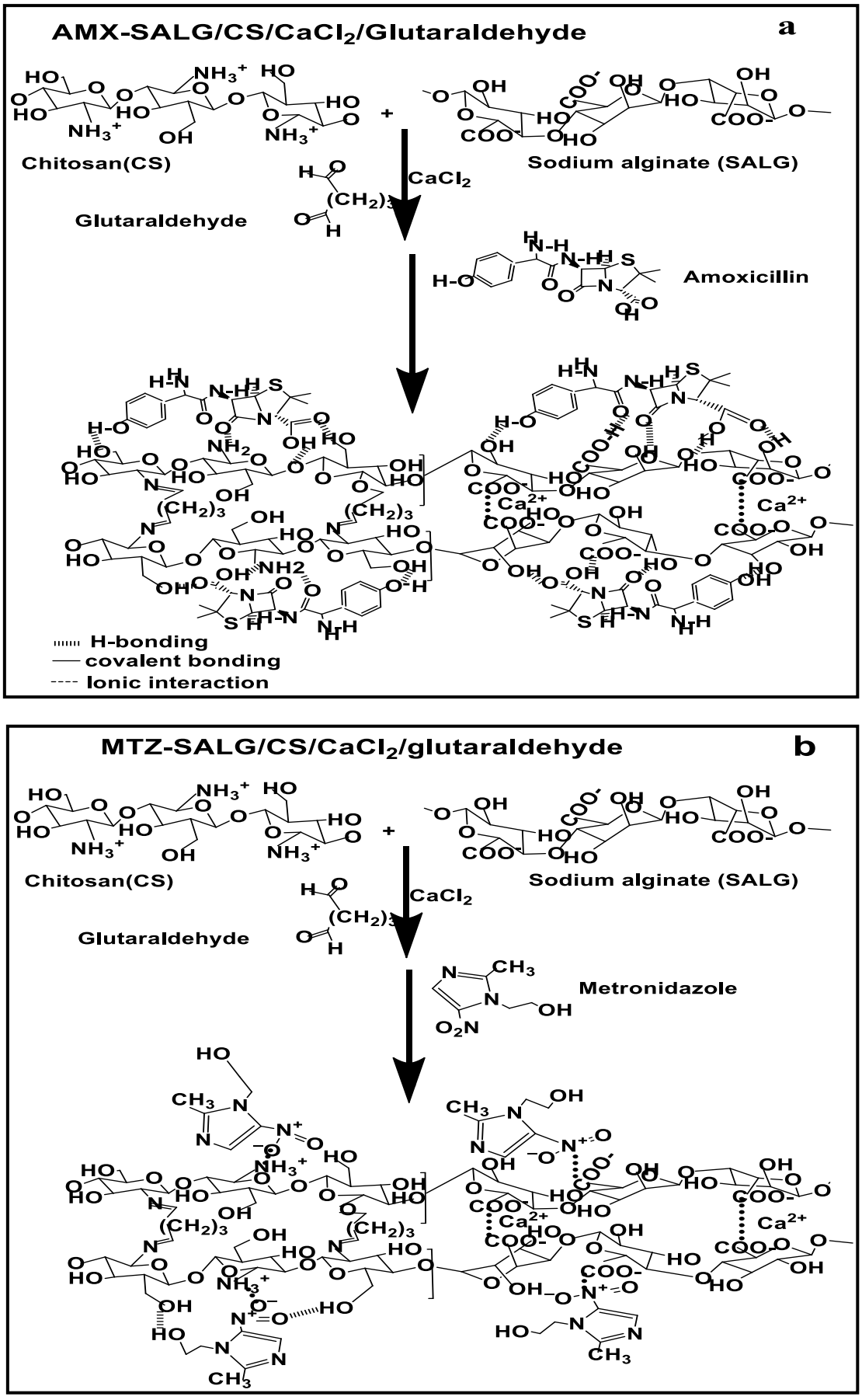

Figure 4. 4 Schematic showing the interaction between (a) CS and SALG (b) CS, SALG, and AMX, (c) CS, SALG, and MTZ using $CaCl_2$ and glutaraldehyde crosslinkers.

4.3. Swelling behavior

Swelling prosperity is one of the essential parameters of crosslinked hydrogels for usage in biological applications. The swelling of hydrogels owing to the absorption of physiological fluids helps the penetration of a drug into the hydrogel scaffolds, causing the diffusion of the drug providing the controlled drug release properties of the hydrogels. In the current study, the swelling behavior of the hydrogels was carried out to investigate the impacts of the polymer weight ratio on the swelling ratio in different simulated physiological fluids (pH 1.2, 6.8, and 7.4). Figure 4.5 depicts the % swelling ratios of the hydrogels H1, H2, H3, H4, and H5 in SGF, SIF, and SCF. It is observed that in each physiological fluid, the degree of swelling of CS/PVP hydrogels decrease with increasing CS content and increases with increase PVP content. The hydrogel H5 (CS/PVP weight composition of 30/70) displays the maximum swelling ratio in all physiological fluids in comparison to other CS/PVP hydrogels with maximum values of approximately 535.47%, 522.22%, and 488.19% in SGF, SIF, and SCF respectively after 240 minutes, and the lowest swelling ratio was observed for system H1 (CS/PVP weight ratio of 70/30) with maximum values of approximately 475.55%, 452.98%, and 368.82 % in SGF, SIF and SCF respectively in 240 minutes (Appendix I, a-c). The increased swelling ratios of the hydrogels as PVP concentration increases are connected with PVP's more hydrophilic character than CS (Garakani et al., 2020). In the CS/PVP hydrogel network, glutaraldehyde crosslinks the amino groups of CS through hydrogen bonding, thereby decreasing the hydrophilic functional groups of CS. PVP is interlaced to the CS network by electrostatic interactions forming semi-interpenetrating network structures (semi-IPNs). During the CS/PVP crosslinking, the ring chain of PVP forms void spaces inside the hydrogel network owing to the irregular arrangement of the polymer matrix. As a result, the physiological fluids diffuse into the matrix, occupying the open empty spaces and swelling the hydrogel films.

The observed swelling behaviour of the hydrogels during the beginning stages of immersing in each physiological fluids is caused by the formations of hydrogen bonding between water molecules and the hydrophilic groups of the polymer chains. Following this, more water tries to cluster about this bound water, which causes more significant swelling. Finally, any additional fluid enters the gel network freely. The Pearson correlation analysis shows a strong positive correlation between PVP content and the swelling ratios in SGF ($r^2 = 0.993$), SIF ($r^2 = 0.993$), and SCF ($r^2 = 0.997$), and the reverse correlation with CS content with a significantly ($P < 0.005$) observed difference between the swelling ratio values in all the simulated physiological fluids.

The NH_2 and OH functional ends of the CS chains with a strong affinity for water, cause the polymer to be unstable in moist conditions (El Achaby et al., 2014).

Figure 4.5 also shows the swelling ratio of the CS/PVP hydrogels in simulated physiological fluids of different pH values. It is observed that the swelling ratio of the hydrogels displays a similar pattern regardless of the variations in the pH of the testing media used but with varied levels of fluid uptake. Hydrogels H1 to H5, show the highest degree of swelling in simulated gastric fluid (pH 1.2) in comparison to the simulated intestinal and colon fluids (pH 6.8 and 7.4). The swelling ratios of all the hydrogels in simulated intestinal fluid (pH 6.8) are lower than the values obtained in simulated gastric fluid (pH 1.2) and slightly higher than that of in simulated colon fluid (pH 7.4). The difference in the swelling ratios in each physiological fluids indicates the pH-sensitivity of the CS/PVP hydrogels because of the protonation and deprotonation capability of the amino ($-NH_2$) groups of CS (Emami et al., 2021) and the ring structure of PVP which causing chain expansion, rapid hydrogen bond breakage, and hence greater SGF diffusion.

pH-sensitive hydrogels for oral drug delivery must possess minimal swelling and drug release properties in the acidic medium (stomach) and optimal swelling as well as drug release in the intestinal tract where drug absorption is the highest. Therefore, the optimal polymer ratio in this study should indicate a relatively lower swelling ratio in the SGF (pH 1.2) and a relatively higher swelling ratio in the SIF (pH 6.8). Hence, CS/PVP at a 60/40 weight ratio is selected as the optimal polymer ratio. The hydrogel H_2 (CS/PVP, weight ratio of 60/40) has been studied in the literature as an optimal composition for applications in CDDSs (Gull et al., 2019; Nematollahi et al., 2021; Garakani et al., 2020). Therefore, further to determine the influence of the glutaraldehyde concentration on the degree of swelling, the hydrogel system H_2 was chosen as the model system as it displayed an optimal balance of low swelling in simulated gastric fluid and higher swelling in simulated intestinal fluid. The concentration of the crosslinker was varied between 200 µL to 1000 µL, and the swelling ratio was measured in the three-different simulated physiological fluids.

Figure 4.6 (a, b, c) depicts the percentage swelling ratios of the hydrogels H2-G1, H2-G2, H2-G3, H2-G4, and H2-G5 in SGF, SIF, and SCF. The figure shows that the swelling ratio, irrespective of glutaraldehyde concentration and simulated physiological fluids, shows a similar trend of an initial rapid swelling up to about 180 minutes. The hydrogel H2-G3 (CS/PVP, weight ratio of 60/40 and 600 µL glutaraldehyde) showed the highest swelling ratio in all physiological fluids in comparison to the other hydrogels with maximum values of approximately 588.4%, 557.44%, and 502.96% in SGF, SIF and SCF respectively in 240 minutes, and the lowest swelling

ratio was observed for system H2-G5 (CS/PVP, weight ratio of 60/40 and 1000 µL glutaraldehyde) with maximum values of approximately 257.24%, 235.54%, and 179.31% in SGF, SIF and SCF respectively in 240 minutes (Appendix I, d-f).

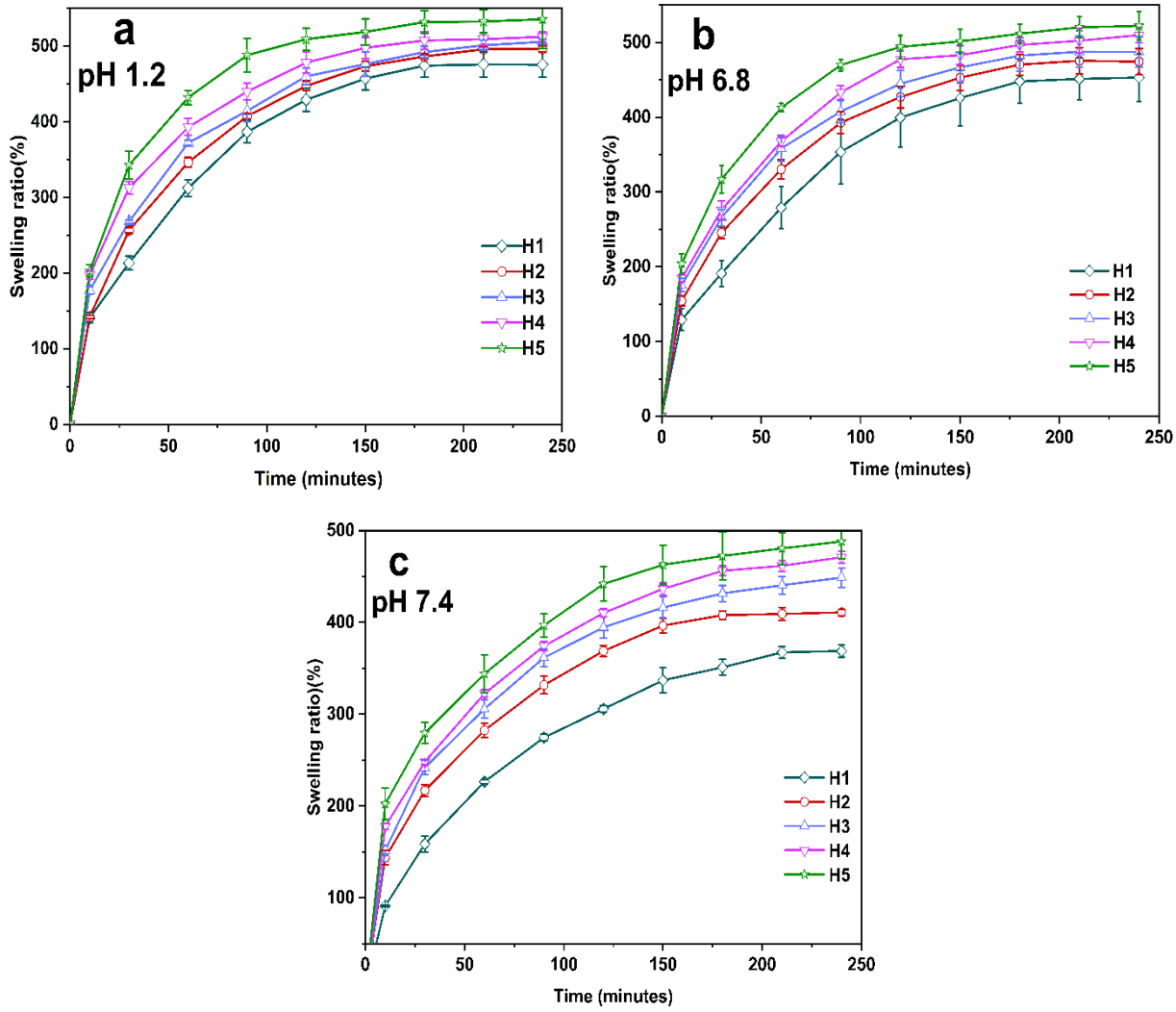

Figure 4. 5 Swelling ratios of hydrogels H1 to H5 in (a) SGF, (b) SIF, and (c) SCF.

At lower concentrations of glutaraldehyde (200 µL and 400 µL), a lower crosslinking density resulted in reduced inter-connected channels or less porous network structures; thus, low swelling ratios are observed. The increased swelling ratio obtained with glutaraldehyde concentration up to 600 µL is due to the establishment of improved interconnected structural networks and covalent bonding between glutaraldehydic groups. These improved structural networks result in a greater degree of physical intertwining of PVP chains, resulting in a more stable porous structure. Furthermore, the osmotic pressure difference between physiological fluids and this hydrogel system is increased, allowing extra water molecules to permeate into the structure (Anwar et al., 2021). The decrease in the sewlling ratio in the hydrogel systems with 800 µL and 1000 µL of glutaraldehyde is attributable to an increase in crosslinking density, which leads in

highly compact structural networks, which reduces porosity. The results agree with the literature (Gull et al., 2020b).

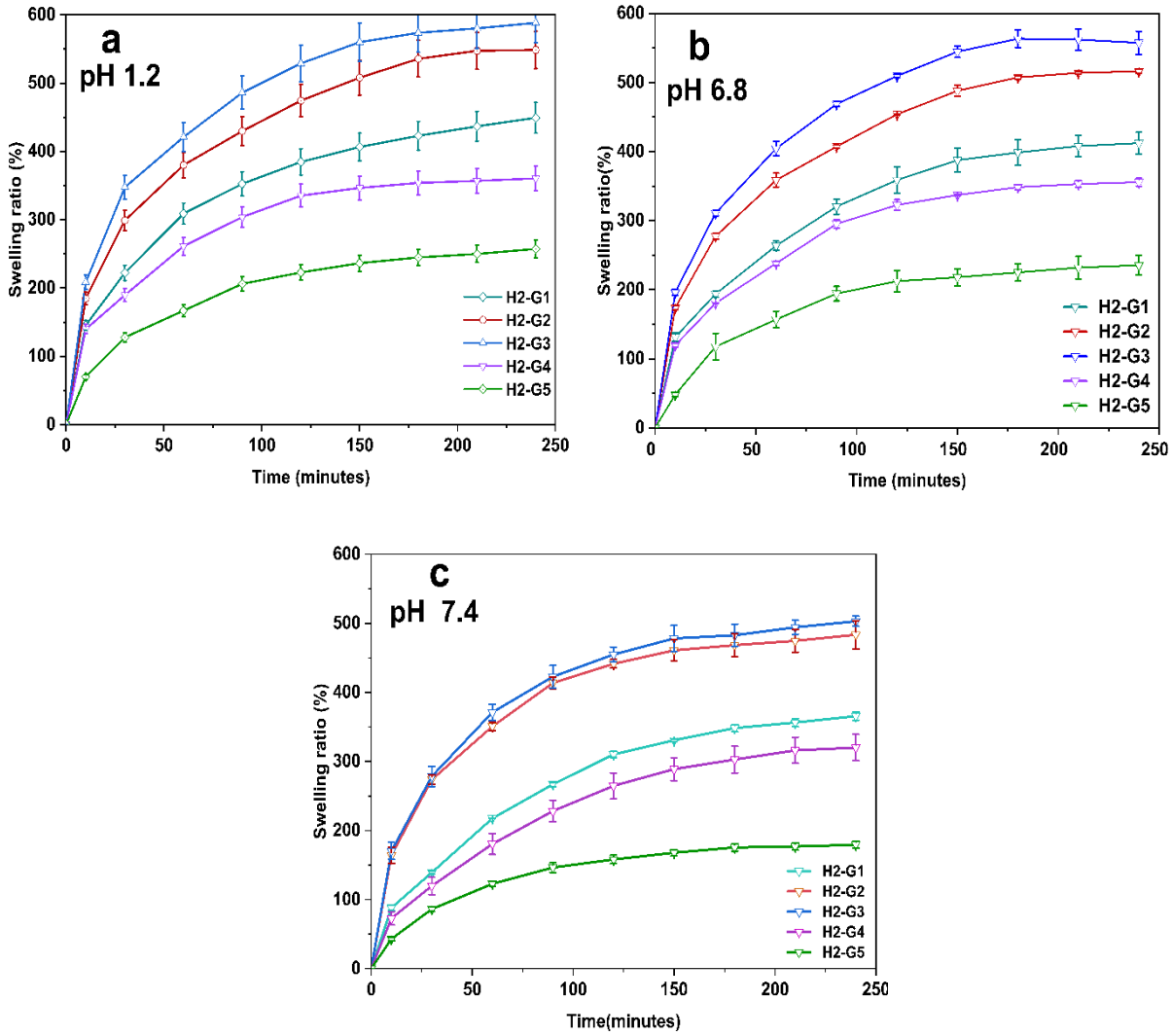

Figure 4. 6 Swelling ratio of hydrogel H_2 with increasing glutaraldehyde content in (a) SGF, (b) SIF, and (c) SCF.

The observed swelling ratios based on varied amounts of glutaraldehyde also support the results of the swelling behavior of the hydrogels as a function of CS/PVP polymer ratio (H1 to H5), wherein it is seen that in the SGF the hydrogels displayed the highest swelling ratio. As previously noted, these results are atributed due to the protonation and deprotonation nature of of NH_2 groups of CS leading to polymer volume expansion or shrinkage (Peers et al., 2020).

A strong positive correlation between glutaraldehyde content from 200 µL to 600 µL and the swelling ratios in SGF (r^2 = 0.982), SIF (r^2 = 0.983), and SCF (r^2 = 0.908) with significant difference ($P < 0.005$) observed in all the simulated physiological fluids. Increasing the concentration of glutaraldehyde further from 800 µL and 1000 µL leads to a dramatic reduction

in the degree of swelling although the sensitivity to pH is related, and the strong negative correlation (r^2 = -1.00) between glutaraldehyde content and the swelling ratio was observed as apparent from the figure 4.6.

The swelling ratios of the SALG/CS hydrogels B1 to B5 (Table 3.3) in SGF (pH 1.2), SIF (pH 6.8), and SCF (pH 7.4) at 37.2 °C in 240 minutes are presented in Figure 4.7 (a, b, c). The swelling behavior of the SALG/CS hydrogels is observed to differ based on the pH of the simulated physiological fluids and the polymer composition (the amount and hence hydrophilicity of CS and SALG). At pH 1.2 (SGF), the swelling ratio of SALG/CS hydrogels increased with increasing CS percentage and decreased with increasing SALG percentage.

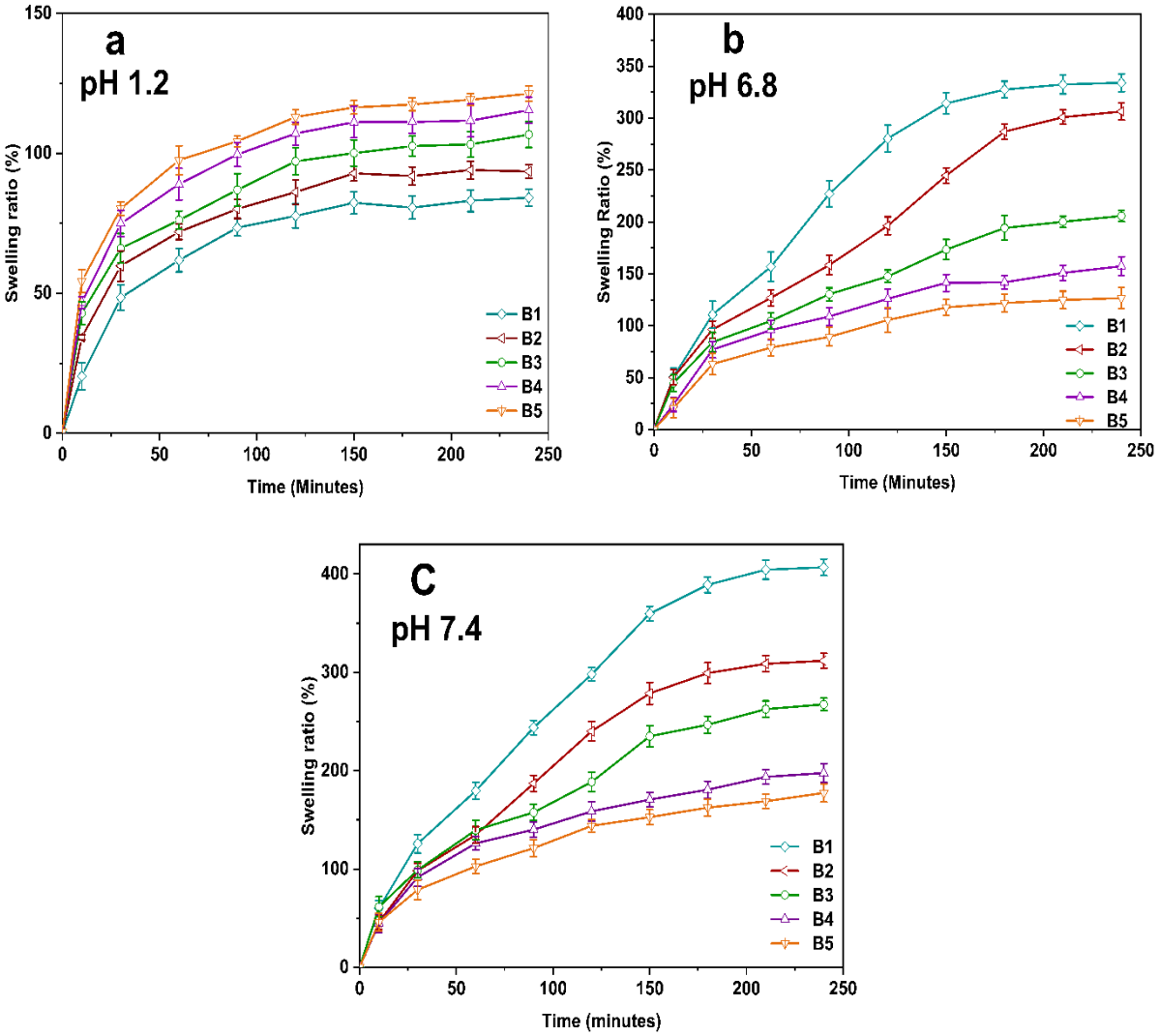

Figure 4. 7 Swelling ratio of hydrogel beads B1to B5 in (a) SGF, (b) SIF, and (c) SCF.

For instance, in acidic media (SGF), the SALG/CS hydrogel with a weight percentage of 75/25 (B1), shows the lowest swelling ratio of 84.14% compared to the SALG/CS hydrogel with a

weight percentage of 25/75 (B5), with the maximum swelling ratio of approximately 121.27% in 240 minutes. In SGF, the swelling ratio of hydrogel bead B1 was about 37% times lower than B5 in 240 minutes. Hydrogels B2 to B4 also displayed similar swelling ratio patterns in an acidic media. The higher swelling ratio of SALG/CS hydrogel with a weight percentage of 25/75 (B5) in SGF is attributed to in SGF (pH 1.2), the amino (NH_2) groups of CS chains are protonated forming NH_3^+. As a result, significant electrostatic interactions between the cationic CS networks cause polymer chain relaxation, thus the diffusion of the fluids into the hydrogel networks causing noticeable swelling (volume expansion). However, in an acidic medium (SGF, pH 1.2), hydrogels with higher SALG percentage contain higher carboxylate ions (COO-) on SALG chains, which protonated and exist as (-COOH) (pka for SALG is 3.4) (Pan et al., 2021).

Consequently, electrostatic repulsion between the polymer networks is reduced, and a strong hydrogen bond between -COOH and -OH is promoted, leading to a reduced swelling ratio of the hydrogel beads. This suggests that SALG is stable in an acidic environment. Furthermore, in acidic media, the hydrogels (B1 to B5) experience ionic interactions between the carboxylate ions (COO-) in SALG chains, and ammonium cations (NH_3^+) in CS chains, which lead to a reduced degree of swelling (T.Wu et al., 2020). In SIF (pH 6.8) and SCF (pH 7.4), however, the tendency of the swelling behavior was reversed. The swelling ratio of SALG/CS hydrogels rose as SALG content increased. The hydrogels show a larger swelling ratio in SIF (pH 6.8) than SGF (pH 1.2) and a slightly lower swelling ratio than SCF (pH 7.4).

As it is observed from Figure 4.7 (b and c) as well as Appendix II (a-c), the hydrogel B1 (SALG/CS, 75/25 wt.%) has a swelling ratio of approximately 334.21% and 406.84% in SIF and SCF respectively after 240 minutes. In comparison, hydrogel B5 (SALG/CS, 25/75 wt.%) had the lowest swelling ratios of approximately 127.77% and 177.34% in SIF and FCF, respectively. After 240 minutes, the swelling ratio of hydrogel B1 was about 72% higher in SCF than in SIF. The observed swelling behavior of SALG/CS is related to the characteristics of CS and SALG in slightly alkaline media where the ammonium cation (NH_3^+) groups of CS release H^+ and invert to -NH_2 groups.

As a result, the swelling ratio of hydrogels is affected by the existence of more carboxylate ions (COO-) because of the deprotonation of the -COOH groups of SALG in slightly alkaline medium. Strong electrostatic repulsion forces among the carboxylate ions drive polymer chain expansion, resulting in the uptake of additional physiological fluids (swelling ratio increases) (Jana & Jana, 2020). The swelling pattern of the hydrogels (B1 to B5) in SIF (pH 6.8) and SCF (pH 7.4) suggests that when the SALG concentration increases, the swelling ratio increases, and CS

provide stability of the hydrogel networks. A strong positive correlation between SALG content and the swelling ratios in SIF (r^2 = 0. 984) and SCF (r^2 = 0.965) with a significant difference (P < 0.005) was seen in all the simulated physiological fluids.

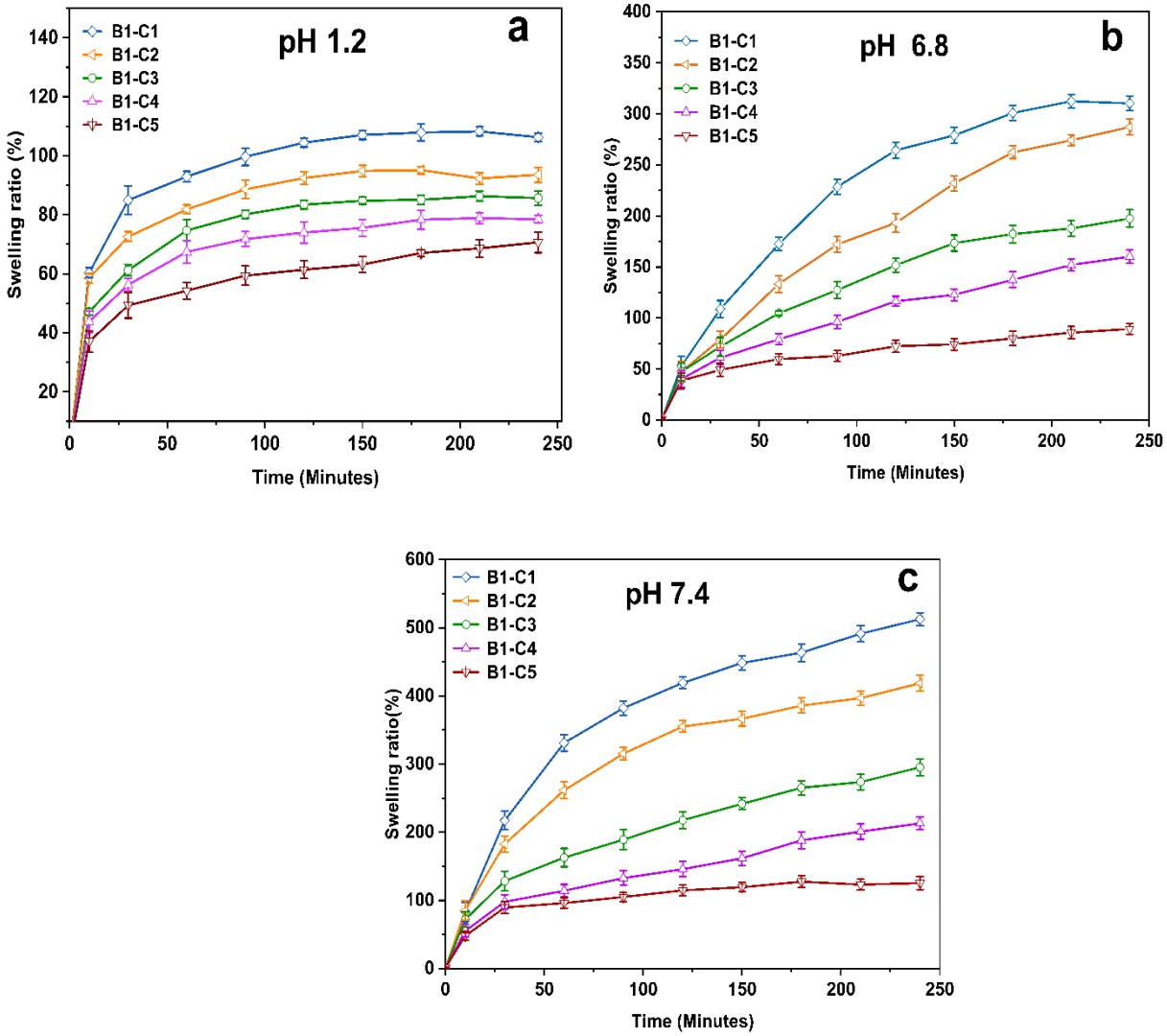

Figure 4. 8 Swelling ratio of hydrogel B1 with increasing $CaCl_2$ content in (a) SGF, (b) SIF, and (c) SCF.

However, a strong negative correlation (r^2 = - 0.990) was found between SALG content and swelling ratio in SGF (r^2 = -0.990). Based on the swelling behavior of the hydrogels B1 through B5, the results reveal that hydrogel B1, with a low swelling ratio in SGF and higher swelling behaviour in SIF and SCF, could be an optimal composition for AMX and MTZ drug loading and release. Thus, SALG/CS with a weight percentage of 75/25 (B1) was further studied to evaluate the effect of $CaCl_2$ concentration on the swelling behavior of hydrogels. The concentration of $CaCl_2$ was varied between 2% to 10%, and the swelling ratio was measured in the three-different simulated physiological fluids (SGF, SIF, and SCF).

Figure 4.8 (a, b, c) displays the swelling behaviour of the hydrogels B1-C1 to B1-C5 as a function of increasing $CaCl_2$ concentration from 2% to 10% in SGF, SIF, and SCF. It is seen that while a similar trend of increasing swelling ratio with pH as for the hydrogel B1 is obtained in all three physiological fluids, there is a reduction in the swelling ratio with increasing concentration of $CaCl_2$ with initial rapid swelling lasting up to 120 minutes.

It was seen that, the swelling ratios of SALG/CS hydrogel beads in SCF in general higher than in SIF and SGF for all crosslinker concentrations ($CaCl_2$), which is attributed to the stability of SALG polymer in acidic medium (pH 1.2) as discussed above. The hydrogel B1-C1 (SALG/CS, weight ratio of 75/25 and 2% $CaCl_2$) showed the highest swelling ratio in all physiological fluids in comparison to the other hydrogels with maximum values of approximately 106.26%, 310.23%, and 512.65% in SGF, SIF and SCF respectively in 240 minutes and the lowest swelling ratio was observed for system B1-C5 (SALG/CS, weight ratio of 75/25 and 10% $CaCl_2$) with maximum values of approximately 70.64%, 89.29%, and 125.39% in SGF, SIF and SCF respectively in 240 minutes (Appendix II, d-f). At higher pH, the –COOH group deprotonated forming more carboxylate groups (COO-). Consequently, the electrostatic repulsions between carboxylate groups (COO-) causes polymer relaxation and the diffusion of simulated fluids into the hydrogel networks. In each simulated fluid, when the concentration of $CaCl_2$ increased from 2%-10% the swelling ratios of each hydrogel were decreased. This condition is associated with more ionotropic crosslinking of the –COO- groups of SALG and Ca^{2+} resulting in dense structures that reduce the diffusion of simulated fluids into the hydrogel networks (Zhang et al., 2019).

A strong negative correlation between $CaCl_2$ content and the swelling ratios in SGF (r^2 = -0.997), SIF (r^2 = -0.998), and SCF (r^2 = -0.989) with significant difference ($P < 0.005$) seen in all the simulated physiological fluids. The obtained degree of swelling reflects the crosslinked network density, which increases with $CaCl_2$ concentration. Due to this, the hydrogels become more compact and rigid, and the extent of swelling decreases (Khajuria et al., 2020). Among the different $CaCl_2$ concentrations, the 2% (B1-C1) is considered optimal as it displays the highest and most stable swelling behavior in all the three simulated physiological fluids, and has been studied in the literature as an optimal composition for applications in CDDSs (Jana & Jana, 2020; Khajuria et al., 2020; T.Wu et al., 2020).

4.4. Porosity

Porosity is a critical feature of hydrogels utilized in CDDSs as it influences swelling capacity, and hence drug diffusion. It is determined by the dimensions and number of pores in the hydrogel

networks and the gel content (crosslinking density) of the hydrogel systems (Siboro et al., 2021). Figure 4.9a shows the change in the porosity of the CS/PVP hydrogels with respect to the polymer ratio (H1 to H5). The result (Appendix III, a) shows that an increase in porosity is obtained with an increasing ratio of PVP. The hydrogel system CS/PVP with 30/70 wt.% (H5) has the highest porosity (83.1%), while the hydrogel H1 (CS/PVP, 70/30 wt%) has the lowest porosity (61%).

The formation of a more significant number of crosslinked channels comprised of void spaces formed during the entanglement of PVP ring structures into the CS chains is related to the monotonic increase in porosity with increasing PVP ratio (Khanum et al., 2018). Furthermore, with increasing PVP content, the viscosity of the polymer mixture increases during synthesis, which inhibits the removal of bubbles from the polymer matrix partially and produces an interconnected porous structure, resulting in enhanced porosity. The effect of crosslinking agent on porosity is apparent for the hydrogels H2-G1, H2-G2, and H2-G3 (Figure 4.9b), where porosity increases linearly from about 77%, 80%, and 95%, respectively (Appendix III, b).

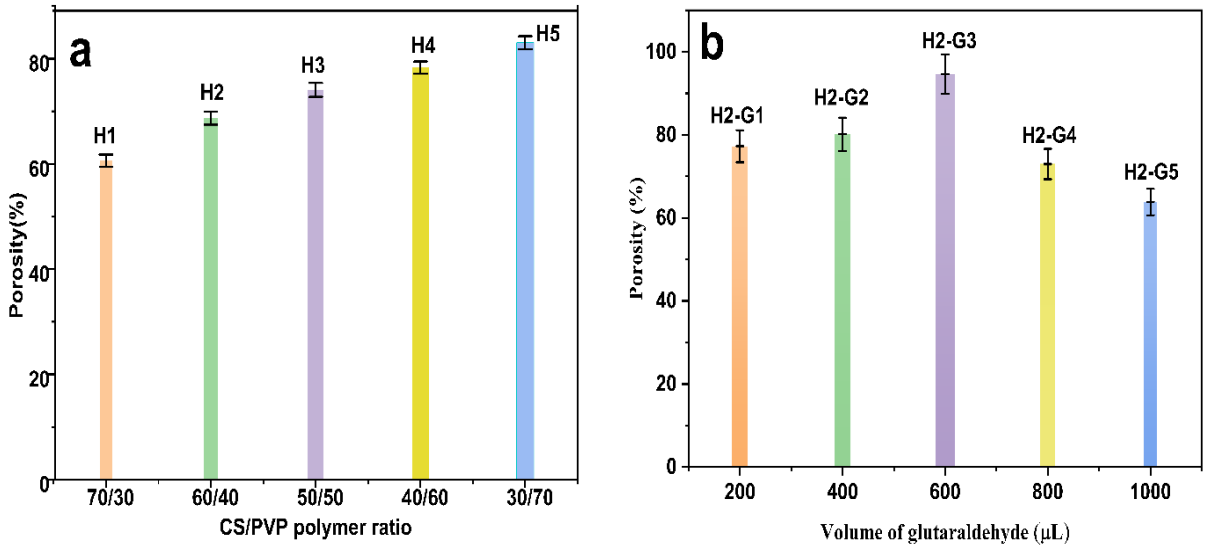

Figure 4. 9 Porosity of hydrogels (a) H1 to H5, and (b) H2-G1 to H2-G5.

Nevertheless, porosity drastically decreased approximately to 73% and 64% when the crosslinker concentration is increased to 800 µL (H2-G4) and 1000 µL (H2-G5) respectively. This is owing to the increased interlacement of PVP between CS networks resulting in highly compact structures due to the high crosslinking density. Above 600 µL, it is evident that the viscosity effect was overcome by the crosslinking of CS with a glutaraldehyde, resulting in highly crosslinked structures. For the incorporation of AMX and MTZ drugs, the hydrogel H2-G3 (CS/PVP, 60/40 wt. % with 600 µL was chosen based on the observations mentioned above.

The change in porosity of the SALG/CS hydrogels with respect to the polymer ratio (B1 to B5) is shown in Figure 4.10a. The obtained porosity values suggest that increasing the SALG content leads to an increase in porosity. The highest porosity (about 92%) was obtained for hydrogel bead SALG/CS with 75/25 wt.% (B1), whereas hydrogel bead with 25/75 wt.% (B5) had the lowest porosity of about 75% (Appendix III, c). This increase in porosity with increasing SALG ratio is attributed to the formation of an increased amount of crosslinked channels as a result of CS crosslinking by glutaraldehyde producing Schiff base (C=N) and physical crosslinking (such as hydrogen bonding) between CS and SALG.

Porosity is decreased due to the change in polymer chain alignments caused by crosslinking, which also decreases the free space in the hydrogels' matrix (Radhakrishnan et al., 2015). Figure 4.10b demonstrates the variation in porosity of the SALG/CS hydrogels B1-C1 to B1-C5 as a function of the crosslinker ($CaCl_2$). The figure shows that the hydrogels' porosity decreases in proportion to the amount of the crosslinker, with the hydrogel B1-C1 having the highest porosity (about 87%) and the hydrogel B1-C5 having the lowest porosity (about 69%). This suggests that as the hydrogels' crosslink density increases, less porous structures are formed. Depending on the obtained results, B1-C1 was selected for the incorporation of the drugs (AMX and MTZ).

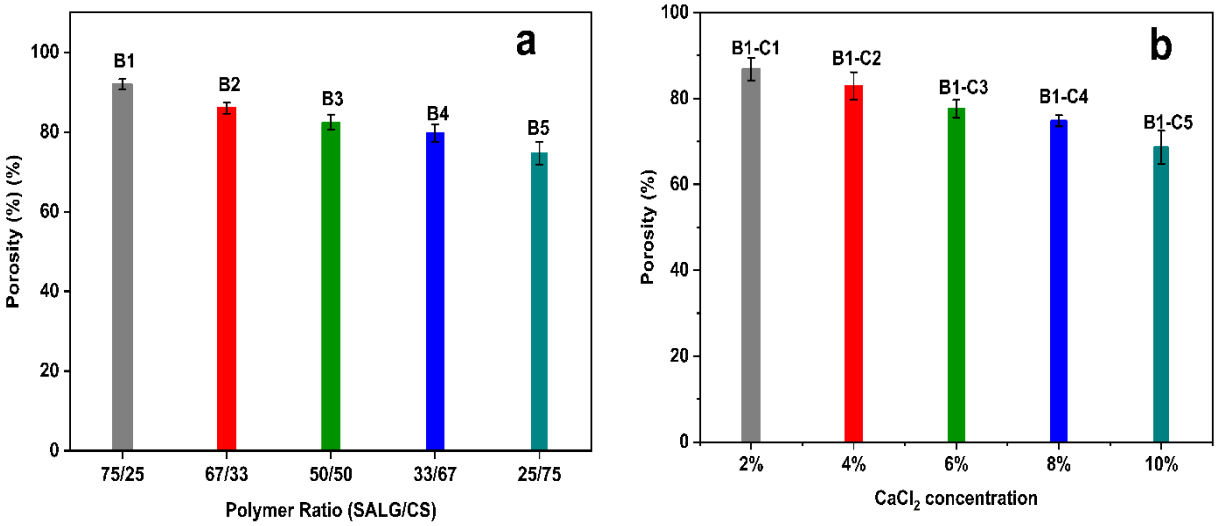

Figure 4. 10 Porosity of hydrogels (a) B1 to B5, and (b) B1-C1 to B1-C5.

4.5. Functional group analysis

In the synthesis of a three-dimensional (3D) semi-IPN CS/PVP hydrogels, the aldehydic groups of glutaraldehyde interact with CS chains through covalent bonding forming schiff base and PVP is interlaced between the crosslinked CS networks (Figure 4.2). FTIR analysis investigated the polymers functional groups, interactions between polymer components, and the polymer-drug

interactions. The FTIR results showed variations in the appearance and disappearance of some peaks of the FTIR spectra relative to the bands of the individual polymers, drugs, and the crosslinking agent in the crosslinked hydrogel, which is due to the various interactions among components of the polymer blend and the drug as described in previous studies (Afriani & Sutanti Budikania, 2020; Garakani et al., 2020). Figure 4.11 displays the FTIR spectra of PVP, CS, MTZ, and AMX, CS/PVP hydrogels H2-G1 to H2-G5, AMX-H2-G3, and MTZ-H2-G3.

Figure 4.11a shows that the stretching vibrations of the O-H groups and the N-H bonds of the primary amine (NH_2) groups in the CS spectrum overlap, forming a broad peak between 3000, and 3600 cm^{-1}. The stretching vibrations of the C-H of the methyl ($-CH_3$) and methylene ($-CH_2-$) groups in CS chain are detected at 2920 and 2853 cm^{-1} respectively (Budianto & Amalia, 2020). The peak noticed at 1600-1800 cm^{-1} in the CS spectrum is associated to amide carbonyl (-CONR2) stretching vibration, indicating the presence of chitin due to inefficient CS deacetylation. The characteristic strong peaks at 1638, 1554, 1315, and 605 cm^{-1} are attributable to the carbonyl (C=O) stretching vibrations of primary amide ($-CONH_2$), secondary amide (-CONHR), tertiary amide ($-CONR_2$), and N-H out-of-plane vibration, respectively in CS chains (Ghauri et al., 2021). The weak peaks detected at 1418 and 1381 cm^{-1} are ascribed to the symmetric bending vibration of the methyl group ($-CH_3$). The peaks at 1150 and 897 cm^{-1} are due to C-O stretching vibrations, which are characteristic of CS saccharide chains .

The FTIR spectrum of pure PVP indicates a broad absorption band between 3600 and 3000 cm^{-1}, attributed to symmetric vibration produced by the O-H bond of water because of the polymer's intrinsic hygroscopiic character (Rahma et al., 2016). The characteristic peaks of pure PVP are detected at 2923 cm^{-1} ($-CH_2$ symmetric stretching), 1655 cm^{-1} (C=O stretching vibrations), 1495 cm^{-1} (-C-N-C stretching), 1423 cm^{-1} (C-H bending), 1285 and 1024 cm^{-1} (out-of-plane rings bending and rocking of $-CH_2$) (Afriani & Sutanti Budikania, 2020; Rahma et al., 2016).

Figure 4.11a shows the FTIR spectra of the produced hydrogels with increasing glutaraldehyde content (H2-G1 to H2-G5) in comparison to pure CS and PVP. It is noticed that when CS is crosslinked with increasing amounts of the crosslinker (glutaraldehyde), the absorption band becomes weaker between 3000-3600 cm^{-1}, which is due to CS interactions with glutaraldehyde resulting in Schiff-base (imine linkage, C=N) (Nematollahi et al., 2021). A difference observed between the spectra of the crosslinked hydrogels (H2-G1 to H2-G5) is the reducing strength of the $CS–NH_2$ bending vibration at 1554 cm^{-1} with increasing glutaraldehyde content as CS reacts with glutaraldehyde resulting in Schiff-base.

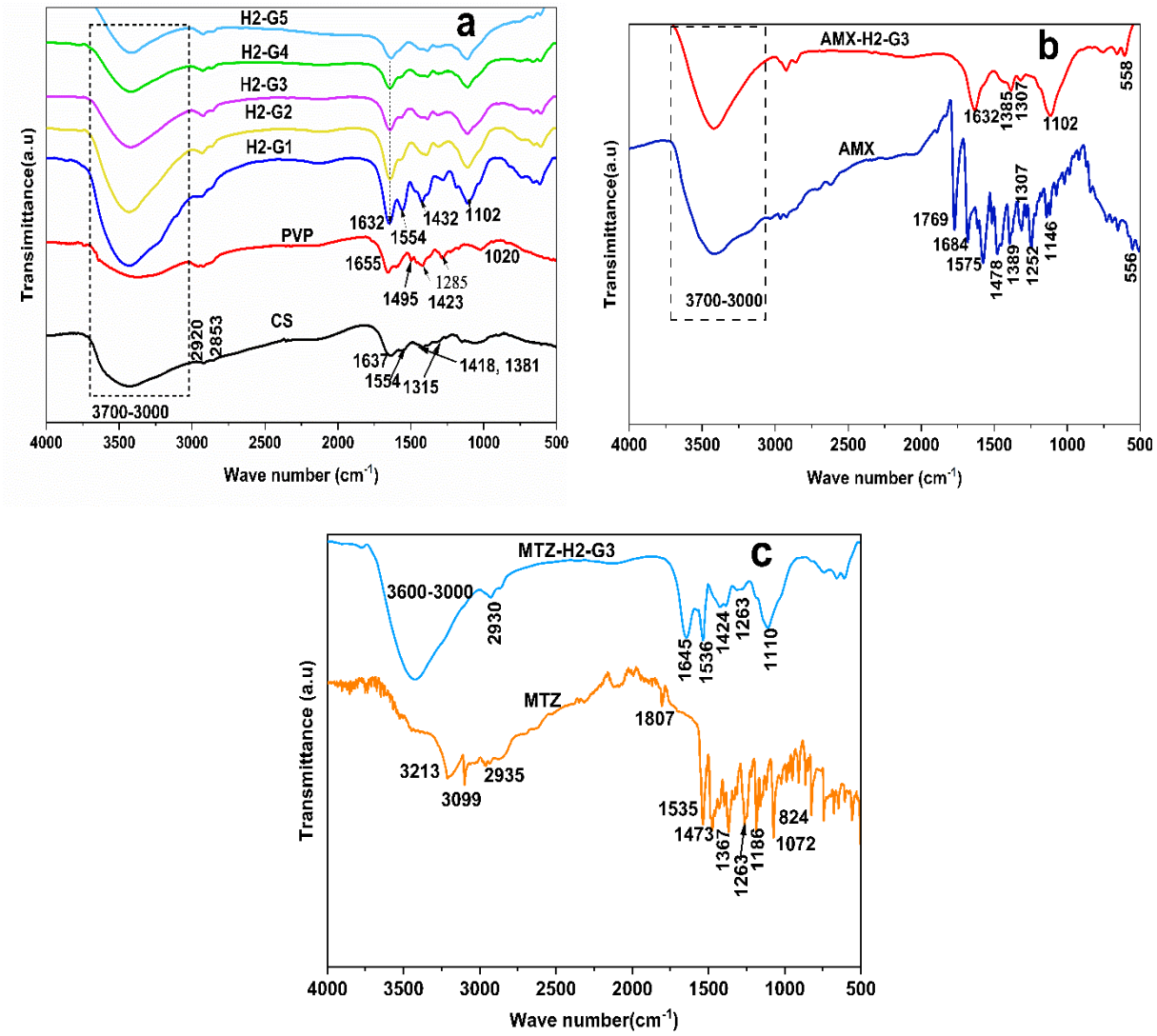

Figure 4. 11 FTIR spectra of (a) CS and PVP, and hydrogels H1-G1 to H2-G5, (b) AMX and hydrogel AMX-H2-G3, and (c) MTZ and hydrogel MTZ-H2-G3.

The peak at 1638 cm^{-1} reflects the imine bonds (N=C). The stretching strength of the C-H at 2922 cm^{-1} increased. These observations were attributed to the enhanced contribution of the crosslinking between the carbonyl groups of glutaraldehyde and amine ($-NH_2$) groups of CS chains, forming semi-IPNs and increased crosslinking density. The weak peak observed at 1389 cm^{-1} is ascribed to $-CH_3$ deformation frequency. The carbonyl (C=O) absorption changes to lower frequencies with an increase in intensity with glutaraldehyde concentration at 1632 cm^{-1} because of the crosslinking between the CS chains and interlaced PVP chains (El Achaby et al., 2014).

Figure 4.11b illustrates the FTIR spectrum of pristine AMX and AMX-H2-G3. Both spectra show a broad peak from 3600–3000 cm^{-1} because of overlapping N–H and O–H stretching frequencies. Aliphatic C-H bonds in $-CH_2-$ exhibit symmetric stretching frequencies at 2945 cm^{-1} and 2856 cm^{-1}. The characteristic sharp absorption bands because of stretching frequencies of C=O of the

β-lactam, amide, and carboxylic groups of AMX are detected at 1769 cm^{-1}, 1684 cm^{-1}, and 1575 cm^{-1}, respectively. Other bands observed on the AMX molecule include those at 1478 cm^{-1} (alphatic C-N bending vibrations), 1146 cm^{-1} (aliphatic C-C stretching), and 1017 cm^{-1} (C-O stretching), 1389 and 1252 cm^{-1} (asymmetric and symmetric stretching of carboxylate group), and 556 cm^{-1} (C-S stretching).

Most of the characteristic peaks of pristine AMX are absent in the FTIR spectrum of AMX-H2-G3, indicating the existence of crosslinking between functional ends of CS chains and AMX. The distinctive strong absorption band of AMX at 1769 cm^{-1} due to the stretching vibration of the carbonyl bond (C=O) of the β-lactam was not noticed in AMX-H2-G3. However, the AMX absorption bands at 1684 and 1575 cm^{-1} (stretching vibration of C=O of, amide, and carboxylic end) shifted into broad stronger band at 1632 cm^{-1} in AMX-H2-G3. The absorption band at 1385 cm^{-1} and weak band at about 1320 cm^{-1} are attributable to the carboxylate group's (COO-) asymmetric and symmetric stretching frequencies. The band at 1102 cm^{-1} in AMX-H2-G3 hydrogel is assigned to the saccharine chain of CS. Furthermore, the shift of the C=O bond stretchibg peaks of AMX in the drug-loaded hydrogel (AMX-H2-G3) to 1632 cm^{-1} and the C-S band observed at 557 cm^{-1} indicates that AMX is incorporated into the hydrogel.

The FTIR spectra of MTZ and MTZ-H2-G3 hydrogels are presented in Figure 4.11c. The spectra of MTZ displays an absorption band about 3221 cm^{-1}(O-H stretching vibrations) and at 3099 cm^{-1} attributed to imidazole (C=CH) symmetric stretching frequency of MTZ (Heragh et al., 2022; Myhal et al., 2016). The stretching vibrations of the C-H of methyl ($-CH_3$) and methylene ($-CH_2-$) groups are observed at 2937 cm^{-1} and 2853 cm^{-1} respectively (Naseem et al., 2022). The nitro group (NO_2) exhibits bands at 1807 cm^{-1} (N-O bond asymmetric stretching) and 1473 cm^{-1} (N-O bond symmetric stretching). Other specific absorption bands of MTZ include 1535 and 1367 cm^{-1} corresponding to the nitroso group (R-N=O), 1263 cm^{-1} due to ethylenic group (-C=C-), 1186 cm^{-1} attributed to the imine (-C=N), 1072 cm^{-1} corresponding to the carbon oxygen bond (C-O) stretching vibrations, and at 824 cm^{-1} due to the alphatic C-H rock vibrations (Heragh et al., 2022). The absorption bands in MTZ-H2-G3 spectrum correspond to carbonyl (C=O) stretching frequency at 1645 cm^{-1}, benzene ring (C-H) bending frequency at 1110 cm^{-1}, and alphatic C-H bond deformation frequency at 1424 cm^{-1}. The newly observed absorption band at 1536 cm^{-1} is associated with the MTZ's nitro (N-O) bond stretching frequency, suggesting its existence in the H2-G3 hydrogel (Naseem et al., 2022). The absence of more bands of MTZ in the MTZ-H2-G3 hydrogel provides proof of the drug-polymer interaction. MTZ's interaction with the polymer

components shows that MTZ is effectively loaded into the hydrogel via various physical crosslinking, for example hydrogen bonding (Figure 4.2b). Furthermore, the result point out the stabiliity of MTZ in the hydrogel.

The FTIR spectra of the pristine CS, SALG, AMX, MTZ, unloaded hydrogels (B1-C1, B1-C2, B1-C3, B1-C4, and B1-C5) and the drug loaded hydrogel (AMX-B1-C1 and MTZ-B1-C1) are presented in Figure 4.12. The spectrum of SALG in Figure 4.12a has a distinctive broad absorption band between 3000 and 3700 cm^{-1} that is owing to hydroxyl group (O-H) stretching frequencies of SALG chains. The FTIR spectrum of SALG exhibits significant absorption bands at 2920 cm^{-1} (aliphatic C-H stretching vibrations), 1595 cm^{-1} (asymmetricstretching frequency of C=O of COO-), and 1394 cm^{-1} symmetric stretching vibrations of C=O of carboxylate group (COO-) in SALG chains. Other absorption bands of SALG includes at approximately 1287 cm^{-1} (C-C stretching vibration), weak band at about 1084 cm^{-1} (C-O and C-Cstretching), and a strong band intensity at 1017 cm^{-1} is ascribed to carbon-carbon single bond (C-C) and the saccharide structure of SALG (C-O-C) stretching vibrations (Nastaj et al., 2016). The distinctive absorption band at around 816 cm^{-1} corresponds to Na-O (Baysal et al., 2013). As discussed above, CS shows characteristic strong bands at approximately 1638, 1554, 1315, and 605 cm^{-1} are attributable to the carbonyl (-C=O) stretching vibrations of primary amide (-CONH2), secondary amide (-CONHR), tertiary amide (-CONHR2), and N-H out-of-plane vibration, respectively. The peaks at 1150 and 897 cm^{-1} are due to C-O stretching vibrations, which are characteristic of CS saccharide chains.

The FTIR spectra of the double crosslinked hydrogels B1-C1, B1-C2, B1-C3, B1-C4, and B1-C5 as a function of $CaCl_2$ concentrations are presented in Figure 4.12b. All of the hydrogels have the Ca-O weak absorption band associated with SALG at around 816 cm^{-1}. The absorption band at 1385 cm^{-1} bending vibrations of the -CH_2- group. The absorption band observed at 1634 cm^{-1} is attributed to the stretching frequency of C=N bond formed due to the covalent interactions between aldehydic group of glutaraldehyde and CS amino groups. The carbonyl bond (C=O) absorption band of SALG at 1595 cm^{-1} and stretching vibrations of amide I (at 1642 cm^{-1}) and amide II of CS chains are disappered confirming the presence of interactions between the carboxylic groups (-COOH) on SALG the adjacent CS networks (Baysal et al., 2013). Figure 4.12c, illustrates the FTIR spectra of AMX and AMX-loaded hydrogel (AMX-B1-C1). Both spectra show a large absorption band from 3600 to 3000 cm-1 owing to overlapping stretching vibrations of N-H and O-H bonds. The characteristic absorption bands at 2945 and 2856 cm-1

are ascribed to the symmetric stretching frequencies of aliphatic C-H bonds of methyl (-CH3) and methylene (-CH2-) groups.

As discussed above, the characteristic sharp absorption bands of of AMX molecule are the stretching viberations of carbonyl bond (C=O) of β-lactam ring, amide (-CON-), and carboxylic (-COOH) groups of AMX detected at 1769 cm^{-1}, 1684 cm^{-1}, and 1575 cm^{-1}, respectively, 1478 cm^{-1} (alphatic C-H bending vibrations), 1146 cm^{-1} (aliphatic C-C stretching), 1017 cm^{-1} (C-O stretching), 1389 and 1252 cm^{-1} (asymmetric and symmetric stretching of carboxylate group), and 556 cm^{-1} (C-S stretching). Most of the characteristic peaks of pristine AMX are absent in the FTIR spectrum of AMX-B1-C1, indicating the presence of interactions between functional ends of CS and SALG chains with AMX molecules. The strong absorption band of AMX at 1769 cm^{-1} (C=O, lactam stretching) was not noticed in AMX-B1-C1. However, the AMX absorption bands at 1684 and 1575 cm^{-1} (C=O of amide, and carboxylic end stretching) shifted into broadband at 1638 cm^{-1} in AMX-B1-C1.

The absorption bands at 1385 and 1320 cm^{1} are attributable to the carboxylate group's (COO-) asymmetric and symmetric stretching frequencies. An absorption band at 1110 cm^{-1} in AMX-B1-C1 hydrogel is assigned to the saccharine chain of CS. Furthermore, the shift of the AMX peak in the drug loaded hydrogel (AMX-H2-G3) from 1769 to 1638 cm^{-1} and the existence of C-S stretching frequency at about 557 cm^{-1} indicate that AMX is incorporated into the hydrogel. The FTIR spectra of MTZ and the drug-loaded hydrogel (MTZ-B1-C1) are shown in Figure 4.12d. As mentioned above MTZ shows characteristic absorption bands at 3221 cm^{-1} (O-H stretching), 3099 cm^{-1} (imidazole, C=C-H stretching) 2937, and 2853 cm^{-1} (alphatic C–H stretching), 1807 cm^{-1} and 1473 cm^{-1} (N=O, nitroso symmetric and asymmetric stretching of NO_2), 1535 and 1367 cm^{-1} N-O symmetric and asymmetric stretching of NO_2, 1263 cm^{-1} (–C=C– stretching), 1186 cm^{-1} (–C=Nstretching), 1072 cm^{-1} (C-O stretching), 824 cm^{-1}(C-N stretching). In the MTZ-B1-C1 spectra, the absorption bands correspond to 1645 cm^{-1} (C=O stretching), 1110 cm^{-1} (C-H benzene ring bending), and 1381 cm^{-1} (alphatic C-H deformation). The newly observed absorption band at 1534 cm^{-1} is related to the MTZ's nitro (N-O) bond stretching vibration, suggesting its existence in the B1-C1 hydrogel. The non-appearance of other characteristic bands of MTZ in the MTZ-B1-C1 hydrogel provide proof of the drug-polymer interaction. MTZ interaction with the polymer components shows that it is effectively loaded into the hydrogel via various ppysical interactions, such as hydrogen bonding as illustrated in Figure 4.4c. Furthermore, the result reveals the stability of MTZ in the SALG/CS hydrogel.

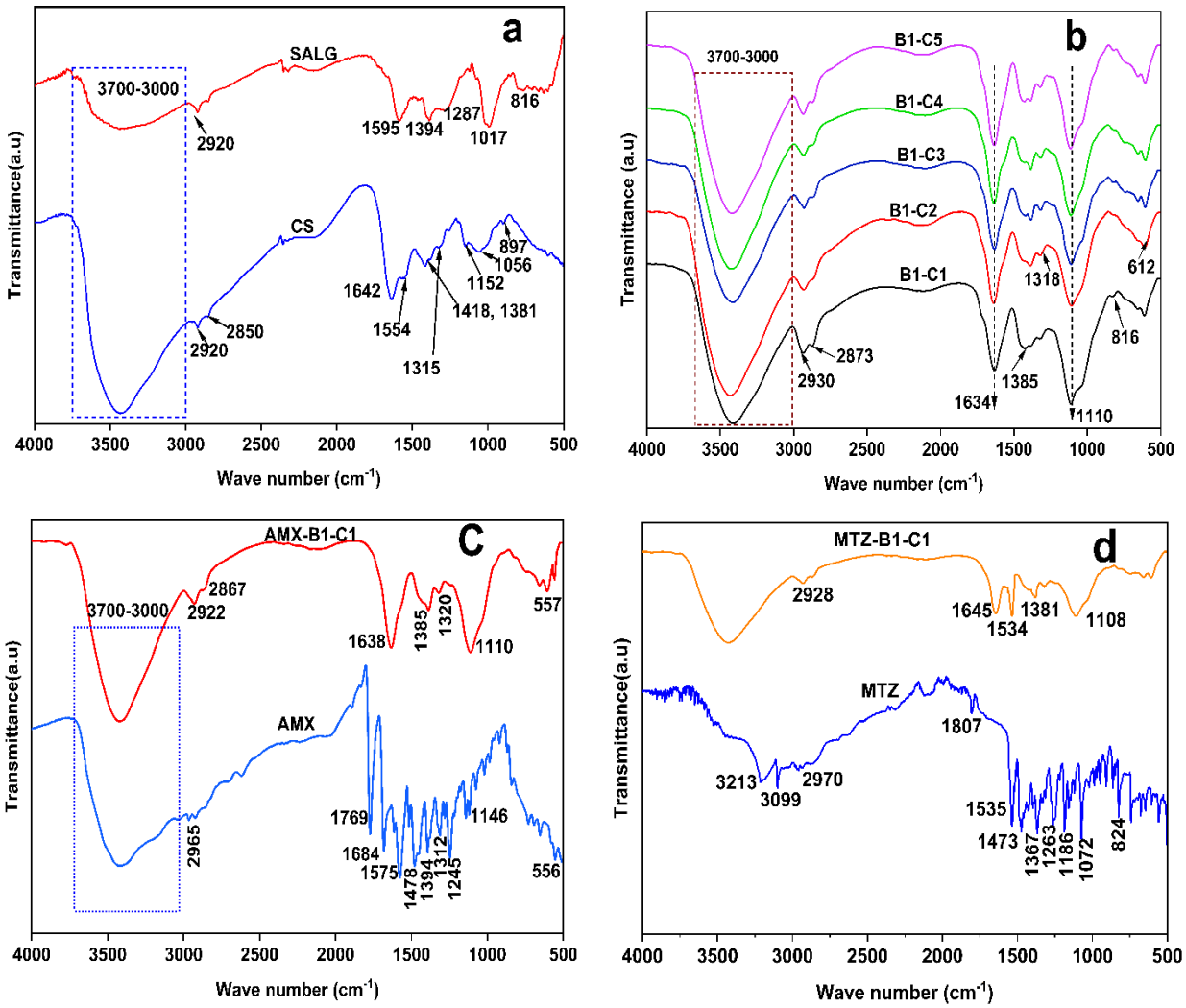

Figure 4. 12 FTIR spectra of (a) CS and SALG, (b) hydrogel beads B1-C1 to B1-C5, (c) AMX and hydrogel AMX- B1-C1, and (d) MTZ and hydrogel MTZ-B1-C1.

4.6. Phase structure

XRD investigation was done to study the effect of concentration of crosslinking agent and drug loading on the phase nature of the hydrogel systems. The XRD patterns of the polymers CS, PVP, selected hydrogels (H2-G2, H2-G3, H2-G4), and drug loaded hydrogels (AMX-H2-G3 and MTZ-H2-G3) are presented in Figure 4.13a. It is observed that CS displays typical crystalline peaks at 2θ values of 9.6º and 20.2º due to the X-ray diffiraction from the α and β chains which match the (020) and (200) diffiraction planes respectively (Mogilevskaya et al., 2006). According to the International Center of Diffiraction Data (JCPDS 39-1894) database, CS displays two characteristic peaks at 2θ, 13.57°, and 23° that represent its semi-crystalline nature because of the existence of -OH and -NH_2 groups.

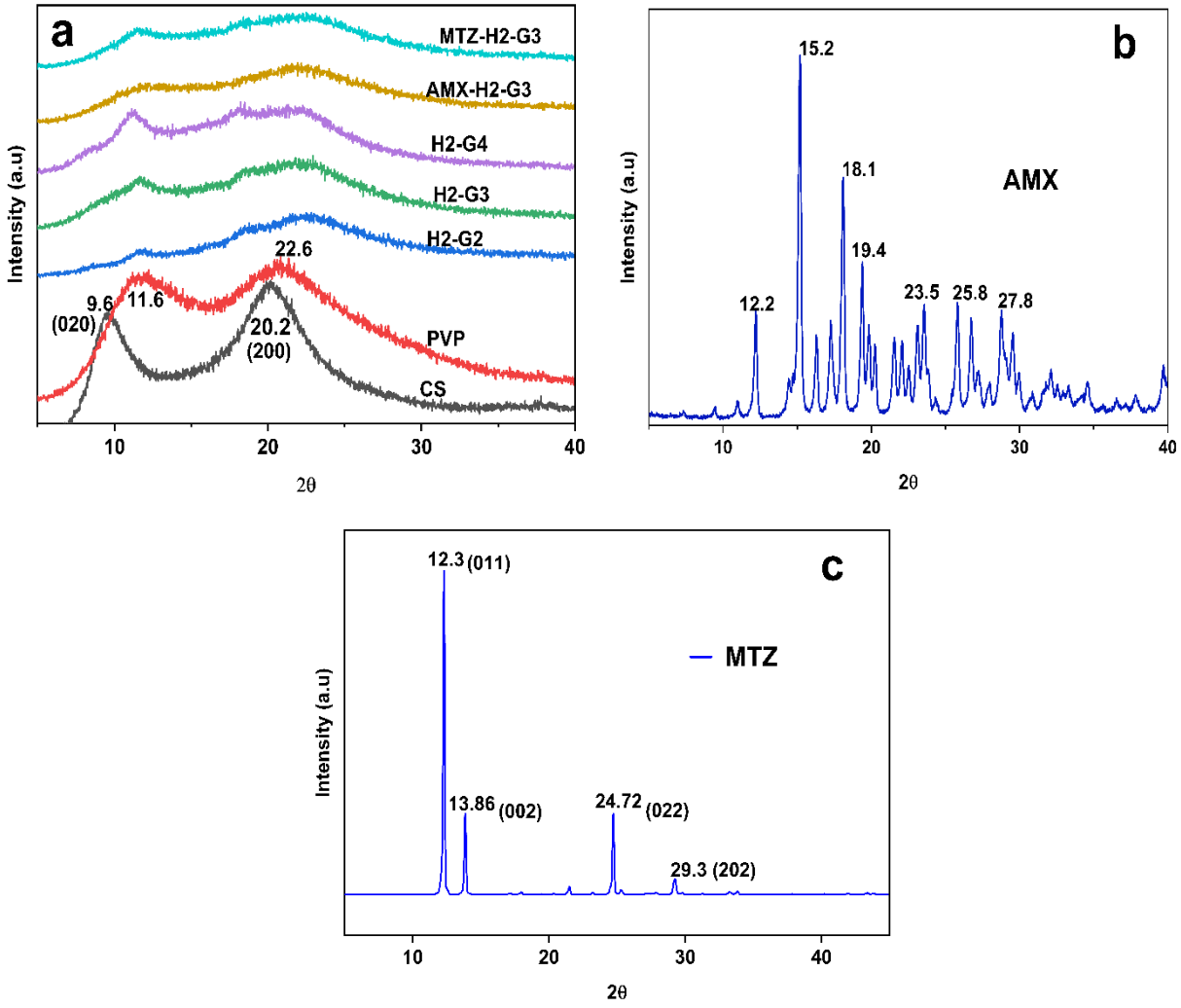

Figure 4. 13 XRD diffractograms of (a) CS, PVP, hydrogels H2-G2 to H2-G4, AMX-H2-G3 and MTZ-H2-G3 (b) AMX (c) MTZ.

The 2θ values at 9.6º and 20.2º are somewhat lower than that of the α and β values of CS, suggesting that the polymer (CS) contains moisture. For PVP, a pair of peaks 2θ values of 11.6º and 20.6º is detected. The peak observed at 2θ value of 11.6º is due to the scattering emanating from short-range arrangements in the amorphous structure of PVP, while the second is attributed to a pseudocrystalline phase (Lewandowska, 2011). The diffraction patterns of the hydrogels H2-G2, H2-G3, and H2-G4 are significantly different from the peak of CS (020), as the amount of water present in its hydrated form is lowered because of the reaction between CS and glutaraldehyde. The values of 2θ indicate that the semi-crystalline nature of the crosslinked CS/PVP hydrogel films and remarkable compatibility and crosslinking between the polymer chains (Nematollahi et al., 2021). The sharpness of the peaks was increased as the crosslinker content increased. The increased in intensity of the peaks is because of an increase in crosslinking density and strong hydrogen bonds between CS, PVP, and glutaraldehyde leading to increased crystallinity.

It is observed that each of the crosslinked CS/PVP hydrogels (H2-G2, H2-G3, and H2-G4) show broad hump peaks at 2θ values around 11° and 23° due to the reflection CS planes (Gull et al., 2020) . This indicates that the dialdehyde alters the components liable for water bonding (Beppu et al., 2007). The first peak of PVP decreases initially decreases in intensity (H2-G2) and then increases and sharpens with increasing glutaraldehyde content. This is attributed to the fact that at low glutaraldehyde content or gel content, the crystalline region of CS has nearly disappeared with the appearance of broad bands representing the amorphous morphology of the hydrogels because of robust interactions between CS and PVP (Archana et al., 2015). On increasing the glutaraldehyde content (H2-G3 and H2-G4), the increase in intensity and sharpness of the first peak of PVP are observed. This is attributed to an increase in the rearrangement of the short-range order of PVP chains in the amorphous regions of the hydrogels as the crosslinking between CS and PVP reduce with crosslinking of CS. This enhanced crosslinking also induces stress in the matrices with the PVP chains held rigidly.

The pristine AMX powder is crystalline, as presented in Figure 4.13b. The distinctive peaks are observed at 2θ values of approximately 12.2°, 15.2°, 16.3°, 17.26°, 18.2°, 19.4°, 23.12°, 15.8°, 26.74°, 28.78° and 29.56° that confirms the AMX is a crystalline material. The crystallinity of hydrogel H2-G3 is reduced due to drug loading. The development of a broader peak validated the amorphous nature of the drug-loaded hydrogel (AMX-H2-G3), which indicates characteristic peaks at 2θ values of 11.68° and 22.18°. The notable decrease in the diffraction peaks of the drug-loaded hydrogel (AMX-H2-G3) shows that the drug's molecular miscibility and interaction with the polymer matrix. The XRD pattern of drug loaded hydrogel (AMX-H2-G3) is similar to that of unloaded hydrogels in which the diffraction peaks of AMX are not observed. This shows that the loaded AMX existed as a dispersed amorphous form in the hydrogel matrix and not as the crystalline form (Nia et al., 2020). Pristine MTZ (Figure 4.13c) shows XRD peaks at 2θ values of 12.3°, 13.8°, 24.7° and 29.3° corresponding to (011), (002), (022), and (202) diffiraction planes (Mirică et al., 2021) and is comparable to that previously described in literature (Kader et al., 2020; Sabbagh et al., 2019). The drug loading reduced the crystallinity of the unloaded hydrogel (H2-G3), confirming the amorphous characteristics of MTZ-H2-G3. Furthermore, the XRD pattern of the MTZ-H2-G3 hydrogel reveals the drug's molecular miscibility and interaction with the polymer matrix.

The diffractograms of the polymer CS, SALG, hydrogels B1-C1 to B1-C5, AMX-B1-C1, and MTZ-B1-C1 are shown in Figure 4.14. SALG is typically a semi-crystalline natural polymer due to the robust intermolecular hydrogen bonding within its chains. The SALG diffractogram (Figure

4.14a) displays peaks at 2θ values of 13.6º due to the diffiraction of their (110) plane from the polyguluronate unit at 21.5º due to the diffraction their (200) plane from polymannuronate and, at 39º due to the diffiraction from the amorphous halo area of SALG chains (Kaur et al., 2022). As mentioned above CS displays characteristic diffraction peaks at 2θ values of 9.6º and 20.2º, which match the (020) and (200) planes, respectively.

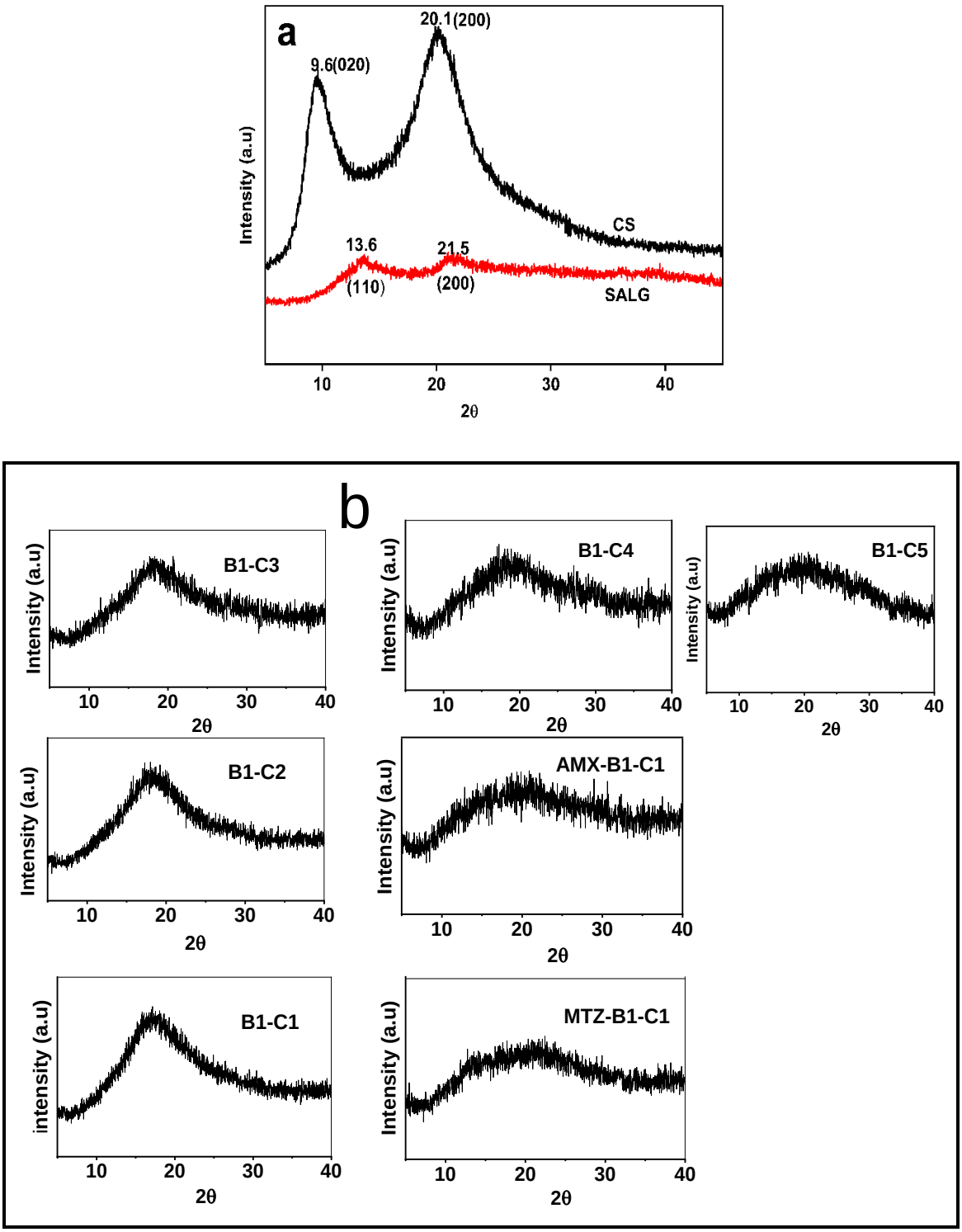

Figure 4. 14 XRD diffractograms of (a) SALG and CS (b) hydrogels B1-C1to B1-C5, AMX-B1-C1, and MTZ-B1-C1.

In the case of SALG/CS hydrogels, crosslinking of SALG and CS resulted in the disappearance of the characteristic XRD peaks of each polymer component because of the crosslinking between the anionic end (COO-) of SALG and the cationic end (NH_3^+) of CS. In the XRD spectra of hydrogels B1-C1 to B1-C5 (Figure 4.14b), with increasing $CaCl_2$ amount, the CS and SALG peaks shifted and broader peak ranging between 2θ values of 17º- 30º observed suggested the increase in the amorphous nature of the crosslinked hydrogels (loss in crystallinity). Both the inter- and intra-molecular hydrogen bonding between the amino (NH_2) and hydroxyl (OH) groups of CS chains, as well as between the COOH groups of SALG, increase the polymers' chain-to-chain secondary bonding (orders), thus enhancing crystallinity. However, when double crosslinked SALG/CS hydrogels are formed, the hydrogen bonds between the amino (NH_2) and hydroxyl (OH) ends of CS as well as between the COOH groups of SALG are disrupted due to crosslinking effect, resulting in amorphous frameworks (semi-crystalline structure) of SALG /CS matrix (Wang et al., 2017).

As the amount of $CaCl_2$ increased, the hydrogels' reducing crystallinity with the absence of well defined scattering planes obseved in B1-C4 and B1-C5 further suggests that the ionic crosslinking between SALG and CS caused their outstanding compatibility. In the drug-loaded hydrogels (AMX-B1-C1 and MTZ-B1-C1), the XRD patterns are similar to the unloaded hydrogels. The sharp peaks observed in the diffraction patterns of pristine AMX and MTZ are suppressed, probably due to the predominance of the amorphous charactersitic of the drug-loaded hydrogels, revealing the drug's molecular miscibility and interaction with the polymer matrix (Nia et al., 2020). The results confirm that AMX and MTZ are successfully loaded into the hydrogels.

4.7. Thermal stability

TGA was used to examine the thermal stability of the polymers, the synthesized drug loaded and unloaded hydrogels. Figure 4.15 displays the thermograms of CS, PVP, unloaded hydrogels (H2-G2, H2-G3, H2-G3), and hydrogels loaded with drugs (AMX-H2-G3 and MTZ-H2-G3). The mass loss percentage and corresponding temperature range of the thermograms of the hydrogels are shown in Table 4.1. The figure indicates three distinct degradation phases visible on the thermogram curve for CS. The initial weight loss phase of approximately 7% up to temperature of 105 °C is attributable to the removal of readily eliminated unbound (free) water that is not interacting through secondary interactions, and is followed by a slow rise until 214 °C with an additional weight loss of approximately 8% owing to the elimination of trapped water. The subsequent weight loss phase of approximately 32% occurs between temperature ranges of 214 °C to 367 °C is due to partial polymer decomposition, and the final phase of weight loss to 700

°C is attributable to total decomposition of the polymers with an ultimate residual weight of 17%. PVP also exhibits three stages of decomposition.

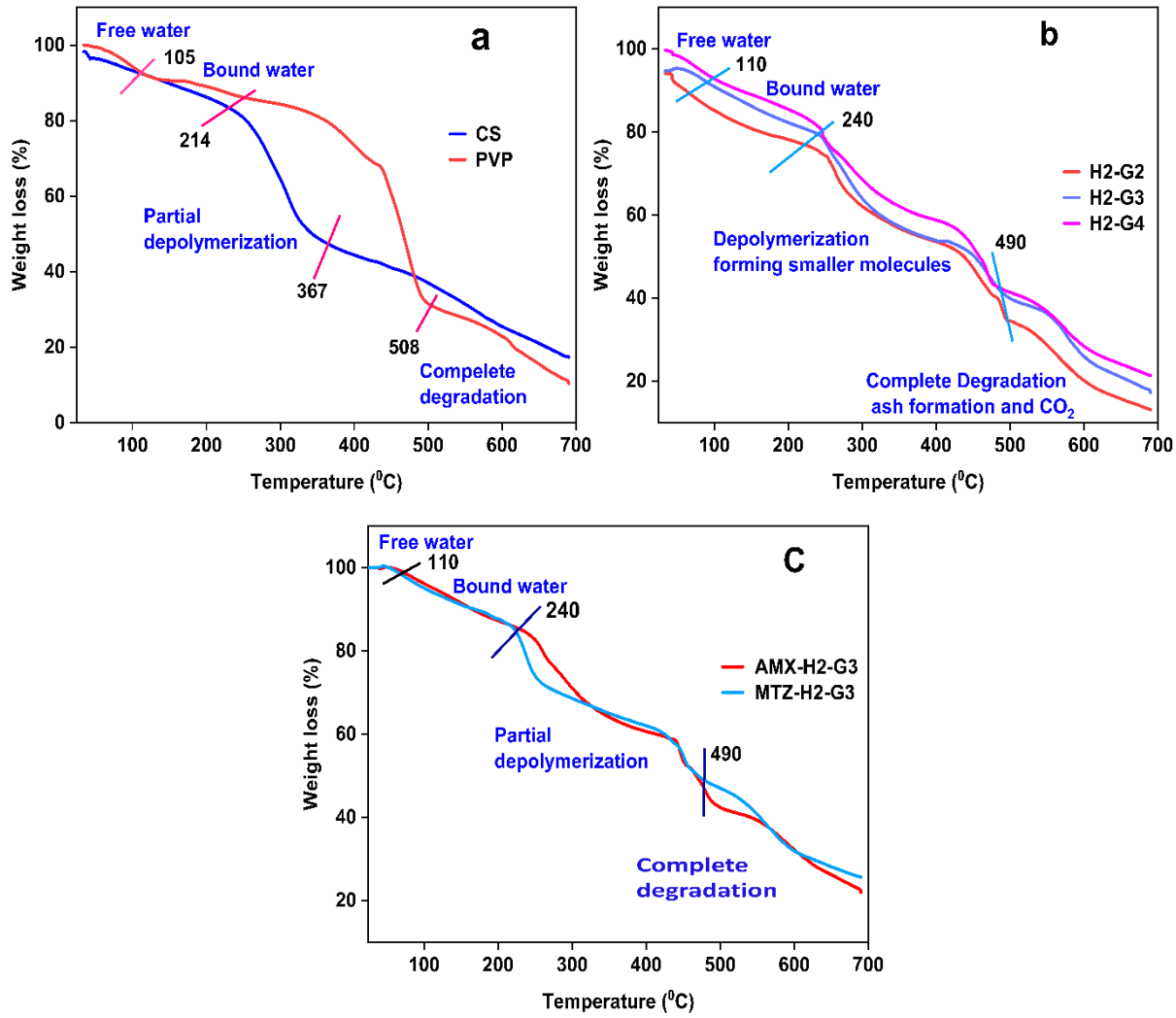

Figure 4. 15 TGA thermograms of a) pristine CS, PVP, b) hydrogels H2-G2 to H2-H4 c) AMX-H2-G3, and MTZ-H2-G3.

The initial weight loss phase of 9.0% occurs from 45 °C to 135 °C owing to the removal of bound water, subsequently followed by a slope from 135 °C through 238 °C with weight loss of approximately 5% attributable to the evaporation of the bound water. The next weight loss phase of approximately 56% from 238 °C to 508 °C is caused by partial polymer decomposition, and the final (third) phase up to 700 °C is owing to the total decomposition of polymers with a final residual weight of 10%. Figure 4.15 also indicates that unloaded hydrogels (H2-G2, H2-G3, H-G4) and drug-loaded hydrogels (AMX-H2-G3 and MTZ-H2-G3) pass through four weight loss phases. The initial phase of weight loss is noticed for each of the hydrogels up to 110 °C. The subsequent phase of weight loss is noted till 240 °C owing to the removal of unbound water, which can be readily eliminated because it is non-interaction, above which the elimination

freezing water forming weak interactions with both polymer components (CS and PVP) and bound water forming hydrogen bonding.

As shown in the figure 4.15, the mass loss percentage in each step is different for the hydrogels, owing to their difference in water absorption capacity. The thermal robustness of these instances is also associated with covalent links among CS chains and the crosslinker (glutaraldehyde), as well as the interactions involving hydrogen bonds with PVP (Archana et al., 2015). The third weight loss phase occurs at 490 °C owing to the partial decomposition of the polymers and the breakdown of secondary forces among the polymer components and the crosslinking agent. The final weight loss phase occurs in the temperature range of 490 °C to 700 °C forming stable aromatic compounds, CO_2 and ash because of the complete hydrogel degradation.

Table 4. 1: Weight loss percentage and corresponding temperature range of CS/PVP hydrogels

Hydrogel Sample Code	**Degradation phases**								**Char yield at 700 °C (%)**
	I		**II**		**III**		**IV**		
	wt . loss (%)	Temp. **(°C)**	**wt . loss (%)**	Temp. **(°C)**	**wt . loss (%)**	Temp. **(°C)**	**wt . loss (%)**	Temp. **(°C)**	
CS	15	25-214	32	214-367	83	367- 700			17
PVP	14	25-238	56	238-508	90	508-700			10
H2-G2	9	25-110	19	110-240	58	240-490	82	490-700	18
H2-G3	5	25-110	15	110-240	56	240-490	78	490-700	22
H2-G4	5	25-110	14	110-240	56	240-490	79	490-700	22
AMX-H2-G3	6	25-110	14	110-240	54	240-490	83	490-700	17
MTZ-H2-G3	5	25-110	16	110-240	48	240-490	76	490-700	24

The thermograms of the drug-loaded hydrogels (AMX-H2-G3 and MTZ-H2-G3) similarly display four weight loss phases. The initial weight loss observed in the temperature range of 33 °C to 175 °C, results in a 10% mass reduction due to unbound water loss. The next phase weight loss is recorded in the temperature range of 175 °C to 238 °C exhibiting a weight loss of approximately 16% due to partial degradation of the polymer. The third weight loss phase happened in the temperature range of 238 °C to 516 °C, with weight loss of around 38% due to the breaking of glycoside linkage, producing smaller molecules such as acetic acid, butyric acid, smaller fat acids and other volitile products. The last phase of thermal degradation observed between 516°C and 700°C with a final mass remains of 24% corresponds a decomposition stage foring a more stable aromatic compounds from the polymers (Kader et al., 2020).

For the SALG/CS hydrogels, the thermograms of SALG, CS, the unloaded hydrogels (B1-C1, B1-C1, B1-C1, B1-C1, and B1-C5), and the drug-loaded hydrogels (AMX-B1-C1 and MTZ-B1-C1) are presented in Figure 16. The mass loss percentage and corresponding temperature range of SALG/CS based hydrogels are shown in Table 4.2. The thermogram of SALG indicates three

thermal degradation phases. In the initial phase, the temperature is raised to 158 ºC with a weight loss of around 12% caused by the loss of water, which includes unbound water (that evaporates between 40 ºC to 60 ºC), water interacting with OH groups (which is released till 120 ºC), and water linked to -COOH group, which is released till 205 ºC (Wang et al., 2022).

Table 4. 2: Mass loss percentage and corresponding temperature range of SALG/CS hydrogels.

Hydrogel Sample Code	**Degradation steps**						**Char yield (residue) at 700 ºC**
	I		**II**		**III**		
	wt . loss (%)	Temp. **(ºC)**	**wt . loss (%)**	Temp. **(ºC)**	**wt . loss (%)**	Temp. **(ºC)**	
CS	15	25-214	32	214-367	83	367-700	17
SALG	16	25-205	38	205-345	73	350-700	26
B1-C1	14	25-220	50	220-380	77	380-700	23
B1-C2	13	25-220	51	220-380	75	380-700	25
B1-C3	13	25-220	54	220-380	74	380-700	26
B1-C4	12	25-220	56	220-380	74	380-700	26
B1-C5	11	25-220	58	220-380	72	380-700	28
AMX-B1-C1	14	25-220	50	220-380	75	380-700	25
MTZ-B1-C1	13	25-220	53	220-380	79	380-700	21

The next phase of weight loss, a pronounced main decomposition stage, observed in the temperature range of 205 ºC to 345 ºC, with a mass loss of approximately 38%, is attributed to the complexity of decomposition of SALG chains (glucosidic bonds), resulting in the formation of water (H_2O), methane (CH_4), and the emission of carbondioxide (CO_2) by the carboxylate (COO-) groups, as well as the formation of sodium carbonate (Na_2CO_3). The third mass loss of approximately 26% noted in the temperature range of 350 ºC to 700 ºC is related to the decomposition of SALG fragment units into Na_2CO_3, which further decompose to NaO and CO_2. A final weight residue at 700 °C is approximately 22.7% is obtained. As discussed above CS shows three distinct degradation phases with initial weight loss phase about 105 °C due to free water loss which extended up to 214 °C, the second weight loss phase occured between 214 °C and 367 °C (partial polymer decomposition) and the final weight loss to 700 °C (due to total polymer decomposition) with an ultimate residual weight of 17%.

Thermograms of the hydrogels B1-C1 to B1-C5, AMX-B1-C1, and MTZ-B1-C1 (Figure 4. 16) show that mass loss occurs in three phases. In general, in comparison with SALG and CS, all the cross-linked hydrogels (B1-C1 to B1-C5) exhibited less unbound water mass loss during the initial phase. They needed higher temperatures for the release of the water taken up, equal to approximately 175 ºC. The absorbed water was more tightly immobilized between the cross-linked CS networks. The interactions of the polymers reduce their functional ends, resulting in a

decreased water absorption capacity of the hydrogels (Rassu et al., 2016). The hydrogels are more thermally stable as crosslinking density increases, as evidenced by the increasing temperatures at which 10% weight loss occurred with increasing $CaCl_2$ content.

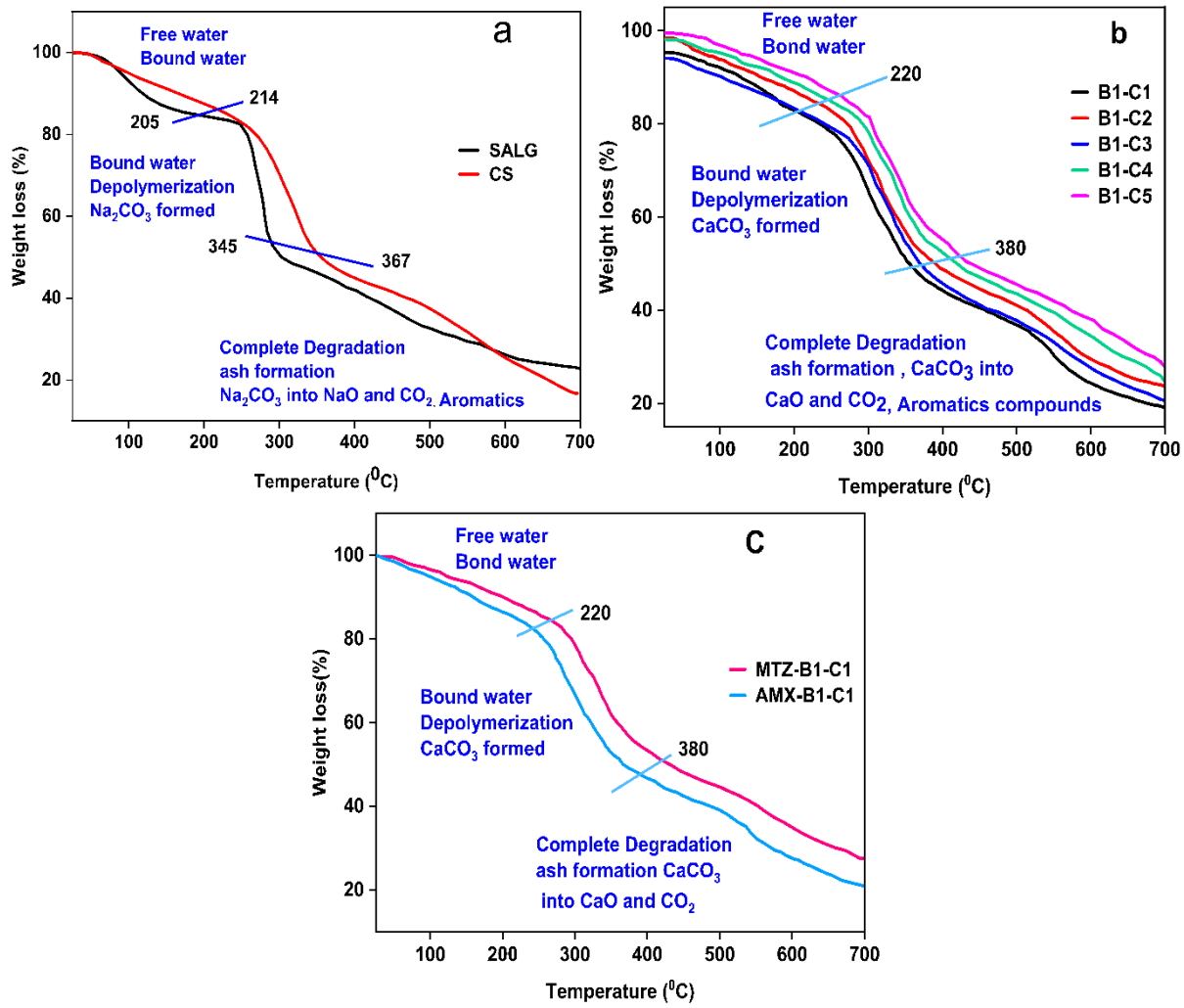

Figure 4. 16 TGA thermograms of a) pristine SALG and CS, b) hydrogels B1-C1 to B1-C5, an and c) MTZ-B1-C1.

Beyond 220 ºC, the most significant changes occur. The second, most crucial weight loss phase takes place between approximately 220 ºC and approximately 380 ºC and entails the release of trapped water to the functional end of both polymers (SALG and CS) that was not eliminated during the initial phase of water release, the partial decomposition of the polymers. The subsequent weight loss occurs between approximately 380 ºC to 700 ºC and is related to the breaking of glycoside linkage, producing smaller molecules such as acetic acid, butyric acid, smaller fat acids and evantually forming stable aromtic compounds and ash (Naghshineh et al., 2019). The crosslinking of SALG with CS improve the thermal stability of the hydrogels. In overall, the temperature ranges where the polymers thermal decompositions of the hydrogels

occurs is greater than the typical human body temperature (37.2ºC), implying that hydrogels are appropriate for oral CDDSs.

4.8. Gel fraction

The gel content represents the covalent linkage of polymer networks, which is directely related to the stiffness of a polymer chain structures (Gower & Shanks, 2004; Mondal et al., 2018). In their pristine state, CS chains are fragile, with unpredictable porosity and quick breakdown in the acidic conditions of the stomach. Because of their poor capability to control drug release, they are limited in their utility for drug administration through the oral route. Similarly, hydrogels of PVP alone exhibit weak mechanical charactersitics and swelling properties. By crosslinking PVP with CS, structures with features including controllable porosity can be resulted, which is required for drug delivery applications. Furthermore, the degree of CS cross-linking in the polymer matrix determines the quality of the hydrogel structures, which consecutively effects the mechanical and water absorbing capabilities of the hydrogels.

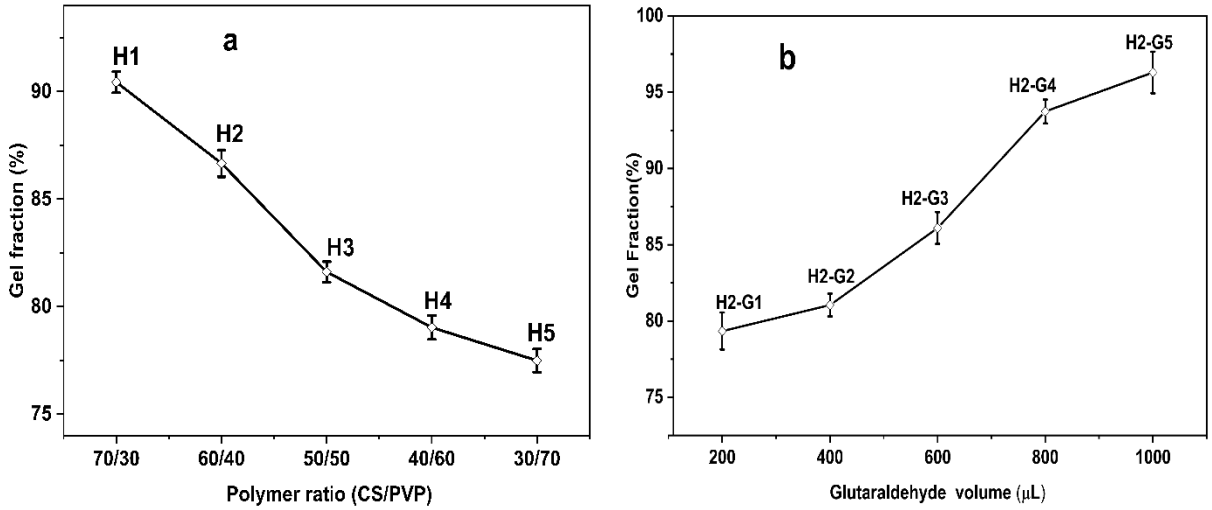

Figure 4. 17 Gel fraction of (a) hydrogels H1 to H5 as a function of CS/PVP ratio and (b) hydrogels H2-G1 to H2-G5 as a function of glutaraldehyde concentration.

Figure 4.17(a) shows a progressive reduction in the gel fraction percentage from approximately 82% for the hydrogel H1(CS/PVP, 70/30 wt.%) to approximately 71% (Appendix IV, a) for the hydrogel H5 (CS /PVP, 30/70 wt.%). The results reveal that while crosslinking of CS with glutaraldehyde happens during hydrogel preparation, the gel fraction reduces owing to the rising PVP percentage, which is highly hydrophilic polymer. Furthermore, the reduction of gel fraction is not significant in an interval of approximately 11%, meaning that at a fixed glutaraldehyde concentration of 200 μL and when the CS percentage decreases, improved cross-linking of the CS chains is to be anticipated, that is insufficient to overcome the viscosity effect. Figure 4.17b indicates for the hydrogel H2(CS/PVP, 60/40 wt.%), increasing glutaraldehyde

concentration from 200 µL to 1000 µL leads to increase in gel content from approximately 79% (H2-G1) to 96% (H2-G5) with about 17% increment. The results show that CS is partly cross-linked at a glutaraldehyde concentration of 600 µL (H2-G3) and nearly entirely cross-linked at glutaraldelyde concentration of 1000 µL, despite having a high gel content of around 86%. The considerable reduction in swelling ratio and porosity of the hydrogels H2-G4 and H2-G5 owing to the restricted mobility of polymer networks reflects the significant stiffness of these materials as a result of their high gel contents (Wong et al., 2015). Figure 4.18(a, b) indicates the gel fractions of the hydrogels B1 to B5 and hydrogels B1-C1 to B1-C5, respectively. Figure 4.18a indicates that hydrogel B1 (SALG / CS, 75/25 wt.%) has the lowest gel content of approximately 77%, and hydrogel B5 (SALG / CS, 25/75 wt.%) has the highest gel content of around 90%, indicating that gel fraction increases with CS percentage. As the crosslinking density of the SALG/CS hydrogel increases, a compact and interconnected network structure develops, resulting in a reduced rate of dissolving medium entry into the polymer matrix.

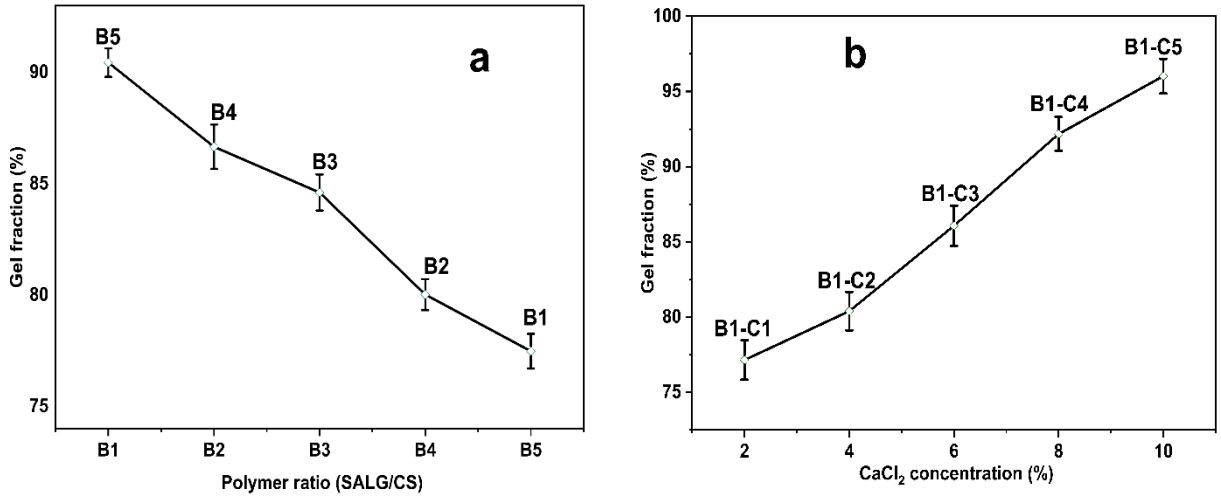

Figure 4. 18 Gel fraction of (a) hydrogels B1 to B5 and (b) hydrogel B1 as a function of $CaCl_2$ concentration.

The gel content of the select hydrogel B1 as a function of concentrations of calcium chloride ($CaCl_2$) is presented in Figure 4.18b. It is observed from the figure that as the $CaCl_2$ concentration in hydrogel B1 (SALG/CS ratio 75/25) is increased from 2% (B1-C1) to 10% (B1-C5), the gel content increased in a range of approximately 19% from approximately 77% (B1-C1) to about 96% (B1-C5) (Appendix IV, d). The gel fraction increases as $CaCl_2$ content rises, leading to the formation of rigid hydrogel networks. Moreover, as more Ca^{2+} ions interact with the carboxyl groups (COOH) of SALG, the quantity of carboxylate (COO-) groups decreases. As a result, the electrostatic repulsion between the carboxylate (COO-) groups of SALG reduces, and the

hydrogel mixture change into compact and stronger networks which resist the entrance of the dissolving medium (water) at higher rates (Ibrahim et al., 2014; Rassu et al., 2016).

4.9. In vitro biodegradation assay

In vitro, biodegradation refers to the breakdown of larger polymeric material into smaller molecules in simulated physiological fluids. The tests evaluate the biodegradability of hydrogels in simulated physiological fluids determining the drug's diffusion and release rates. It is associated to the crosslinking density of the hydrogels. Because of their superior biodegradability and ease of clearance after a useful lifetime, CS and PVP-based hydrogels have received attention for CDDSs. Figure 4.19 illustrates the in vitro biodegradation of the unloaded hydrogels (H2-G1, H2-G2, H2-G3, H2-G4, and H2-G5) in SCF (pH 7.4) at human body temperature (37.2 ºC) for 30 days as a function of increasing crosslinker concentration. The figure demonstrates that the degradation pattern of the hydrogels is similar, with the main difference being a decrease in mass loss with increasing glutaraldehyde concentration. H2-G1, H2-G2, H2-G3, H2-G4, and H2-G5 hydrogels showed weight loss of approximately 95%, 89%, 78%, 66%, and 56%, respectively in 30 days (Table 4.3).

Table 4. 3: In vitro biodegradation assay of CS/PVP based hydrogels.

Days	H2-G1	SD	H2-G1	SD	H2-G3	SD	H2-G4	SD	H2-G5	SD	AMX-H2-G3	SD	MTZ-H2-G3	SD
30.00	4.23	3.41	10.63	2.11	22.09	2.41	34.15	2.31	43.74	1.34	28.15	1.81	24.09	2.41
27.00	6.40	2.45	15.61	2.43	24.16	2.25	35.90	1.85	45.31	1.75	30.90	1.95	26.16	2.25
25.00	7.72	3.24	17.29	2.25	27.12	1.96	36.43	2.45	47.22	1.64	34.43	1.95	29.12	1.96
23.00	9.98	3.12	20.90	2.32	29.61	1.82	39.75	1.87	50.21	1.95	36.75	1.77	31.61	1.82
21.00	15.35	2.75	23.24	2.71	30.06	1.62	42.53	1.81	53.55	2.12	39.53	1.81	32.06	1.62
19.00	17.40	2.14	26.90	2.13	33.54	1.91	49.50	2.24	58.77	1.17	43.50	2.04	35.54	1.91
17.00	20.86	2.50	29.51	2.31	40.89	2.45	52.27	1.62	59.76	1.34	45.27	1.72	43.89	2.45
15.00	25.91	1.82	33.88	2.12	49.92	1.91	60.23	1.92	68.14	1.72	52.23	1.92	51.92	1.91
13.00	28.44	2.27	43.56	1.65	52.56	2.51	62.17	2.34	71.17	1.43	55.17	1.84	54.56	2.51
11.00	39.51	2.58	50.15	2.87	59.52	1.88	69.21	1.74	82.85	1.72	62.21	1.64	61.52	1.88
9.00	48.02	3.18	64.87	2.17	70.62	2.41	78.31	2.08	87.36	1.82	73.31	1.78	71.62	2.41
7.00	67.56	2.05	72.41	1.98	81.40	2.11	88.24	1.85	94.10	1.83	83.24	1.58	81.90	2.11
5.00	72.84	2.75	81.32	2.05	87.97	1.84	90.92	1.69	97.14	1.88	88.92	1.46	88.97	1.84
3.00	77.35	2.46	83.17	2.62	89.95	1.97	94.20	1.59	98.77	1.61	90.20	1.49	90.95	1.97
1.00	87.21	1.84	90.88	1.93	94.68	1.95	97.60	1.78	99.58	1.75	95.60	1.68	94.81	1.95

The in vitro biodegradations of the drug-loaded hydrogels AMX-H2-G3 and MTZ-H2-G3 are observed to be lower than that of the corresponding unloaded hydrogel (H2-G3) with a weight loss of about 62% and 66%, respectively in 30 days. This might be associated with improved interactions among the polymer matrixes, and the drug forming a more stable crosslinked structure. The mass loss pattern also demonstrates that, regardless of the glutaraldehyde

concentration, the rate of disintegration is considerably slower between days 1 and 7 and then increases to a maximum between days 7 and 17. The degradation rate starts to decline between days 17 and day 30. CS itself is not stable in moist conditions because of the hydrophilic ends of CS (-NH_2 and -OH), which cause hydrolytic breakdown of the polymer (El Achaby et al., 2014).

PVP is also hydrophilic polymer, however when combined with CS, the -NH_2 and -OH groups of CS crosslinking with the C=O groups of PVP to produce an intricate 3D network, resulting in a more hydropobic structure. Additionally, due to the stereoregularity of the carbon and hydrogen atoms in their chains, CS and PVP combine to produce helical structures that are slightly hydrophobic (Garakani et al., 2020). The polymer blend's hydropobicity is further strengthened by CS crosslinking in CS/PVP hydrogels, which increases with glutaraldehyde concentration in the present investigation results. This suggests that, despite the formation of highly dense crosslinked networks, some excess amine (-NH_2) and hydroxyl (-OH) groups still exist in CS networks. These residual non-interacting groups (-NH_2, -OH, and -C=O) are accountable for the hydrolytic decomposition of the crosslinked CS/PVP hydrogels (El Achaby et al., 2014; Najaf et al., 2019). The degradation proceeds via the breaking down of internetworks connections of CS, PVP, and glutaraldehyde as well as the disruption of secondary forces.

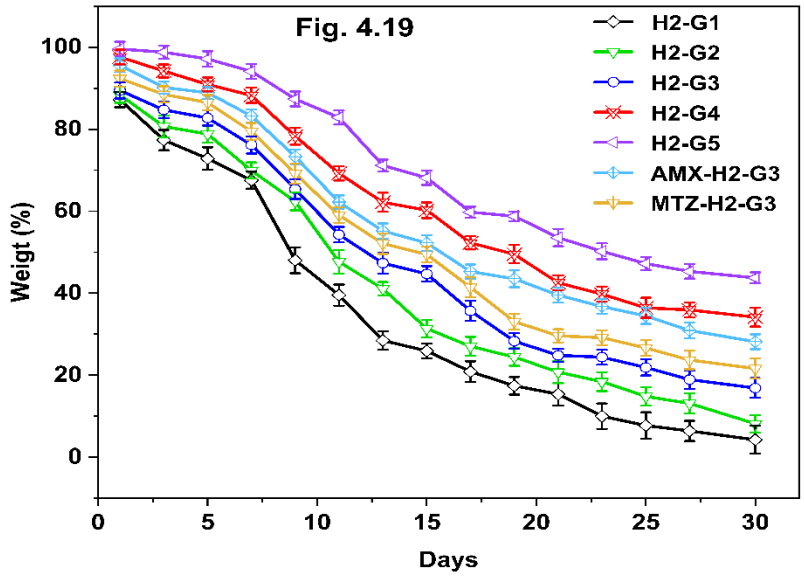

Figure 4. 19 In vitro degradation of hydrogels H2-G1 to H2-G5 in SCF (pH 7.4) at 37 ºC.

The degradation (in vitro) pattern of the SALG/CS based unloaded hydrogels (B1-C1, B1-C2, B1-C3, B1-C4, and B1-C5) and drug-loaded hydrogels (AMX-B1-C1 and MTZ-B1-C1) performed in simulated colon fluid (pH 7.4) at human body temperature (37.2 °C) for 30 days is presented in Figure 4. 20. It is observed from figure that with the sole variation of decrease in mass loss as the crosslinker ($CaCl_2$) concentration increases, the hydrogels display similar

degradation pattern. Hydrogels B1-C1 and B1-C2 degraded at a relatively higher rate and reached weight loss of 39.58 % and 35.38%, respectively, between day 1 and day 7. While hydrogels B1-C3, B1-C4, and B1-C5 showed weight loss of approximately 24.5%, 14.8%, and 11.5% within the first 7 days. The hydrogels B1-C1, B1-C2, B1-C3, B1-C4, and B1-C5 showed weight loss of approximately 80%, 66%, 55%, 44%, and 33% respectively in 30 days (Table 4.4). The decrease in weight loss with increasing $CaCl_2$ concentration is caused by an increase in the SALG polymer inter-networking with Ca^{2+} linked to the polyguluronic acid units of the SALG chains, resulting in a more rigid and compact "egg-box" dimer structures (T.Wu et al., 2018).

The Na^+ in the physiological fluid replaces the Ca^{2+} that connects the SALG chains via physical ionotropic interactions in the polymannurate units, which loosens the egg-box frameworks and causes degradation of the hydrogel (erosion). In SCF, CS is more stable due to its increased amount of amine (NH_2) groups, which help to retain the structural integrity of the hydrogel via electrostatic and hydrogen bonding interactions, hence decreasing the degree of swelling and prolonging hydrogel degradation.

Table 4. 4: In vitro biodegradation assay of SALG/CS/ based hydrogels.

Days	B1-C1	SD	B1-C2	SD	B1-C3	SD	B1-C4	SD	B1-C5	SD	AMX-B1-C1	SD	MTZ-B1-C1	SD
1.00	7.87	1.18	7.20	1.69	4.45	1.78	1.15	1.78	1.00	1.66	4.93	1.18	5.93	1.66
3.00	22.20	2.53	15.69	1.44	8.98	1.54	3.55	1.54	2.38	1.85	11.80	2.53	13.80	1.85
5.00	32.06	2.59	27.91	2.03	18.54	1.28	10.00	1.28	5.81	2.47	21.99	2.59	23.99	2.47
7.00	39.58	2.34	35.38	1.60	24.55	2.55	14.84	2.55	11.50	2.47	26.78	2.34	28.78	2.47
9.00	46.18	2.43	37.26	1.91	28.41	3.20	18.47	3.20	13.22	2.09	31.14	2.43	33.14	2.09
11.00	49.61	2.74	42.95	1.26	31.99	1.98	20.93	1.98	15.02	1.34	36.06	2.74	38.06	1.34
13.00	57.87	1.38	47.60	1.64	35.27	3.52	24.54	3.52	17.01	2.32	39.28	1.38	41.28	2.32
15.00	61.34	2.29	50.55	2.46	39.39	1.12	26.51	1.12	19.84	2.07	43.72	2.29	45.72	2.07
17.00	67.30	2.31	55.70	1.79	43.85	2.31	29.56	2.31	23.21	2.37	45.65	2.31	47.65	2.37
19.00	68.99	1.95	58.00	1.23	45.65	2.31	34.83	2.31	25.88	2.48	48.38	1.95	50.38	2.48
21.00	71.23	2.31	60.38	1.07	48.37	2.42	37.69	2.42	28.04	1.83	51.88	2.31	53.88	1.83
23.00	75.12	1.61	63.09	1.80	50.93	2.73	39.82	2.73	29.22	2.20	53.16	1.61	55.16	2.20
25.00	76.21	1.74	63.94	1.37	52.74	3.39	41.58	3.39	30.34	2.73	55.88	1.74	57.88	2.73
27.00	77.76	2.26	64.87	1.14	53.32	3.04	43.02	3.04	32.04	2.22	58.07	2.26	60.07	2.22
30.00	79.56	1.73	66.69	1.07	55.40	2.09	44.28	2.09	33.67	2.06	60.09	1.73	62.09	2.06

The degradation of the drug-loaded hydrogels AMX-B1-C1 and MTZ-B1-C1 are observed to be lower than that of the corresponding unloaded hydrogel B1-C1 with a weight loss of about 60% and 62.09% in 30 days respectively. As previously noted, the weight loss trends could be attributed to enhanced interactions among the polymer matrixes and the drugs, leading to enhanced crosslinked frameworks. In general, the decomposition rate of the SALG/CS hydrogels in this work is low due to the double-crosslinking of SALG and CS using $CaCl_2$ and glutaraldehyde crosslinking agents, allowing the hydrogels endure the impacts of GI fluids for

AMX and MTZ in CDDSs. The in vitro degradation of the SALG/CS hydrogels in the present study is in good agreement with the literature (Sharma et al., 2016).

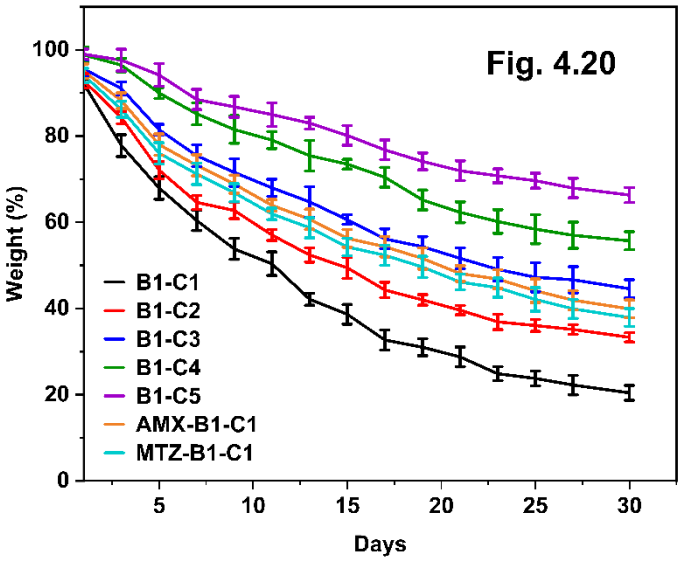

Figure 4. 20 In vitro degradation of hydrogels B1-C1 to B1-C5 in SCF at 37 ºC for 30 days.

4.10. Morphology

Figure 4.21 illustrates the FESEM images of the morphology of the hydrogels H2-G2 to H2-G5, AMX-H2-G3, and MTZ-H2-G3. Figure 4.21(a-e) illustrates that the dimensions of the pore networks increase when the glutaraldehyde concentration increases from 200 µL to 600 µL (H2-G1 to H2-G3). Increasing the glutaraldehyde concentration from 800 µL (H2-G4) to 1000 µL (H2-G5) reduces the size of the pores. The pore size distributions of the hydrogels H2-G1, H2-G2, H2-G3 and H2-G4, and H2-G5 are about 64 ± 14 µm, 81 ± 20 µm, 132 ± 42 µm, 44 ± 21 µm, and 32 ± 17 µm respectively. Hydrogel AMX-H2-G3 (Figure 4.21f) shows a pore dimension of approximately 117 ± 18 µm. The increasing swelling ratio in SGF, SIF, and SCF till for H2-G3 (discussed in section 4.3) is associated with this increased porous structure. For H2-G4 and H2-G5, the pore dimension reduction with increasing glutaraldeyde is associated with higher matrix crosslink denSification. The pores in the network structures of the hydrogels are areas in which water diffuses and serve as regions for interaction with external stimuli and the loaded drug in the hydrogels. Therefore, the pore structure of the hydrogel H2-G3 is considered a potent candidate for the controlled-release of the drugs (AMX and MTZ).

The electron microscopic images of AMX-H2-G3 and MTZ-H2-G3 indicate that AMX and MTZ are incorporated into the hydrogels. Because of the drug loading, the surfaces of the hydrogels AMX-H2-G3 and MTZ-H2-G3 appear compact. The morphology of the drug-loaded hydrogels (AMX-H2-G3 and MTZ-H2-G3) reveals the presence of interactions among the components and

the drugs, thus indicating their miscibility. Electron microscopic images of unloaded hydrogels (B1-C1, B1-C2, B1-C3, B1-C4, and B1-C5) and drug-loaded hydrogels (AMX-B1-B1 and MTZ-B1-C1) are shown in Figure 4.22 (a-g). Each hydrogel exhibits a porous outer layer framework, but the $CaCl_2$ concentration has a noticeable effect on the diameter (size), consistency, and depth of the hydrogel wall around the openings.

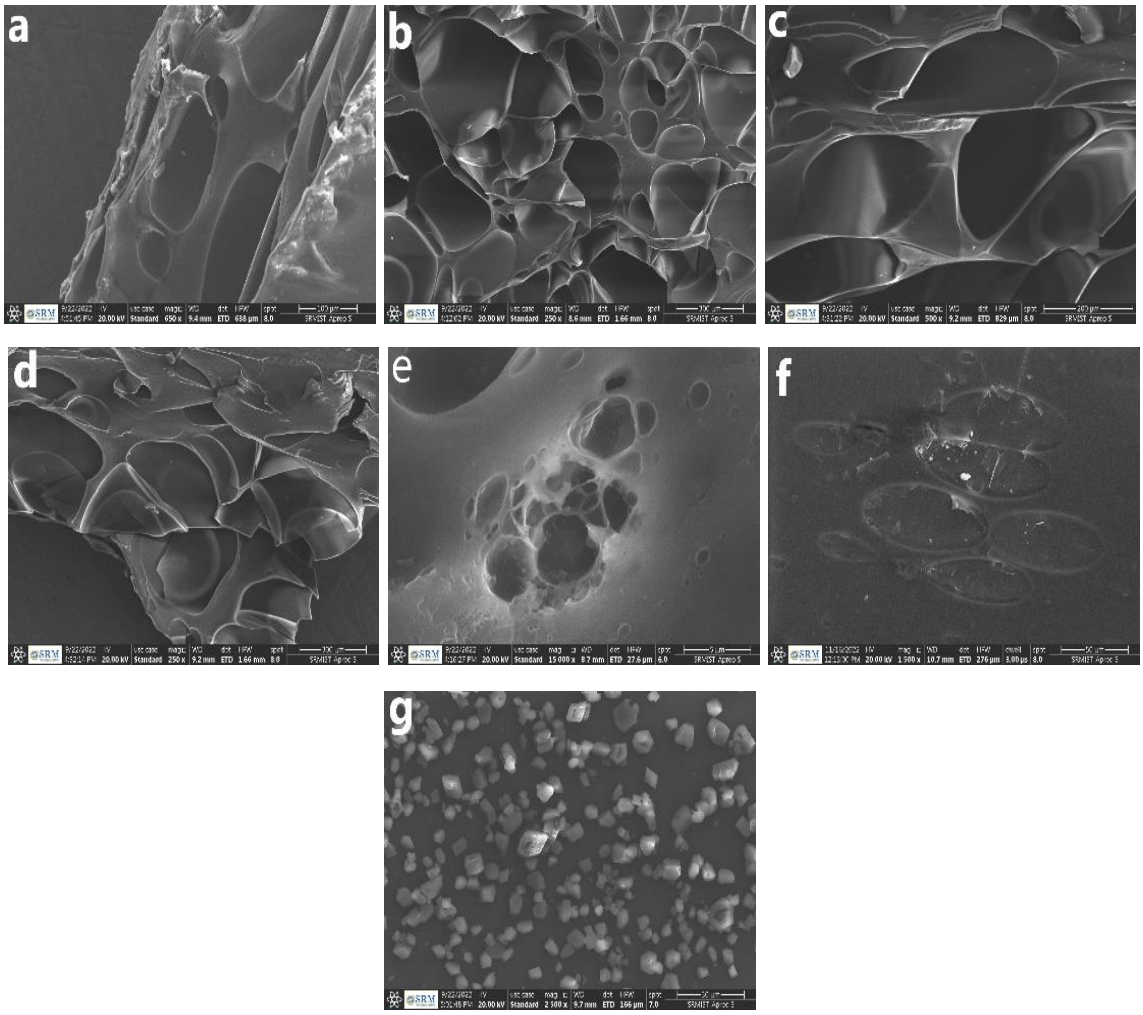

Figure 4. 21 FESEM micrographs of (a-e) hydrogels H2-G1 to H2-H5 and (f) AMX-H2-G3 (g) MTZ-H2-G3.

Figure 4.22(a-e) displays a porous, spongy, and rough three dimensional network frameworks of the hydrogels B1-C1 to B1-C5, which is used as water channels. As the concentration of crosslinker ($CaCl_2$) increases, so does the crosslinking density, resulting in more stiff and denser porous structures with smaller pores. The characteristics mentioned above of the hydrogels are consistent with their swelling capacities. For instance, hydrogels B1-C4 and B1-C5 have highly compact frameworks and small pores, which lessens the swelling capacity of the hydrogels.

The hydrogel AMX-B1-C1 (Figure 4.22f) has a surface appearance that is related to that of the corresponding unloaded hydrogel (B1-C1) which exhibits relatively the highest swelling ratio but is a more crosslinked three dimensional structure and less porous than B1-C1. This reveals the inclusion of AMX into the hydrogel. Figure 4.22g illustrates the hydrogel MTZ-B1-C1's surface appearance, which is comparatively densely granulated yet smooth surface, with less porous, revealing the miscibility of the drug particles into the polymer matrix. As a result, the electron micrograph of MTZ-B1-C1 indicates that MTZ particles are incorporated into the hydrogel. Thus, porous structure of the hydrogel is thought to be a strong option for the controlled release of AMX and MTZ.

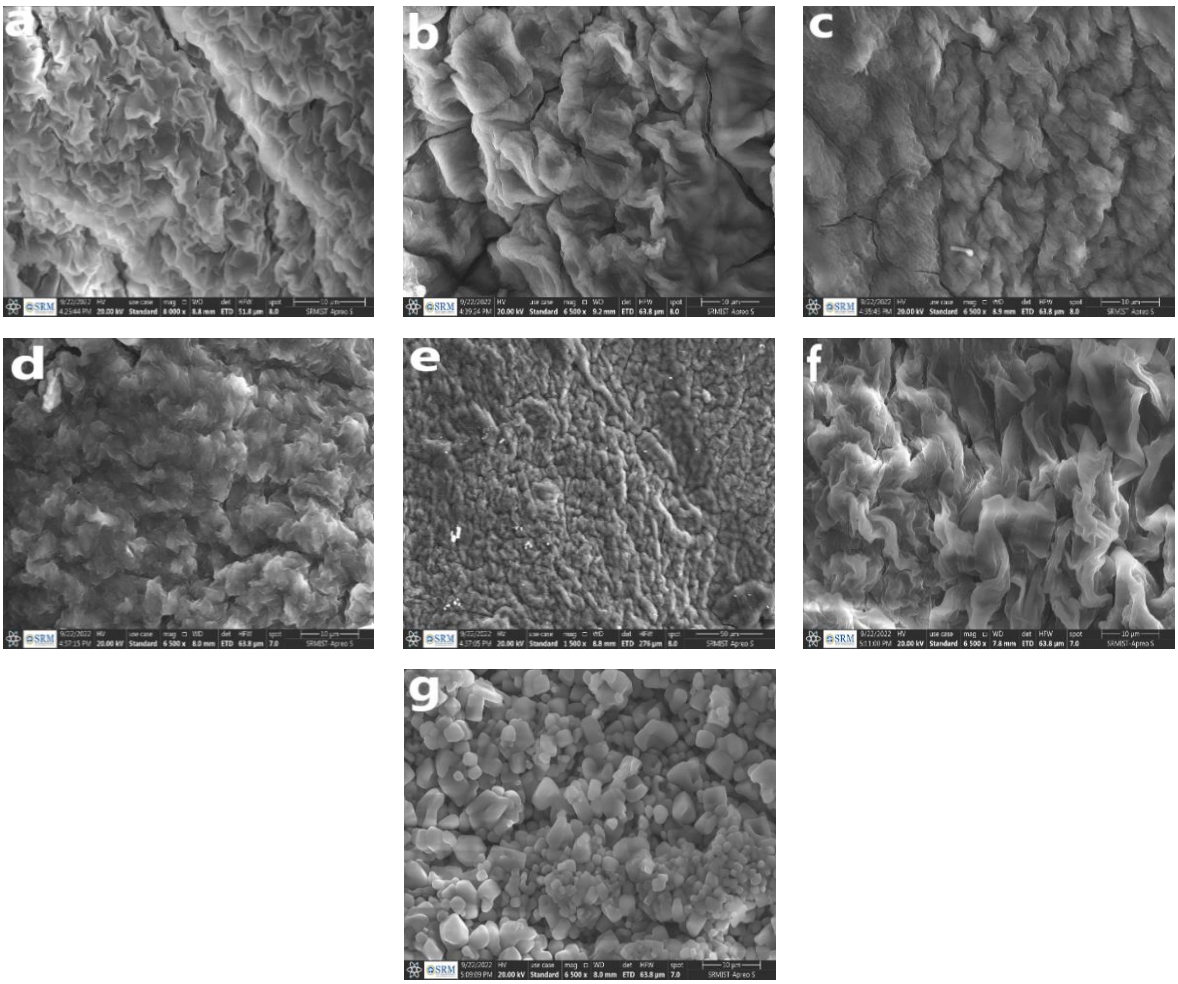

Figure 4. 22 FESEM micrographs of (a-e) hydrogels B1-C1 to B1-C5, (f) AMX-B1-C1 and (g) MTZ- B1-C1.

4.11. In vitro drug release

The cumulative drug release of the model drugs (AMX and MTZ) from the optimum hydrogel systems (H2-G3 and B1-C1) was studied in vitro for 25 hours in simulated physiological fluids of different pH including SGF (pH 1.2), SIF (pH 6.8), and SCF (pH 7.4) at human body

temperature (37.2 °C). Figure 4.23a indicates the cumulativee release patterns of the drug AMX from AMX-H2-G3 in each simulated physiological fluid. The cumulative release percentage of the drug (AMX) in SGF, SIF, and SCF is approximately 18.5%, 14.96%, and 12.45% in the first 2 hours, respectively (Appendix V, a). Subsequently, the release progressively increased in a monotonic pattern with time, regardless of the simulated physiological fluid pH. After that, regardless of pH the media, the release progressively increased linearly with time. At 25h, the cumulative percentage release of the drug in SGF, SIF, and SCF is about 61.25%, 55.24%, and 46.52%, respectively, revealing an anticipated effects of pH of the simulated physiological fluids because the CS/PVP hydrogel is a pH-responsive system determined by its swelling behavior. Figure 4.23b displays the cumulative release patterns of MTZ over 25 hours in SGF, SIF, and SCF at 37 °C with approximately 16.71%, 11.98%, and 7.22%, respectively in the first 2 hours (Appendix V, b). Following that, regardless of pH the releasing media, it progressively increased over time linearly. The cumulative drug release percentage in SGF, SIF, and SCF is approximately 71.03%, 58.22%, and 52.13%, respectively, at 25 hours.

Because the size of the drug particles is significantly smaller than the dimension of the pores of the drug-loaded hydrogels, AMX-H2-G3 (Figure 4.21f) and MTZ-H2-G3 (Figure 4.21g), the drug diffusion coefficient (release pattern) is related to the porosity of the hydrogels. Moreover, the drug release profile is determined by the degree of water up take capacity of the drug-loaded hydrogels in various swelling media. The uncrosslinked amine groups ($-NH_2$) of CS (pKa 6.3) in SGF (pH, 1.2) atract H^+ from the solution and become protonated forming ammonium cation (NH_3^+). An electrostatic repulsion force enhanced between the cationic polymer matrix leads to polymer relaxation and hence swelling, which rises the rate of drug release in the acidic (de Oliveira et al., 2018). Additionally, the entanglement of the rings PVP structure into the hydrogel networks provide void spaces, enabling additional volumes for physiological fluids (Garakani et al., 2020).

However, in slightly alkaline media [SIF pH (6.8) and SCF (pH 7.4)], the CS chain release H^+ (deprotonated) and forms hydrogen bonding with the hydrogel components and water decreasing rates of swelling and drug release. Both for AMX and MTZ in each physiological fluid, less than 25% of the loaded drugs were released in 4 hours. The percentage of the release of both AMX and MTZ is significantly low. The slow release rate of each drug implies it requires an extended-release time; because each drug has a slow release rate, prolonged release duration is required; thus, the hydrogels for each drug (AMX and MTZ) have the potential to be employed in CDDSs. The drug release pattern from the synthesized hydrogels in this study agrees with the findings of

other studies (Gull et al., 2020a; Rahimzadeh et al., 2021; Garakani et al., 2020). In addition, the interactions among the carbonyl groups (C=O) of PVP, the amino (-NH_2) and hydroxyl (OH) groups of CS chains, and the drugs functional ends cause the slower release of AMX and MTZ from the optimal hydrogels. It is reported that PVP can absorb a drug it is achieved by the hydrogen bonds, which cause a rapid release of the drug, especially when the ratio of CS to PVP is low in the structure of a hydrogel. However, if the content of CS is more than PVP, the release is delayed but not ultimately achieved because the release of the drug is prevented by the ordered domains of CS (Ipate et al., 2020). The optimal CS/PVP concentration in the present study contributes to the extended-release of AMX and MTZ, which is consistent with results previously reported in the literature (Xiong et al., 2016).

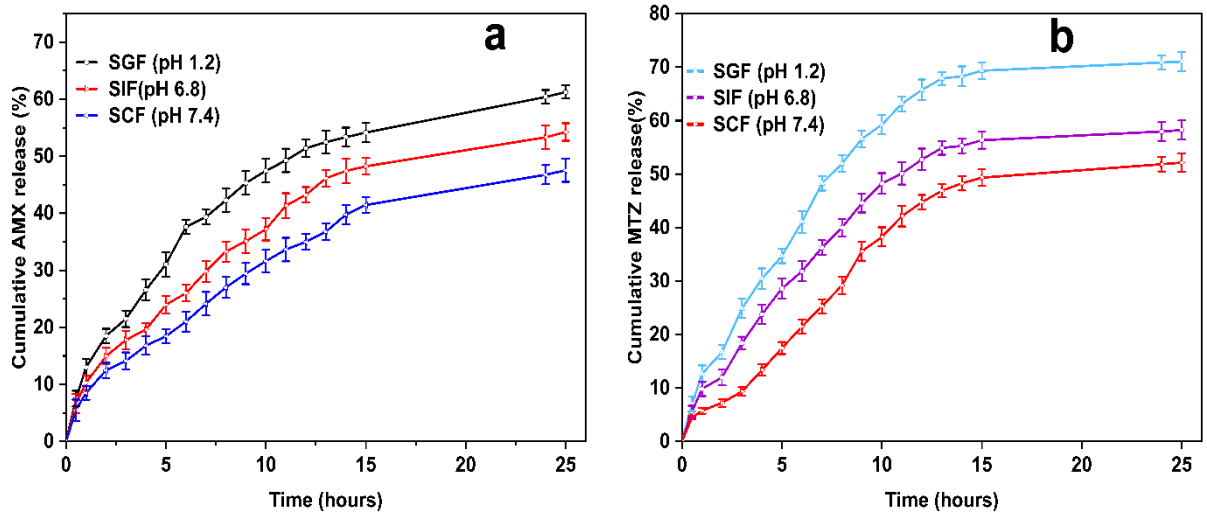

Figure 4. 23 Cumulative release of (a) AMX from hydrogel AMX-H2-G3, (b) MTZ from the hydrogel MTZ-H2-G3 in SGF, SIF, and SCF at 37.2 ºC.

In CDDS employing hydrogels, drug release behavior is strongly associated with release medium and hydrogel physical features including swelling behaviour and porosity. The swelling ratio of the optimal hydrogel (H2-G3) and the in vitro cumulative drug release data of AMX and MTZ from the drug-loaded hydrogels in each of the simulated physiological fluid (SGF, SIF, and SCF) were correlated by Pearson's correlation coefficient (r^2) at $P < 0.05$ using Origin 2021b software (Appendix VI, a and b). As expected, a strong positive correlation between swelling ratios and in vitro release pattern of AMX and MTZ in each physiological fluid was observed. For instance, for AMX-H2-G3, the correlation between the swelling ratio in SGF (SW-SGF) and the in vitro release data of the drugs in all three physiological fluids (DR-SGF, DR-SIF, and DR-SCF), a strong positive correlation with Pearson's correlation coefficients r^2 = 0.98369, 0.98119 and 0.97015 ($P < 0.05$) respectively.

For MTZ-H2-G3 hydrogel, the correlation between swelling ratio in SGF (SW-SGF) and the in vitro release data of each drug in all three physiological fluids (DR-SGF, DR-SIF, and DR-SCF) showed a strong positive correlation with Pearson's r^2 = 0.97941, 0.98106 and 0.97155 respectively. Furthermore, for AMX and MTZ, the correlations of the swelling ratios of the optimal hydrogel (H2-G3) in the SIF and SCF with the respective in vitro drug release in all three physiological fluids at $P < 0.05$ showed similar strong linear positive correlation trends. In all cases, the correlation coefficient's $p < 0.05$ indicated a significant linear dependence between swelling ratio and the cumulative AMX and MTZ release from H2-G3 in all the three physiological fluids, indicating that a greater degree of hydrogel swelliing enhances the rapid release of the drugs.

Figure 4.24 (a, b) exhibits the cumulative drug release pattern of AMX and MTZ from the optimal SALG/CS hydrogel (AMX-B1-C1 and MTZ-B1-C1) in each physiological fluid [SGF (pH 1.2), SIF (pH 6.8), and SCF (pH 7.4)] at 37.2 °C over 25 hours. The cumulative release percentage of AMX after two hour is approximately 13.58%, 15.72%, and 22.28% in SGF, SIF, and SCF, respectively. Following that, regardless of the variations in pH of the releasing media, the release profile exhibits a monotonic pattern as a function of time. At 25 hours, the cumulative drug release percentage of AMX in each physiological fluid SGF, SIF, and SCF is approximately 55.70%, 68.14%, and 74.34%, respectively at 37.2 ºC (Appendix VII, a). The cumulative release percentage of MTZ from the hydrogel MTZ-B1-C1 in in each physiological fluid SGF, SIF, and SCF at 37.2 ºC as a function of time is presented in Figure 4.24b.

The cumulative MTZ release percentage after two hours is approximately 13.02%, 19.34%, and 25.87% in SGF, SIF, and SCF, respectively (Appendix VII, b). Similar to AMX the release, following that, regardless of the variations in pH of the releasing media, the release profile exhibits a monotonic pattern as a function of time. At 25 hours, the cumulative drug release percentage in each physiological fluid SGF, SIF, and SCF is about 63.99%, 73.94%, and 81.96% in SGF, SIF, and SCF, respectively. The difference in the release patterns of AMX and MTZ in each simulated physiological fluids show the effects of the pH of the releasing media since both SALG and CS are pH-responsive polysaccharides depending on their swelling nature. Furthermore, both for AMX and MTZ, the correlation of the swelling ratios of the hydrogel B1-C1 in the SCF, SIF, and SCF with the respective in vitro drug release in all three physiological fluids at $p < 0.05$ showed similar linear positive correlation trends (Appendix VIII, a and b). In all cases, the correlation coefficient's $P < 0.05$ indicated a significant linear dependence between the degree of swelling and the percentage of AMX and MTZ released in all three physiological

fluids, indicating that a higher swelling behaviour of the hydrogel enhances the rapid release of the drugs.

In SGF, the low AMX and MTZ release can be described by the development of the insoluble form of alginic acid due to the protonation of SALG. In SGF (pH 1.2 < pKa 3.4 of SALG), SALG chains protonate, forming the carboxyl (COOH) groups. Hydrogen bonds are formed between the carboxyl (-COOH) and the hydroxyl(-OH) groups, creating an insoluble SALG block on the hydrogel surface, which protects the structure from fluid ingress and hinders swelling (Yang et al., 2013). In the meantime, CS restricts drug release due to the strong interactions of its cationic groups (NH_3^+) with SALG, limiting hydrogel swelling and, thus, drug release. As the pH increases to 6.8 and 7.4, the increasing deprotonation of SALG with pH causes the disintegration of the hydrogel via stretching of the SALG chains releasing its free surface as a result of the repulsion force between the carboxylate (COO-) anions. This expansion of the polymer chains increases fluid ingress into the hydrogel structure and, thus, drug release (Agüero et al., 2017).

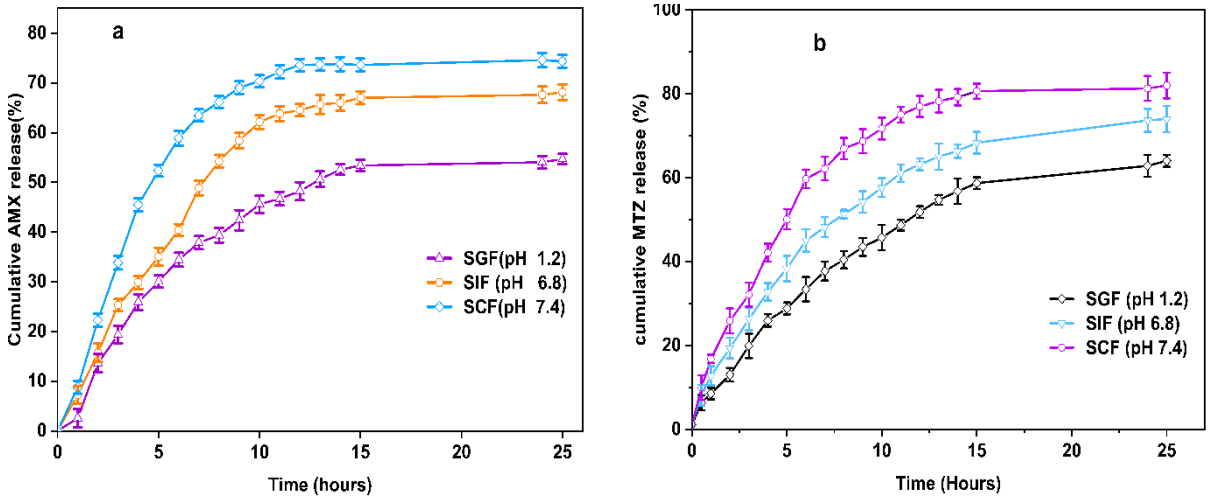

Figure 4. 24 Cumulative release (a) AMX from hydrogel AMX-B1-C1 release (b) MTZ from the hydrogel MTZ-B1-C1 in SGF, SIF, and SGF at 37.2 ºC.

4.12. Drug release mechanisms

To determine the mechanism of the release of each drug (AMX and MTZ) from the optimal CS/PVP and SALG/CS hydrogels, the cumulative percentages of the release results were incorporated into several release kinetic mathematical models including the zero order model, first order model, Higuchi model, and Korsmeyer-Peppas model.

To choose the most appropriate mathematical model that matches the drug's release profile, the most significant coefficient of correlation (R^2) was considered. The findings of each linear

adapted model of the release data of both drugs, AMX and MTZ, in the three physiological fluids (SGF, SIF, and SCF) are presented in Table 4.5 and Table 4.6, respectively, for the drug-loaded CS/PVP based hydrogels. It can be seen from the results of the adapted kinetic models of AMX in SGF acidic medium (SGF, pH 1.2), the Korsmeyer-Peppas kinetic model has the highest coefficient of correlation (R^2 = 0.9777) than the Higuchi model (R^2 =0.9528), the zero-order model (R^2 = 0.8164), and the first-order model (R^2 = 0.6326). The results demonstrate that the Korsmeyer-Peppas kinetic model is most fit for the release of AMX from the AMX-H2-G3 hydrogel.

Similarly, the Korsmeyer-Peppas kinetic model, which has the highest correlation coefficients (R^2) value in slightly basic media [SIF (pH 6.8) or SCF (pH 7.4)], is the best matched kinetic model for AMX release from the optimal CS/PVP hydrogel. Additionally, for the Korsmeyer-Peppas model the determined exponent 'n' was found to be 0.5471, 0.5631, and 0.5743 for AMX in SGF (pH 1.2), SIF (pH 6.8), and SCF (pH 7.4), respectively. This shows that the AMX release from the optimal hydrogel (H2-G3) is a diffusion and swelling-controlled time-dependent non-Fickian mechanism ($0.5 < n < 1$) (Duceac et al., 2020).

Table 4. 5: Drug release kinetics of AMX release from hydrogel AMX-H2-G3.

pH	Zero-order model		First-order model		Higuchi model		Korsmeyer–Peppas model	
	k	R^2	k	R^2	k	R^2	n	R^2
1.2	0.021	0.8164	0.0654	0.6326	0.133	0.9528	0.5471	0.9777
6.8	0.0197	0.876	0.07709	0.7113	0.1217	0.9691	0.5631	0.9881
7.4	0.0174	0.912	0.074	0.741	0.106	0.9806	0.5743	0.9903

As shown in Table 4.6, the release kinetic data of MTZ in acidic medium (SGF), the Korsmeyer-Peppas kinetic model exhibits a higher coefficient of correlation (R^2= 0.9814) in comparison to the Higuchi model (R^2 = 0. 9604), the zero-order model (R^2 = 0.8443), and the first-order kinetic model (R^2 = 0.6652). These outcomes demonstrate that the Korsmeyer–Peppas model is the best fit for the release of MTZ. Likewise, Korsmeyer-Peppas kinetic model shows coefficient of correlation values of R^2 = 0.9826 and R^2 = 0.9753 in SIF (pH 6.8) and SCF (pH 7.4), respectively, and is the best suitable kinetic model for MTZ release from the optimal CS/PVP hydrogel. For MTZ release in SGF (pH 1.2), SIF (pH 6.8), and SCF(pH 7.4), the diffusional exponent 'n' determined using Korsmeyer-Peppas mathematical equation is 0.5848, 0.6347, and

0.7268, respectively. As long as the exponent (n) is higher than 0.45, the diffusion and swelling rate coefficients are comparable. According to the model, drug release is governed by the physical diffusion and swelling controlled time-dependent non-Fickian process (0.45 < 0.85) caused by hydrogel erosion (Duceac et al., 2020).

Table 4. 6: Drug release kinetics of MTZ release from hydrogel MTZ-H2-G3.

pH	Zero-order model		First-order model		Higuchi model		Korsmeyer–Peppas	
	k	R^2	k	R^2	k	R^2	n	R^2
1.2	0.023	0.844	0.0716	0.665	0.145	0.960	0.585	0.981
6.8	0.023	0.877	0.0801	0.711	0.138	0.961	0.635	0.983
7.4	0.022	0.878	0.0921	0.710	0.133	0.957	0.726	0.975

In a similar way, the cumulative percentage release results of both drugs (AMX and MTZ) from the optimal SALG/CS hydrogel (B1-C1) were matched to multiple release kinetic equations. Table 4.7 and Table 4.8 show the related kinetic results matched into zero-order, first-order, Higuchi model, and Korsmeyer-Peppas model in the physiological fluids (SGF, SIF, and SCF).

Table 4. 7: Drug release kinetics of AMX release from hydrogel bead AMX-B1-C1.

pH	Zero-order model		First order model		Higuchi model		Korsmeyer–Peppas		
	k	R	k	R^2	k	R^2	n	R^2	k
1.2	0.019	0.714	0.032	0.439	0.130	0.879	0.804	0.808	0.828
6.8	0.024	0.652	0.028	0.523	0.166	0.844	1.028	0.694	0.904
7.4	0.022	0.557	0.023	0.411	0.158	0.754	1.197	0.604	0.821

Based on the release kinetic data of AMX from hydrogel AMX-B1-C1, Korsmeyer-Peppas kinetic model shows a maximum value of correlation coefficient (R^2) of 0.8276, 0.9039, and 0.8209, respectively. These findings reveal that the Korsmeyer-Peppas kinetic model is the best fitting for the releasing of AMX from AMX-B1-C1 in all the simulated physiological media. Further, the obtained exponent 'n' using the Korsmeyer-Peppas mathematical equation for the controlled release of AMX in SGF(pH 1.2), SIF(pH 6.8), and SCF(pH 7.4) is 0.8082, 0.6941, and 0.6038, respectively, implying that the release of AMX follows an anomalous combination of diffusion and swelling controlled time dependent non-Fickian mechanism (0.43 < n < 0.85).

When considering the release kinetics of MTX from the hydrogel MTZ-B1-C1 in each physiological fluid (SGF, SIF, and SCF), the Korsmeyer-Peppas model provides a maximum R^2

value of 0.9781, 0.9739, and 0.9458, respectively. The results indicate that the Korsmeyer-Peppas kinetic model is the best fitting for the release of MTZ from the optimal SALG/CS hydrogel in SGF, SIF, and SCF.

Table 4. 8: Drug release kinetics for MTZ release from the hydrogel MTZ-B1-C1.

pH	Zero-order model		First-order model		Higuchi model		Korsmeyer–Peppas model	
	k	R^2	k	R^2	k	R^2	k	R^2
1.2	1.2036	0.8424	0.07899	0.6483	7.5386	0.9609	0.652	0.9781
6.8	1.3206	0.8001	0.07047	0.6117	8.4153	0.9444	0.5977	0.9739
7.4	1.3949	0.6883	0.06333	0.5402	9.2154	0.8735	0.5645	0.9458

Additionally, the obtained exponent 'n' from the Korsmeyer Peppas mathematical equation is 0.653, 0.5977, and 0.5645, respectively. This implies that MTZ release from the optimal hydrogel (B1-C1), follows an anomalous combination of diffusion and swelling controlled time-dependent non-Fickian mechanism ($0.43 < n < 0.85$).

4.13. Antimicrobial efficacy test

The antimicrobial efficacy test was performed for AMX-loaded hydrogels (H2-G3 and B1-C1) against *Escherichia coli* (ATCC25922) and *Streptococcus pyogenes* (ATCC19615) and for that of MTZ-loaded hydrogels (H2-G3 and B1-C1) against *Escherichia coli* (ATCC25922) and *Staphylococcus aureus* (ATCC25923). The average inhibition zones of the AMX and MTZ loaded CS/PVP hydrogels (AMX-H2-G3 and MTZ-H2-G3) against the chosen bacterial species are shown in Table 4.9. The chosen images of the zone of inhibition of unloaded (negative control), drug-loaded hydrogels, and the pristine form of AMX and MTZ as the positive control are shown in Fig.4.25. The AMX-H2-G3 and MTZ-H2-G3 hydrogels show substantial inhibitory zone against bacteria because of increased swelling and drug release. The AMX-H2-G3 hydrogel killed *Streptococcus pyogenes* and *Escherichia coli* bacteria with inhibition zones ranging from 27.5 mm to 32 mm and 19.5 mm to 24.5 mm (Table 4.9), respectively.

The MTZ-H2-G3 hydrogel prohibited the *Staphylococcus aureus* and *Escherichia coli* bacteria with inhibitory zones of approximately 24.8 mm and 23.46 mm respectively (Table 4.9). The larger inhibitory zones of the AMX-H2-G3 hydrogel [Figure 4.25(a, b)] than the pristine drug (PC) is related to the antibacterial properties of CS (Ngwabebhoh et al., 2021). CS interacts with the bacterial DNA via its positively charged amine end (NH_3^+), limiting the protein and mRNA

formation in bacterial strains, and its effect is proportional to the number of the positively charged amine (NH_3^+) groups.

Table 4. 9: The inhibition zones diameter of hydrogels AMX-H2-G3 and MTZ-H2-G3.

Bacteria strains	**Zone of inhibition, diameter (mm)**					
	AMX loaded hydrogel			MTZ loaded hydrogel		
	H2-G3 (Negative control)	Pristine AMX	AMX-H2-G3	H2-G3 (Negative control)	Pristine MTZ	MTZ-H2-G3
Streptococcus pyogenes	6.27 ± 0.7	27.17 ± .27	29.33 ±2.36			
Escherichia coli	6.74 ± 1.2	20.16 ± .04	23.33 ±1.04	9.3 ± 0.8	11.6 ± 0.7	23.5 ± 1.3
StapHylococcus aureus				10.2±0.9	13.7 ±1.3	24.8 ± 1.1

AMX acts as an antibacterial by binding to the penicillin-binding proteins of bacterial strains inducing the release of autolytic enzymes in the bacterial cell wall (Fazulbhoy et al., 2021). The autolytic enzymes in the bacteria cell wall inhibit the formation of the peptidoglycan layer of the bacterial cell walls (destruction of the cell wall of bacteria).

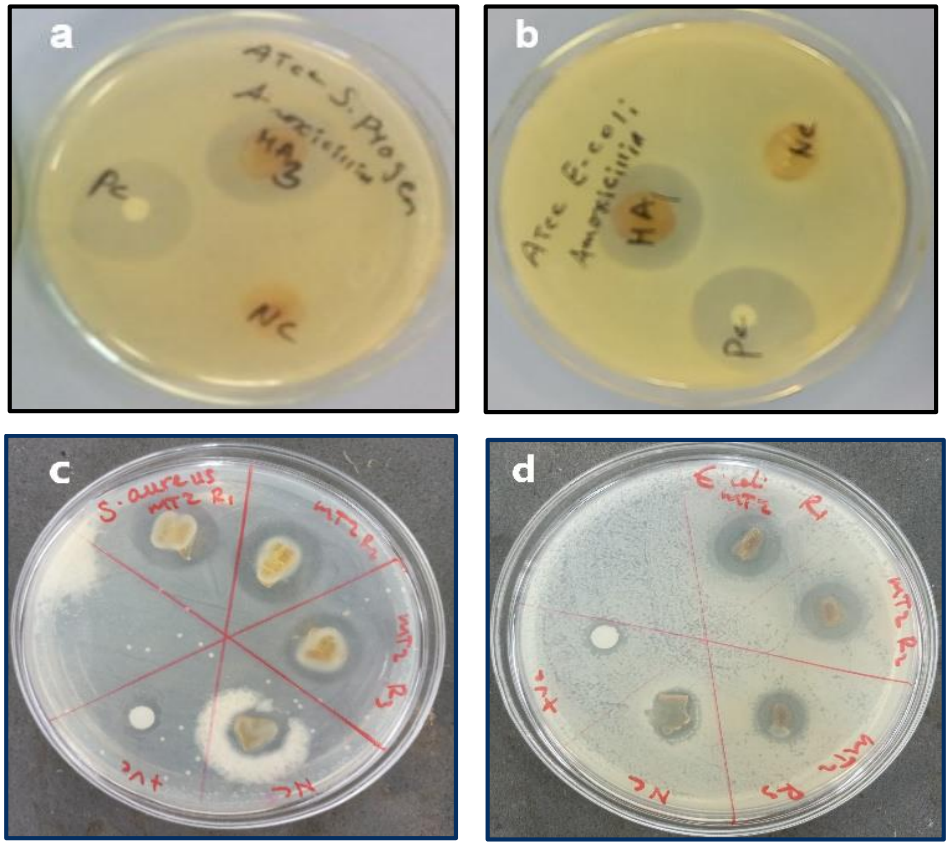

Figure 4. 25 Inhibitory effect of a) AMX-H2-G3 against *Streptococcus pyogenes*, b) AMX-H2-G3 against *Escherichia coli*, c) MTZ-H2-G3 against *Staphylococcus aureus* and d) MTZ-H2-G3 against *Escherichia coli.*

In addition, in *Escherichia coli* bacteria, due to the cationic properties of CS (NH_3^+), it interacts with the cell wall of the negatively charged bacterial cell wall causing the lysis of the cell wall (Ata et al., 2020). MTZ is a type of nitroimidazole drug, which binds to bacterial DNA producing nitroso radicals and hydroxyl amine groups, resulting in the loss of bacterial DNA helical structure, consequently, cell death in vulnerable microbes (Arslan et al., 2017).

The drug-loaded hydrogel (MTZ-H2-G3) has a larger inhibitory zone than the pure drug [Figure 4.25(c, d)] against both *Staphylococcus aureus and Escherichia coli* demonstrates the synergistic effects of MTZ and the hydrogel MTZ-H2-G3 besides to the antibacterial properties of CS (X.Wu et al., 2020). The antimicrobial properties of CS contributed to the significant inhibitory zone surrounding H2-G3 (negative control) in both instances. Based on these findings, the AMX-H2-G3 and MTZ-H2-G3 hydrogels have a bright future for usage in CDDSs. The variation in the inhibition zones of the negative controls (H2-G3) of the AMX and MTZ samples could be attributed to the hydrogel's degree of swelling as well as the pH of the agar and swelling media.

For the SALG/CS hydrogels, the average inhibition zones of the hydrogel AMX-B1-C1 and MTZ-B1-C1 against the selected bacterial species are shown in Table 4.10. The hydrogel AMX-B1-C1 inhibited the reproduction of both *Streptococcus Pyogenes* and *Escherichia coli* bacterial strains having a larger zone of inhibition of 28.7 and 20.8 mm, respectively, in comparison to hydrogels B1-C1(negative control) and AMX (positive control). The pure AMX (PC) inhibition zones against *Streptococcus pyogenes* and *Escherichia coli* are 20.1 and 18.6 mm, respectively (Table 4.10). The hydrogel MTZ-B1-C1 also suppressed the growth of both *Staphylococcus aureus* and *Escherichia coli* bacteria strains with inhibitory zones ranging from 18.35 mm and 17.4, respectively (Table 4.10).

The negative control (B1-C1) also showed a significant inhibition zone ranging from 8.3 to 6.3 mm (Table 4.10) against, while that of pure MTZ (PC) is 10.4, and 10.1 mm against *Staphylococcus aureus*, and *Escherichia coli,* respectively. The findings indicate that the drug-loaded hydrogel (MTZ-B1-C1) effectively limit the growth of the bacterium strains. The difference in the inhibition zones of the negative controls (B1-C1) of the AMX and MTZ samples may be associated to the degree of swelling of the hydrogels and the pH of the swelling media and agar media. Figure 4.26 displays images of the zones of inhibition of pure AMX, MTZ, B1-C1 and drug-loaded hydrogels (AMX-B1-C1 and MTZ-B1-C1) exhibiting considerable inhibition zones against the bacteria strains. The drug-loaded hydrogels (AMX-B1-C1 and MTZ-

B1-C1) have substantial antibacterial properties due to the synergistic effect of CS and the drugs released from the hydrogel matrix upon swelling (X.Wu et al., 2020).

Table 4. 10: The inhibition zones of hydrogels AMX-B1-C1and MTZ-B1-C1.

Bacteria strains	Zone of inhibition, diameter (mm)					
	AMX loaded hydrogel			MTZ loaded hydrogel		
	B1-C1 (Negative control)	Pristine AMX	AMX-B1-C1	B1-C1 (Negative control)	Pristine MTZ	MTZ-B1-C1
Streptococcus pyogenes	12 ± 1.11	20.1 ±1.3	28.7± 1.53			
Escherichia coli	11.2 ±1.3	18.6 ±1.2	20.8 ± 1.6	6.3 ± 0.3	10.1 ± 0.5	17.4 ± 0.2
Staphylococcus aureus				8.3 ± 0.5	10.4 ± 0.7	18.35 ± 0.5

The antibacterial activity of CS depends on to the degree of deacetylation, which varies with the number of protonated amine (NH_3^+) groups. AMX, on the other hand, is an antibacterial drug that binds to the penicillin-binding proteins of bacterial strains causing the release of autolytic enzymes in the bacteria structure (cell wall).

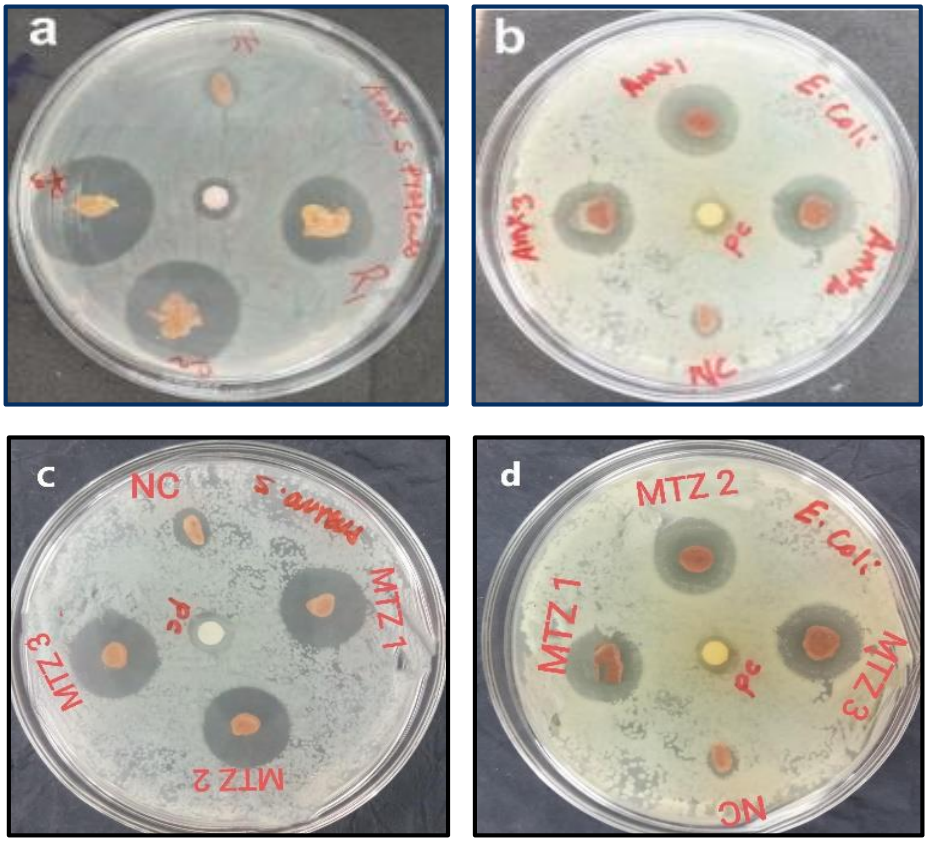

Figure 4. 26 Inhibitory effect of a) AMX-B1-C1 against *Streptococcus pyogenes* and b) AMX-B1-C1 against *Escherichia coli* c) MTZ-H2-G3 against *Staphylococcus aureus* d) MTZ-H2-G3 against *Escherichia coli*.

The autolytic enzymes in the bacteria cell walls inhibit the formation of the peptidoglycan layer of both gram negative and gram positive bacteria cell walls leading to the destruction of the cell walls. For both bacteria species, MTZ (positive control) showed insignificant inhibition zones, owning to that pure MTZ is active only to anaerobes. Antibacterial activity of MTZ-loaded hydrogels (MTZ-B1-C1) tested against *Staphylococcus aureus* and *Escherichia coli* of the present study agree with previous studies (Jeong et al., 2020; Rade et al., 2022). The noticed inhibitory zone of the non-loaded hydrogel is associated to the antibacterial properties of CS. CS fixes to the bacterial DNA via its cationic amine groups inhibiting protein and mRNA production of the bacterial species. From these results, the AMX and MTZ loaded SALG/CS hydrogel possibly will have clinical inferences, and deserve to be further studied for applications in CDDSs.

5 SUMMARY AND CONCLUSIONS

Hydrogels that take into account physiological requirements and release drugs continuously at predetermined rates can offer innovative insights to promote the development of CDDSs that are extremely effective at delivering the desired therapeutic effects. CS-based hybrid crosslinked hydrogels were developed and characterized for the controlled release of AMX and MTZ, the most commonly prescribed broad-spectrum antibiotics for the treatment of different bacterial infections. Different polymer crosslinking methods can be used synthesize hydrogels. However, chemical and ionotropic gelation methods were chosen because they create stable structures with flexible physiological properties. Glutaraldehyde was employed as a crosslinking agent in the chemical crosslinking method (for CS/PVP hydrogels), whereas $CaCl_2$ and glutaraldehyde were used in the ionotropic gelation method to construct stable SALG/CS double crosslinked network systems.

The first set of experiments studied the in vitro controlled release of AMX and MTZ, as well as the antibacterial efficacy of CS/PVP hydrogels. To achieve the intended objectives, the hydrogel synthesis techniques were established in two stages. Using a fixed amount of glutaraldehyde (200 µL), crosslinked CS/PVP hydrogels with varying polymer ratios were synthesized in the first stage. Using the optimum polymer composition determined in step one based on swelling ratios in simulated physiological fluids, the second phase evaluated the influence of glutaraldehyde concentrations ranging from 200 to 1000 200 µL to optimize a formulation for controlled release of AMX and MTZ. Thin film semi-IPN hydrogels were produced by crosslinking CS and PVP polymers with glutaraldehyde. During the hydrogel formation process (in situ method), the drugs (200 mg each) were loaded in the optimal polymer composition.

In the second set of experiments, AMX and MTZ were controlled released in vitro using a biodegradable, pH-sensitive, and double crosslinked SALG/CS hydrogel. As in the first set of experiments, two steps were used to prepare hydrogels in order to achieve the desired results. The first step involved the ionotropic synthesis of SALG/CS hydrogels using $CaCl_2$ (2%), in which varying polymer ratios were used. A double crosslinked network system was then formed by immersing the hydrogels in glutaraldehyde. In the second phase, the optimum polymer composition based on the swelling ratio in simulated physiological fluids was evaluated. This was done to determine whether $CaCl_2$ concentrations ranging from 2 to 10% affected the formulation suitable for controlled rates of the drugs AMX and MTZ. As a result of interactions between SALG and CS polymers using $CaCl_2$ and glutaraldehyde crosslinkers, microbeads were

formed. During the hydrogel synthesis process (in situ approach), drugs (200 mg each) were loaded in the optimal polymer composition.

The swelling nature of hydrogels in simulated physiological fluids of different pH levels (1.2, 6.8, and 7.4) was determined to be influenced by both the concentration of crosslinker (glutaraldehyde), the polymer composition, and pH levels. Due to the protonation of CS in an acidic medium, the CS/PVP hydrogels showed a higher swelling ratio in SGF (pH 1.2) and a relatively lower swelling ratio in slightly alkaline media (pH 6.8 and 7.4). In contrast to the CS/PVP hydrogels, SALG/CS hydrogels showed a lower swelling ratio in acidic media (pH 1.2) and higher swelling values in slightly alkaline media (pH 6.8 and 7.4) due to the deprotonation of SALG in alkaline media, indicating that the hydrogels are pH sensitive. Observed pH-dependence of the swelling ratios of the hydrogels revealed their ability to be used in CDDSs.

The optimal compositions of CS/PVP (60/40 weight ratio) crosslinked with 600 µL and SALG/CS (75/25 weight ratio) crosslinked with 2% $CaCl_2$ and soaked in sufficient glutaraldehyde were chosen for the in situ loading of 200 milligrams each of AMX and MTZ. As a result, optimal hydrogel compositions showed lower swelling ratios in acidic media (pH 1.2) but relatively higher swelling ratios in SIF (pH 6.8), which would limit drug release in the stomach while maximizing drug release in the intestine, where drug absorption occurs. The outcome of the swelling study is that the CS/PVP hydrogels show a higher degree of swelling in acidic media (pH 1.2), i.e., the microenvironment of the stomach, thus, minimizing drug release at higher pH, i.e., in the microenvironment of the intestine and colon. The optimized hydrogel composition can release drugs in the stomach. The SALG/CS hydrogels swell less at lower pH, thus minimizing drug release in the stomach (acidic pH), with potential for drug delivery to the small intestine and colon, i.e., at higher pH.

In both CS/PVP and SALG/CS hydrogels, a rise in CS percentage and crosslinking agent concentrations leads to a decrease in porosity and an increase in the gel fraction. This is due to increasing crosslinking density. In CS/PVP hydrogels, increasing the glutaraldehyde concentration from 200 µL to 600 µL resulted in a rise in porosity ranging from 77 to 94%. Further raising the glutaraldehyde concentration to 1000 µL resulted in a drastic decrease in porosity to 63%. Increasing the $CaCl_2$ concentration in the SALG/CS hydrogels from 2% to 10% decreased porosity from approximately 86 to 66%. In addition, it resulted in an increase in gel fraction ranging from approximately 77 to 96%.

Each polymer's functional groups (CS and PVP), their crosslinking network, and the incorporation of drugs (AMX and MTZ) were revealed by FTIR analysis. There is a well-defined interaction between the polymer components in the crosslinked hydrogels, as indicated by a significant shift in bands. The disappearance of C=O bands in AMX-H2-G3 and AMX-B1-C1 hydrogels around 1772 cm^{-1} and the appearance of a weak C-S band around 557 cm^{-1} indicated the successful incorporation of the AMX into the hydrogels. The appearance of N-O stretching frequency at about 1536 cm^{-1} in the MTZ-H2-G3 and MTZ-B1-C1 hydrogel spectra also indicated successful MTZ loading.

FESEM micrographs of CS/PVP reveal a porous surface morphology with a noticeable increase in pore size and number up to 600 μL (H2-G3) of glutaraldehyde beyond which the number of pores and pore size decreased dramatically, while micrographs of SALG/CS show fibrous and porous channels decreasing with increasing $CaCl_2$ concentration due to increased crosslinking density. The FESEM image of drug-loaded hydrogels showed each drug incorporated into the pores. With increasing crosslinking agent concentrations, XRD analysis revealed that crystalline structures are transformed into amorous structures in both CS/PVP and SALG/CS hydrogels. The drugs are distributed in the amorphous hydrogels.

Thermal analysis confirmed that crosslinked hydrogels were more stable than pristine polymers. The weight loss percentage for CS/PVP and SALG/CS hydrogels decreased with increasing crosslinker concentration due to increasing crosslinking density. Thermal degradation was reduced from about 82% for H2-G2 to 79% for H2-G5, and for SALG/CS hydrogels, from about 77% to 72% for B1-C1. The drug-loaded CS/PVP and SALG/CS hydrogels displayed a lower weight loss percentage than the unloaded hydrogels. Improved interactions are responsible for the improved thermal stability of drug-loaded hydrogels. As a result of the polymer thermal decomposition of the hydrogels occurring at higher temperatures than the typical body temperature (37.2^{o}C), hydrogels may be appropriate for oral CDDS. As crosslinker concentrations increased, both SALG/CS and CS/PVP hydrogels showed a slow and decreasing mass loss in vitro. Increasing the glutaraldehyde concentration (from to ?%) in hydrogels H2-G1 to H2-G5 resulted in weight losses of approximately 95 and 56%, respectively, while increasing the $CaCl_2$ concentration from 2 to 10% in hydrogels B1-C1 to B1-C5 resulted in weight losses of 80 and 33%, respectively.

CS/PVP and SALG/CS hydrogels loaded with drugs (AMX and MTZ) lost less weight in 30 days than the corresponding optimal unloaded hydrogels (H2-G3 and B1-C1). A possible explanation for the weight loss trends is the enhanced interactions between the polymer matrixes and the

drugs, resulting in enhanced crosslinked frameworks. The high crosslinking density of the CS/PVP and SALG/CS hydrogels in this study allows them to withstand the impact of gastrointestinal fluids on AMX and MTZ in CDDSs. This results in low decomposition rates. The in vitro biodegradable hydrogels developed allow for time-dependent controlled and sustained release of drugs.

CS/PVP hydrogel formulations used to load drugs (AMX and MTZ) were selected for their swelling and good release properties under typical conditions. The highest cumulative release of AMX (about 61%) and MTZ (about 71%) from the optimal hydrogel (H2-G3) was obtained in SGF (pH 1.2), and the lowest cumulative release of AMX (about 46%) and MTZ (about 52%) was achieved in SCF (pH 7.4) in 25 hours. Regardless of the simulated physiological fluids, drug release followed a progressive increasing pattern over time: the highest cumulative release of AMX (about 74%) and MTZ (about 81%) from the optimum hydrogel (B1-C1) obtained in SCF (pH 7.4), and the lowest cumulative release of AMX (about 55%) and MTZ (about 62%) was achieved in SGF (pH 1.2) within 25 hours. A slow and sustained drug release pattern was observed in the drug release profile. Across all three physiological fluids the correlation coefficients, $r^2 > 0.95$ ($P < 0.05$) between swelling ratio and cumulative drug release data indicated a strong linear correlation between swelling ratio and cumulative AMX and MTZ released.

Zero-order, first-order, Higuchi, and Korsmeyer-Reppas kinetic models were applied to analyze the cumulative drug release data. There were significantly higher correlation coefficients (R2) for drug release data by the Korsmeyer-Reppas model for drug release from the CS/PVP and SALG/CS hydrogels. The model showed that drug release from the hydrogels followed a diffusion and swelling controlled time dependent non-Fickian mechanism.

CSs' antibacterial properties are attributed to the inhibition zone in CS/PVP and SALG/CS hydrogels (H2-G3 and B1-C1). CS inhibits bacterial protein and mRNA production via its cationic amine groups. In all cases, pure MTZ (positive control) showed insignificant inhibition zones due to pure MTZ being exclusively active against anaerobes. AMX-loaded hydrogels (AMX-H2-G3 and AMX-B1-C1) showed significantly higher inhibition zones than the negative and positive controls against *Streptococcus pyogenes* and *Escherichia coli*. MTZ-containing hydrogels (MTZ-H2-G3 and MTZ-B1-C1) also displayed considerable antibacterial properties against *Staphylococcus aureus* and *Escherichia coli*. The observed significantly enhanced antibacterial properties of the drug-loaded hydrogels are due to the synergistic effect of CS and the drugs released from the hydrogel matrix upon swelling. Based on these findings, AMX and MTZ-loaded CS/PVP and SALG/CS hydrogels may have therapeutic potential and be further studied for applications in CDDSs.

6 RECOMMENDATIONS AND FUTURE PERSPECTIVE

Hydrogels are becoming increasingly important in CDDSs and will continue to produece advanced biomaterials that improve patient compliance. The hydrogels synthesized in this study offer a potential platform for research in biocompatible natural and synthetic polymers as effective drug carrier materials that are manageable and cost-effective for use in CDDSs. Further work can be done to develop new compositions, including the modulation of the physical and chemical properties for specific drug delivery and controlling the nature of the hydrogel formulations, for example, in film, tablet, or microencapsulated form. Moreover, it is essential to investigate the hydrogel compositions in vivo to evaluate their cytotoxicity. Further research should also be expanded to understand better the techno-economic feasibility of such materials as commercial products.

Publications from this work

1- Fabrication of pH-sensitive double cross-linked sodium alginate/chitosan hydrogels for controlled release of amoxicillin.

Polymer Engineering & Science/John Wiley & Sons, Inc.

2- Development of double crosslinked sodium alginate/chitosan based hydrogels for controlled release of metronidazole and its antibacterial activity.

Cell Press/ Heliyon

3- Fabrication of pH-Responsive Chitosan/Polyvinylpyrrolidone Hydrogels for Controlled Release of Metronidazole and Antibacterial Properties.

International Journal of Polymer Science/Hindawi

4- Synthesis and characterization of chitosan/polyvinylpyrrolidone hydrogels for controlled amoxicillin release.

Journal of Bioactive and Compatible Polymers/SAGE

REFERENCES

Adane, F., Seyoum, G., & Alamneh, Y. M. (2022). Non-prescribed drug use and predictors among pregnant women in Ethiopia: systematic review and meta-analysis. *The Journal of Maternal-Fetal & Neonatal Medicine*, *35*(22), 4273-4284.

Afriani, K., & Budikania, T. S. (2020). Synthesis and characterization of hydrogel of chitosan-poly (N-vinyl-2-pirrolidone) (PVP)-alginate for ibuprofen release. *The Journal of Pure and Applied Chemistry Research*, *9*(3), 201-211.

Agüero, L., Zaldivar-Silva, D., Peña, L., & Dias, M. L. (2017). Alginate microparticles as oral colon drug delivery device: A review. *Carbohydrate polymers*, *168*, 32-43.

Ahmadi, F., Oveisi, Z., Samani, S. M., & Amoozgar, Z. (2015). Chitosan based hydrogels: characteristics and pharmaceutical applications. *Research in pharmaceutical sciences*, *10*(1), 1.

Ahmed, E. M. (2015). Hydrogel: Preparation, characterization, and applications: A review. *Journal of advanced research*, *6*(2), 105-121.

Ahmed, T. A., & Aljaeid, B. M. (2016). Preparation, characterization, and potential application of chitosan, chitosan derivatives, and chitosan metal nanoparticles in pharmaceutical drug delivery. *Drug design, development and therapy*, 483-507.

Ajji, Z., Maarouf, M., Khattab, A., & Ghazal, H. (2020). Synthesis of pH-responsive hydrogel based on PVP grafted with crotonic acid for controlled drug delivery. *Radiation Physics and Chemistry*, *170*, 108612.

Akhtar, N., Singh, V., Yusuf, M., & Khan, R. A. (2020). Non-invasive drug delivery technology: Development and current status of transdermal drug delivery deVices, techniques and biomedical applications. *Biomedical Engineering/Biomedizinische Technik*, *65*(3), 243-272.

Alnaief, M., Obaidat, R. M., & Alsmadi, M. T. M. (2020). Preparation of hybrid alginate-chitosan aerogel as potential carriers for pulmonary drug delivery. *Polymers*, *12*(10), 2223.

Alvarez-Lorenzo, C., Grinberg, V. Y., BuroVa, T. V., & Concheiro, A. (2020). Stimuli-sensitive cross-linked hydrogels as drug delivery systems: Impact of the drug on the responsiveness. *International journal of pharmaceutics*, *579*, 119157.

Anwar, M., PerVaiz, F., Shoukat, H., Noreen, S., Shabbir, K., Majeed, A., & Ijaz, S. (2021). Formulation and evaluation of interpenetrating network of xanthan gum and polyvinylpyrrolidone as a hydrophilic matrix for controlled drug delivery system. *Polymer Bulletin*, *78*, 59-80.

Archana, D., Singh, B. K., Dutta, J., & Dutta, P. K. (2015). Chitosan-PVP-nano silver oxide wound dressing: in vitro and in vivo evaluation. *International journal of biological macromolecules*, *73*, 49-57.

Arslan, N., Yılmaz, Ö. & Demiray-Gürbüz, E. (2017). Importance of antimicrobial susceptibility testing for the management of eradication in Helicobacter pylori infection. *World journal of gastroenterology*, *23*(16), 2854.

Ata, S., Rasool, A., Islam, A., Bibi, I., Rizwan, M., Azeem, M. K., & Iqbal, M. (2020). Loading of Cefixime to pH sensitive chitosan based hydrogel and investigation of controlled release kinetics. *International journal of biological macromolecules*, *155*, 1236-1244.

Aycan, D., Yayla, N. A., & Aydin, Y. A. (2020). Chitosan polyvinyl alcohol blend films for ibuprofen encapsulation: Fabrication, characterization and kinetics. *Polymer Degradation and Stability*, *181*, 109346.

Bakhsheshi-Rad, H. R., Hadisi, Z., Ismail, A. F., Aziz, M., Akbari, M., Berto, F., & Chen, X. B. (2020). In vitro and in vivo evaluation of chitosan-alginate/gentamicin wound dressing nanofibrous with high antibacterial performance. *Polymer Testing*, *82*, 106298.

Batista, R. A., Otoni, C. G., & Espitia, P. J. (2019). Fundamentals of chitosan-based hydrogels: elaboration and characterization techniques. *Materials for Biomedical Engineering*, 61-81.

Baysal, K., Aroguz, A. Z., Adiguzel, Z., & Baysal, B. M. (2013). Chitosan/alginate crosslinked hydrogels: Preparation, characterization and application for cell growth purposes. *International journal of biological macromolecules*, *59*, 342-348.

Beads, M., Park, K. H., Choi, Y. W., Ryu, H., Lee, H. J., Moon, J., Song, H., & Park, Y. (2022). Controlled Drug Release Using Chitosan-Alginate-Gentamicin Multi-Component Beads. *Materials*, *15*(21), 7682.

Bezerra, I. C., Moma, M. S., Freitas, E. D., Silva, M. G., & Vieira, M. G. (2021). Development of a modified drug delivery system through the incorporation of furosemide into sericin and alginate matrix using the experimental design approach. *Journal of Chemical Technology & Biotechnology*, *96*(3), 650-661.

Bhatt, P., Trehan, S., Inamdar, N., Mourya, V. K., & Misra, A. (2021). Polymers in drug delivery: an update. In *Applications of polymers in drug delivery* (pp. 1-42). Elsevier.

Bhupathyraaj, M., & Pole, S. (2020). Study on effect of combination of sodium alginate and xanthan gum on drug release from Tacrolimus microbeads. *European Journal of Molecular & Clinical Medicine*, *7*, 4585.

Bialik-Wąs, K., Pluta, K., Malina, D., & Majka, T. M. (2021). Alginate/PVA-based hydrogel matrices with Echinacea purpurea extract as a new approach to dermal wound healing. *International Journal of Polymeric Materials and Polymeric Biomaterials*, *70*(3), 195-206.

Budianto, E., & Amalia, A. (2020). Swelling behavior and mechanical properties of Chitosan-Poly (N-vinyl-pyrrolidone) hydrogels. *Journal of Polymer Engineering*, *40*(7), 551-560.

Chai, Q., Jiao, Y., & Yu, X. (2017). Hydrogels for biomedical applications: their characteristics and the mechanisms behind them. *Gels*, *3*(1), 6.

Chalitangkoon, J., Wongkittisin, M., & Monvisade, P. (2020). Silver loaded hydroxyethylacryl chitosan/sodium alginate hydrogel films for controlled drug release wound dressings. *International journal of biological macromolecules*, *159*, 194-203.

Chatterjee, S., Upadhyay, P., Mishra, M., Srividya, M., Akshara, M. R., Kamali, N., & Misra, S. K. (2020). Advances in chemistry and composition of soft materials for drug releasing contact lenses. *Rsc Advances*, *10*(60), 36751-36777.

Chen, C., Zhou, J. L., Han, X., Song, F., Wang, X. L., & Wang, Y. Z. (2014). A prodrug strategy based on chitosan for efficient intracellular anticancer drug delivery. *Nanotechnology*, *25*(25), 255101.

Chen, X., Yan, H., Bao, C., Zhu, Q., Liu, Z., Wen, Y., ... & Lin, Q. (2022). Fabrication and evaluation of homogeneous alginate/polyacrylamide–chitosan–gelatin composite hydrogel scaffolds based on the interpenetrating networks for tissue engineering. *Polymer Engineering & Science*, *62*(1), 116-128.

Chen, X., Yu, H., Wang, N., Zhang, Q., Zhou, W., & Uddin, M. A. (2020). Preparation of phenylboronic acid-based hydrogel microneedle patches for glucose-dependent insulin delivery. *Journal of Applied Polymer Science*, *138*(5), 49772.

Chowdhury, S., Chakraborty, S., Maity, M., Hasnain, M. S., & Nayak, A. K. (2020). Biocomposites of alginates in drug delivery. *Alginates in Drug Delivery*, 153-185.

Contardi, M., Kossyvaki, D., Picone, P., Summa, M., Guo, X., Heredia-Guerrero, J. A., & Bayer, I. S. (2021). Electrospun polyvinylpyrrolidone (PVP) hydrogels containing hydroxycinnamic acid derivatives as potential wound dressings. *Chemical Engineering Journal*, *409*, 128144.

Couto, J., Dos Santos, L. P., Alves, J. C., López, R., & Maldonado, C. (2017). Amoxicillin crystalluria: a rare side-effect of a commonly prescribed antibiotic. *European Journal of Case Reports in Internal Medicine*, *4*(10).

Das, S., & Subuddhi, U. (2019). Controlled delivery of ibuprofen from poly (vinyl alcohol) − poly (ethylene glycol) interpenetrating polymeric network hydrogels. *Journal of pharmaceutical analysis*, *9*(2), 108-116.

De Oliveira Pedro, R., Hoffmann, S., Pereira, S., Goycoolea, F. M., Schmitt, C. C., & Neumann, M. G. (2018). Self-assembled amphiphilic chitosan nanoparticles for quercetin delivery to breast cancer cells. *European Journal of Pharmaceutics and Biopharmaceutics*, *131*, 203-210.

Demeter, M., Meltzer, V., Călina, I., Scărișoreanu, A., Micutz, M., & Kaya, M. G. A. (2020). Highly elastic superabsorbent collagen/PVP/PAA/PEO hydrogels crosslinked via e-beam radiation. *Radiation Physics and Chemistry*, *174*, 108898.

Demoz, G. T., Kasahun, G. G., Hagazy, K., Woldu, G., Wahdey, S., Tadesse, D. B., & Niriayo, Y. L. (2020). Prescribing pattern of antibiotics using WHO prescribing indicators among inpatients in Ethiopia: a need for antibiotic stewardship program. *Infection and Drug Resistance*, 2783-2794.

Dubey, S. K., Parab, S., Dabholkar, N., Agrawal, M., Singhvi, G., Alexander, A., & Kesharwani, P. (2021). Oral peptide delivery: Challenges and the way ahead. *Drug discovery today*, *26*(4), 931-950.

Duceac, I. A., Verestiuc, L., Dimitriu, C. D., Maier, V., & Coseri, S. (2020). Design and preparation of new multifunctional hydrogels based on chitosan/acrylic polymers for drug delivery and wound dressing applications. *Polymers*, *12*(7), 1473.

Ebrahimi, R., & Salavaty, M. (2018). Controlled drug delivery of ciprofloxacin from ultrasonic hydrogel. *E-Polymers*, *18*(2), 187-195.

El Achaby, M., Essamlali, Y., El Miri, N., Snik, A., Abdelouahdi, K., Fihri, A., & Solhy, A. (2014). Graphene oxide reinforced chitosan/polyvinylpyrrolidone polymer bio-nanocomposites. *Journal of Applied Polymer Science*, *131*(22).

El Nokab, M. E. H., & Van Der Wel, P. C. (2020). Use of solid-state NMR spectroscopy for investigating polysaccharide-based hydrogels: A review. *Carbohydrate polymers*, *240*, 116276.

Elsayed, M. M. (2019). Hydrogel preparation technologies: relevance kinetics, thermodynamics and scaling up aspects. *Journal of Polymers and the Environment*, *27*(4), 871-891.

Emami, S., Pourmadadi, M., Fatoorehchi, H., Yazdian, F., Rashedi, H., & Navaei, M. (2021). Preparation of pH-sensitive chitosan / polyvinylpyrrolidone / α -Fe 2 O 3 nanocomposite for drug delivery application : Emphasis on ameliorating restrictions. *International Journal of Biological Macromolecules*, *173*, 409–420.

Eskandari, P., Abousalman-Rezvani, Z., Hajebi, S., Roghani-Mamaqani, H., & Salami-Kalajahi, M. (2020). Controlled release of anti-cancer drug from the shell and hollow cavities of poly (N-isopropylacrylamide) hydrogel particles synthesized via reversible addition-fragmentation chain transfer polymerization. *European Polymer Journal*, *135*, 109877.

Fazulbhoy, R., Khan, A., D'souza, L. A., Dave, N., & Chandu, P. (2021). A Comparative Analysis of Amoxicillin and Cefuroxime. *International Journal of Scientific Research in Science and Technology*, 96–124.

Franco, P., & De Marco, I. (2020). The Use of Poly (N-vinyl pyrrolidone) in the Delivery of Drugs: A Review. *Polymers*, *12*(5), 1114.

Frenț, O. D., Duteanu, N., Teusdea, A. C., Ciocan, S., Vicaș, L., Jurca, T., & Marian, E. (2022). Preparation and characterization of chitosan-alginate microspheres loaded with quercetin. *Polymers*, *14*(3), 490.

Ganguly, S., Das, P., & Das, N. C. (2020). Characterization tools and techniques of hydrogels. In *Hydrogels based on natural polymers* (pp. 481-517). Elsevier.

Garakani, S. S., Davachi, S. M., Bagher, Z., Esfahani, A. H., Jenabi, N., Atoufi, Z., Ai, J., Abbaspourrad, A., Rashedi, H., & Jalessi, M. (2020). Fabrication of chitosan/polyvinylpyrrolidone hydrogel scaffolds containing PLGA microparticles loaded with dexamethasone for biomedical applications. *International Journal of Biological Macromolecules*, *164*, 356–370.

Gârea, S. A., Voicu, A. I., & Iovu, H. (2017). Clay–polymer nanocomposites for controlled drug release. In *Clay-polymer nanocomposites* (pp. 475-509). Elsevier.

Garg, S., Garg, A., & Vishwavidyalaya, R. D. (2016). Hydrogel: Classification, properties, preparation and technical features. *Asian J. Biomater. Res*, *2*(6), 163-170.

Gebeyehu, E., & Ararsie, M. (2023). Assessment of home storage of antimicrobials and its predictors in Mecha demographic surveillance and field research center: a cross-sectional study. *BMC Infectious Diseases*, *23*(1), 278.

Gebramariam, E. T., & Ahmed, M. (2019). Evaluation of rational medicine use based on WHO core drug use comparative study of the mechanical performance of bitumen indicators in public hospitals in West Shoa Zone, Oromia, Ethiopia. *Advances in Pharmacoepidemiology and Drug Safety*, *8*(1), 1-6.

Gerami, S. E., Pourmadadi, M., Fatoorehchi, H., Yazdian, F., Rashedi, H., & Nigjeh, M. N. (2021). Preparation of pH-sensitive chitosan/polyvinylpyrrolidone/α-Fe2O3 nanocomposite for drug delivery application: Emphasis on ameliorating restrictions. *International Journal of Biological Macromolecules*, *173*, 409–420.

Ghasemiyeh, P., & Mohammadi-Samani, S. (2019). Hydrogels as drug delivery systems; pros and cons. *Trends in Pharmaceutical Sciences*, *5*(1), 7-24.

Ghauri, Z. H., Islam, A., Qadir, M. A., Gull, N., Haider, B., Khan, R. U., & Riaz, T. (2021). Development and evaluation of pH-sensitive biodegradable ternary blended hydrogel films (chitosan/guar gum/PVP) for drug delivery application. *Scientific Reports*, *11*(1), 21255.

Ghotaslou, R., Baghi, H. B., Alizadeh, N., Yekani, M., Arbabi, S., & Memar, M. Y. (2018). Mechanisms of Bacteroides fragilis resistance to metronidazole. *Infection, Genetics and Evolution*, *64*, 156-163.

Giske, A., Nymo, L. S., Fuskevåg, O. M., Amundsen, S., Simonsen, G. S., & Lassen, K. (2017). Systemic antibiotic prophylaxis prior to gastrointestinal surgery–is oral administration of doxycycline and metronidazole adequate? *Infectious Diseases*, *49*(11-12), 785-791.

Gopikrishna, A., Ramu, B., Srikanth, G., & Rajkamal, B. (2016). Formulation of isoniazide sustained release formulation by using carbopol 934 P. *International journal of applied pharmaceutical sciences and research*, *1*(02), 60-69.

Gower, M. D., & Shanks, R. A. (2004). The effect of varied monomer composition on adhesive performance and peeling master curves for acrylic pressure-sensitive adhesives. *Journal of applied polymer science*, *93*(6), 2909-2917.

Grant, J. J., Pillai, S. C., Perova, T. S., Hehir, S., Hinder, S. J., McAfee, M., & Breen, A. (2021). Electrospun fibres of chitosan/PVP for the effective chemotherapeutic drug delivery of 5-fluorouracil. *Chemosensors*, *9*(4), 70.

Gull, N., Khan, S. M., Butt, O. M., Islam, A., Shah, A., Jabeen, S., & Butt, M. T. Z. (2020b). Inflammation targeted chitosan-based hydrogel for controlled release of diclofenac sodium. *International journal of biological macromolecules*, *162*, 175-187.

Gull, N., Khan, S. M., Khalid, S., Zia, S., Islam, A., Sabir, A., & Butt, M. T. Z. (2020a). Designing of biocompatible and biodegradable chitosan based crosslinked hydrogel for in vitro release of encapsulated povidone-iodine: A clinical translation. *International Journal of Biological Macromolecules*, *164*, 4370-4380.

Gull, N., Khan, S. M., Butt, M. T. Z., Khalid, S., Shafiq, M., Islam, A., & Khan, R. U. (2019). In vitro study of chitosan-based multi-responsive hydrogels as drug release vehicles: A preclinical study. *RSC advances*, *9*(53), 31078-31091.

Guo, F., Li, G., Ma, S., Zhou, H., & Yu, X. (2020). Dual-responsive nanocarriers from star shaped poly (N-isopropylacrylamide) coated mesoporous silica for drug delivery. *International Journal of Polymeric Materials and Polymeric Biomaterials*, *69*(18), 1178-1186.

Hanning, S. M., Matiz, S., Krasser, K., Orlu, M., Dodoo, C., Gaisford, S., & Tuleu, C. (2021). Characterisation of rectal amoxicillin (RAMOX) for the treatment of pneumonia in children. *Drug Delivery and Translational Research*, *11*, 944-955.

Hao, Y., Zhao, W., Zhang, L., Zeng, X., Sun, Z., Zhang, D., & Zhou, Q. (2020). Bio-multifunctional alginate/chitosan/fucoidan sponges with enhanced angiogenesis and hair follicle regeneration for promoting full-thickness wound healing. *Materials & Design*, *193*, 108863.

Heng, P. W. S. (2018). Controlled release drug delivery systems. *Pharmaceutical Development and Technology*, *23*(9), 833.

Heragh, B. K., Javanshir, S., Mahdavinia, G. R., & Naimi-Jamal, M. R. (2022). Development of pH-sensitive biomaterial-based nanocomposite for highly controlled drug release. *Results in Materials*, *16*, 100324.

Hernández Ceruelos, A., Romero-Quezada, L. C., Ruvalcaba Ledezma, J. C., & López Contreras, L. (2019). Therapeutic uses of metronidazole and its side effects: An update. *European Review for Medical and Pharmacological Sciences*, *23*(1), 397–401.

Holz, E., & Rajagopal, K. (2020). In situ-forming glucose-responsive hydrogel from hyaluronic acid modified with a boronic acid derivative. *Macromolecular Chemistry and Physics*, *221*(15), 2000055.

Homayun, B., Lin, X., & Choi, H. J. (2019). Challenges and recent progress in oral drug delivery systems for biopharmaceuticals. *Pharmaceutics*, *11*(3), 129.

Ibrahim, S. M., Abou El Fadl, F. I., & El-Naggar, A. A. (2014). Preparation and characterization of crosslinked alginate–CMC beads for controlled release of nitrate salt. *Journal of Radioanalytical and Nuclear Chemistry*, *299*, 1531-1537.

Ilić-Stojanović, S., Nikolić, L., Nikolić, V., Petrović, S., Oro, V., Mitić, Ž. & Najman, S. (2021). Semi-Crystalline copolymer hydrogels as smart drug carriers: In vitro thermo-responsive naproxen release study. *Pharmaceutics*, *13*(2), 158.

İnal, M., Işıklan, N., & Yiğitoğlu, M. (2017). Preparation and characterization of pH-sensitive alginate-g-poly (N-vinyl-2-pyrrolidone)/gelatin blend beads. *Journal of industrial and engineering chemistry*, *52*, 128-137.

Ipate, A. M., Serbezeanu, D., Bargan, Alexandra., Hamciuc, Corneliu., Ochiuz, L. Ă. C. R. Ă. M. I. O. A. R. A., & Gherman, S. I. M. O. N. A. (2021). Poly (vinylpyrrolidone)-chitosan hydrogels as matrices for controlled drug release. *Cellulose Chemistry and Technology*, *55*, 63-73.

Irfan, M., Du, X. Y., Xu, X. R., Shen, R. Q., Chen, S., & Xiao, J. J. (2019). Synthesis and Characterization of pH-sensitive Poly (IA-co-AAc-co-AAm) Hydrogels via Frontal Polymerization. *Journal of Polymer Science Part A: Polymer Chemistry*, *57*(22), 2214-2221.

Jafari, H., Hassanpour, M., Akbari, A., Rezaie, J., Gohari, G., Mahdavinia, G. R., & Jabbari, E. (2021). Characterization of pH-sensitive chitosan/hydroxypropyl methylcellulose composite nanoparticles for delivery of melatonin in cancer therapy. *Materials Letters*, *282*, 128818.

Jain, A., & Jain, S. K. (2016). In vitro release kinetics model fitting of liposomes: An insight. *Chemistry and physics of lipids*, *201*, 28-40.

Jana, S., & Jana, S. (Eds.). (2020). interpenetrating polymer network: biomedical applications. Springer Nature.

Jeong, J. O., Park, J. S., Kim, E. J., Jeong, S. I., Lee, J. Y., & Lim, Y. M. (2019). Preparation of radiation cross-linked poly (Acrylic acid) hydrogel containing metronidazole with enhanced antibacterial activity. *International Journal of Molecular Sciences*, *21*(1), 187.

Jin, S. G., Kim, K. S., Kim, D. W., Kim, D. S., Seo, Y. G., Go, T. G., ... & Choi, H. G. (2016). Development of a novel sodium fusidate-loaded triple polymer hydrogel wound dressing: Mechanical properties and effects on wound repair. *International journal of pharmaceutics*, *497*(1-2), 114-122.

Jithendra, T., Sreekanth Reddy, O., Subha, M. C. S., & Chowdoji Rao, K. (2020). Fabrication of drug delivery system for controlled release of curcumin, intercalated with magnetite nanoparticles through sodium alginate/polyvinylpyrrolidone-co-vinyl acetate semi ipn microbeads. *International Journal of Applied Pharmaceutics*,*12*, 249-257.

Kader Sabbagh, H. A., Hussein-Al-Ali, S. H., Hussein, M. Z., Abudayeh, Z., Ayoub, R., & Abudoleh, S. M. (2020). A statistical study on the development of metronidazole-chitosan-alginate nanocomposite formulation using the full factorial design. *Polymers*, *12*(4), 772.

Kasiński, A., Zielińska-Pisklak, M., Oledzka, E., & Sobczak, M. (2020). Smart hydrogels – synthetic stimuli-responsive antitumor drug release systems. *International Journal of Nanomedicine*, *15*, 4541–4572.

Kassie Netere, A., & Sendekie, A. K. (2022). Antibiotic Use among Patients visiting Primary Hospitals in Northwest Ethiopia: A Multicenter Cross-Sectional Survey. *Advances in Pharmacological & Pharmaceutical Sciences*, *2022*, 1–10.

Katual, M. K., & Harikumar, S. L. (2017). Formulation, optimization and in-vitro evaluation of metronidazole 500 mg floating tablets for the treatment of helicobacter pylori induced gastric inflammatory disorder, 809–835.

Kaur, G., Grewal, J., Jyoti, K., Jain, U. K., Chandra, R., & Madan, J. (2018). Oral controlled and sustained drug delivery systems: Concepts, advances, preclinical, and clinical status. In *Drug targeting and stimuli sensitive drug delivery systems* (pp. 567-626). William Andrew Publishing.

Kaur, I., Agnihotri, S., & Goyal, D. (2022). Fabrication of chitosan–alginate nanospheres for controlled release of cartap hydrochloride. *Nanotechnology, 33*(2), 025701.

Kaur, J., Kour, A., Panda, J. J., Harjai, K., & Chhibber, S. (2020). Exploring endolysin-loaded alginate-chitosan nanoparticles as future remedy for Staphylococcal Infections. *AAPS PharmSciTech, 21*, 1-15.

Khajuria, D. K., Vasireddi, R., Priydarshi, M. K., & Mahapatra, D. R. (2019). Ionic diffusion and drug release behavior of core–shell-functionalized alginate–chitosan-based hydrogel. *Acs Omega*, *5*(1), 758-765.

Khan, S., Ullah, A., & Ullah, K. (2016). Rehman Nu. *Insight into hydrogels. Designed Monomers and Polymers*, *19*(5), 456-478.

Khan, Y. A., Ozaltin, K., Bernal-Ballen, A., & Di Martino, A. (2021). Chitosan-alginate hydrogels for simultaneous and sustained releases of ciprofloxacin, amoxicillin and vancomycin for combination therapy. *Journal of Drug Delivery Science and Technology, 61*, 102126.

Khanum, H., Ullah, K., Murtaza, G., & Khan, S. A. (2018). Fabrication and in vitro characterization of HPMC-g-poly (AMPS) hydrogels loaded with loxoprofen sodium. *International journal of biological macromolecules*, *120*, 1624-1631.

Kiti, K., & Suwantong, O. (2020). Bilayer wound dressing based on sodium alginate incorporated with curcumin-β-cyclodextrin inclusion complex/chitosan hydrogel. *International Journal of Biological Macromolecules*, *164*, 4113-4124.

Komatsu, S., Tago, M., Ando, Y., Asoh, T. A., & Kikuchi, A. (2021). Facile preparation of multi-stimuli-responsive degradable hydrogels for protein loading and release. *Journal of Controlled Release*, *331*, 1-6.

Korsmeyer, R. W., Gurny, R., Doelker, E., Buri, P., & Peppas, N. A. (1983). Mechanisms of solute release from porous hydrophilic polymers. *International journal of pharmaceutics*, *15*(1), 25-35.

Kumar, D., Kumar, S., Kumar, S., Rohatgi, S., & Kundu, P. P. (2021). Synthesis of rifaximin loaded chitosan-alginate core-shell nanoparticles (Rif@ CS/Alg-NPs) for antibacterial applications. *International Journal of Biological Macromolecules*, *183*, 962-971.

Kumar, S., Prasad, M., & Rao, R. (2021). Topical delivery of clobetasol propionate loaded nanosponge hydrogel for effective treatment of psoriasis: Formulation, physicochemical characterization, antipsoriatic potential and biochemical estimation. *Materials Science and Engineering: C, 119*, 111605.

Kupnik, K., Primožič, M., Kokol, V., & Leitgeb, M. (2020). Nanocellulose in drug delivery and antimicrobially active materials. *Polymers*, *12*(12), 2825.

Kurakula, M., & Rao, G. K. (2020). Pharmaceutical assessment of polyvinylpyrrolidone (PVP): As excipient from conventional to controlled delivery systems with a spotlight on COVID-19 inhibition. *Journal of drug delivery science and technology*, *60*, 102046.

Lee, J. H., Youm, J. S., Ju, H. T., & Kim, J. C. (2020). Influence of N-vinyl-2-pyrrolidone and methacrylic acid on thermal curing process of 2-hydroxyethyl methacrylate hydrogel. *Journal of Applied Polymer Science*, *137*(17), 48622.

Lehner, E., Liebau, A., Syrowatka, F., Knolle, W., Plontke, S. K., & Mäder, K. (2021). Novel biodegradable round window disks for inner ear delivery of dexamethasone. *International Journal of Pharmaceutics*, *594*, 120180.

Lewandowska, K. (2011). Miscibility and interactions in chitosan acetate/poly (N-vinylpyrrolidone) blends. *Thermochimica Acta*, *517*(1-2), 90-97.

Maestrelli, F., Jug, M., Cirri, M., Kosalec, I., & Mura, P. (2018). Characterization and microbiological evaluation of chitosan-alginate microspheres for cefixime vaginal administration. *Carbohydrate polymers*, *192*, 176-183.

Maitra, J., & Shukla, V. K. (2014). Cross-linking in hydrogels-a review. *American Journal of Polymer Science*, *4*(2), 25-31.

Majcher, M. J., & Hoare, T. (2019). Applications of hydrogels 14. *Functional polymers*, *453*.

Malcolm, W., Baxter, L., McNicol, M., & Sneddon, J. (2020). Enough is enough–is it time for the Scottish Antimicrobial Prescribing Group (SAPG) to develop the third age of antimicrobial stewardship in primary care in Scotland? *Access Microbiology*, *2*(2), 3-24.

Mandal, Piyali, and Raja Shunmugam. "Polycaprolactone: a biodegradable polymer with its application in the field of self-assembly study." *Journal of Macromolecular Science, Part A* 58, no. 2 (2020): 111-129.

Marques, M. R., Loebenberg, R., & Almukainzi, M. (2011). Simulated biological fluids with possible application in dissolution testing. *Dissolution Technology*, *18*(3), 15-28.

Melnyk, Y., Stetsyshyn, Y., Skorokhoda, V., & Nastishin, Y. (2020). Polyvinylpyrrolidone-graft-poly (2-hydroxyethylmethacrylate) hydrogel membranes for encapsulated forms of drugs. *Journal of Polymer Research*, *27*, 1-11.

Mimura, Y., Yahiro, M., Masumoto, M., Fukui, R., Okamoto, R., Aichi, M., & Kuragano, T. (2020). The pharmacokinetics of oral metronidazole in patients with metronidazole-induced encephalopathy undergoing maintenance hemodialysis. *Hemodialysis International*, *24*(4), 528-533.

Mirică, I. C., Furtos, G., Lucaciu, O., Pascuta, P., Vlassa, M., Moldovan, M., & Campian, R. S. (2021). Electrospun Membranes based on polycaprolactone, nano-hydroxyapatite and metronidazole. *Materials*, *14*(4), 931.

Misiak, P., Markiewicz, K. H., Szymczuk, D., & Wilczewska, A. Z. (2020). Polymeric drug delivery systems bearing cholesterol moieties: A review. *Polymers*, *12*(11), 2620.

Mogilevskaya, E. L., Akopova, T. A., Zelenetskii, A. N., & Ozerin, A. N. (2006). The crystal structure of chitin and chitosan. *Polymer Science - Series A, 48*(2), 116–123.

Mohsen, M., Gomaa, E., Mazaid, N. A., & Mohammed, R. (2017). Synthesis and characterization of organic montmorillonite-polyvinyl alcohol-co-polyacrylic nanocomposite hydrogel for heavy metal uptake in water. *AIMS Materials Science, 4*(5), 1122-1139.

Mondal, R. K., Dubey, K. A., Kumar, J., Jagannath, Bhardwaj, Y. K., Melo, J. S., & Varshney, L. (2018). Carbon Nanotube Functionalization and Radiation Induced Enhancements in the Sensitivity of Standalone Chemiresistors for Sensing volatile Organic Compounds. *ACS Applied Nano Materials, 1*(10), 5470–5482.

Moshayedi, S., Sarpoolaky, H., & Khavandi, A. (2021). Fabrication, swelling behavior, and water absorption kinetics of genipin-crosslinked gelatin–chitosan hydrogels. *Polymer Engineering & Science*, *61*(12), 3094-3103.

Mujtaba, M. A., & Alotaibi, N. M. (2020). Chitosan-sodium alginate nanoparticle as a promising approach for oral delivery of rosuvastatin calcium: Formulation, optimization and in vitro characterization. *Journal of pharmaceutical research international*, *32*(1), 50-56.

Myhal, A. V., Golovchenko, O. S., Krutskikh, T. V., Gubar, S. M., & Georgiyants, V. A. (2016). IR-spectroscopy research into the structure of products of interaction between metronidazole and metal salts. *Der Pharma Chemica*, *8*(19), 148–154.

Najaf Oshani, B., Davachi, S. M., Hejazi, I., Seyfi, J., Khonakdar, H. A., & Abbaspourrad, A. (2019). Enhanced compatibility of starch with poly(lactic acid) and poly(ε-caprolactone) by incorporation of POSS nanoparticles: Study on thermal properties. *International Journal of Biological Macromolecules*, *141*, 578–584.

Nalini, T., Basha, S. K., Sadiq, A. M. M., Kumari, V. S., & Kaviyarasu, K. (2019). Development and characterization of alginate/chitosan nanoparticulate system for hydrophobic drug encapsulation. *Journal of Drug Delivery Science and Technology*, *52*, 65-72.

Naghshineh, N., Tahvildari, K., & Nozari, M. (2019). Preparation of Chitosan, Sodium Alginate, Gelatin and Collagen Biodegradable Sponge Composites and their Application in Wound Healing and Curcumin Delivery. *Journal of Polymers and the Environment*, *27*(12), 2819–2830. https://doi.org/10.1007/s10924-019-01559-z.

Narayanaswamy, R., & Torchilin, V. P. (2019). Hydrogels and their applications in targeted drug delivery. *Molecules*, *24*(3), 603.

Naseem, F., Shah, S. U., Rashid, S. A., Farid, A., Almehmadi, M., & Alghamdi, S. (2022). Metronidazole based floating bioadhesive drug delivery system for potential eradication of H. pylori: preparation and in vitro characterization. *Polymers*, *14*(3), 519.

Nastaj, J., Przewłocka, A., & Rajkowska-Myśliwiec, M. (2016). Biosorption of Ni (II), Pb (II) and Zn (II) on calcium alginate beads: equilibrium, kinetic and mechanism studies. *Polish Journal of Chemical Technology*, *18*(3), 81-87.

Nawaz, S., Khan, S., Farooq, U., Haider, M. S., Ranjha, N. M., Rasul, A., & Hameed, R. (2018). Biocompatible hydrogels for the controlled delivery of anti-hypertensive agent: Development, characterization and in vitro evaluation. *Designed Monomers and Polymers*, *21*(1), 18-32.

Nayak, A. K., Hasnain, M. S., Pal, K., Banerjee, I., & Pal, D. (2020). Gum-based hydrogels in drug delivery. In *Biopolymer-based formulations* (pp. 605-645). Elsevier.

Nematollahi, E., Pourmadadi, M., Yazdian, F., Fatoorehchi, H., Rashedi, H., & Nigjeh, M. N. (2021). Synthesis and characterization of chitosan/polyvinylpyrrolidone coated nanoporous γ-Alumina as a pH-sensitive carrier for controlled release of quercetin. *International Journal of Biological Macromolecules*, *183*, 600-613.

Ngwabebhoh, F. A., Zandraa, O., Patwa, R., Saha, N., Capáková, Z., & Saha, P. (2021). Self-crosslinked chitosan/dialdehyde xanthan gum blended hypromellose hydrogel for the controlled delivery of ampicillin, minocycline and rifampicin. *International Journal of Biological Macromolecules*, *167*, 1468-1478.

Nia, S. B., Pooresmaeil, M., & Namazi, H. (2020). Carboxymethylcellulose/layered double hydroxides bio-nanocomposite hydrogel: A controlled amoxicillin nanocarrier for colonic bacterial infections treatment. *International journal of biological macromolecules*, *155*, 1401-1409.

Niu, Y., Yang, T., Ke, R., & Wang, C. (2019). Preparation and characterization of pH-responsive sodium alginate/humic acid/konjac hydrogel for L-ascorbic acid controlled release. *Materials Express*, *9*(6), 563-569.

Nogami, S., Uchiyama, H., Kadota, K., & Tozuka, Y. (2021). Design of a pH-responsive oral gel formulation based on the matrix systems of gelatin/hydroxypropyl methylcellulose phthalate for controlled drug release. *International Journal of Pharmaceutics*, *592*, 120047.

Noor, S., Salam, F. B. A., Hima, H. N., Bhuiyan, S., & Chowdhury, S. (2017). Comparative in-vitro quality evaluation of some brands of Metronidazole tablet available in Bangladesh. *International Journal of Applied Research*, *3*(7), 753-8.

Noshadi, I., Walker, B. W., Portillo-Lara, R., Shirzaei Sani, E., Gomes, N., Aziziyan, M. R., & Annabi, N. (2017). Engineering biodegradable and biocompatible bio-ionic liquid conjugated hydrogels with tunable conductivity and mechanical properties. *Scientific reports*, *7*(1), 4345.

Oliveira, I. M., Gonçalves, C., Shin, M. E., Lee, S., Reis, R. L., Khang, G., & Oliveira, J. M. (2021). Enzymatically crosslinked tyramine-gellan gum hydrogels as drug delivery system for rheumatoid arthritis treatment. *Drug Delivery and Translational Research*, *11*, 1288-1300.

Onnainty, R., & Granero, G. (2019). Chitosan-based nanocomposites: Promising materials for drug delivery applications. In *Biomedical applications of nanoparticles* (pp. 375-407). William Andrew Publishing.

Oucif, A., Haddadine, N., Zakia, D., Bouslah, N., Benaboura, A., Beyaz, K., ... & El-Shall, M. S. (2021). Poly (hydroxyethyl methacrylate-co-hydroxyethyl acrylate) soft contact lenses for acetazolamide release. *Polymer Bulletin*, 1-20.

Oustadi, F., Haghbin Nazarpak, M., Mansouri, M., & Ketabat, F. (2022). Preparation, characterization, and drug release study of ibuprofen-loaded poly (vinyl alcohol)/poly (vinyl pyrrolidone) bilayer antibacterial membrane. *International Journal of Polymeric Materials and Polymeric Biomaterials*, *71*(1), 14-23.

Pacheco, Murilo Santos, Gustavo Eiji Kano, Letícia de Almeida Paulo, Patricia Santos Lopes, and Mariana Agostini de Moraes. "Silk fibroin/chitosan/alginate multilayer membranes as a system for controlled drug release in wound healing." *International journal of biological macromolecules* 152 (2020): 803-811.

Pal, D., Nayak, A. K., & Saha, S. (2018). Interpenetrating polymer network hydrogels of chitosan: applications in controlling drug release. *Cellulose-based superabsorbent hydrogels*, 1-41.

Pan, J., Li, Y., Chen, K., Zhang, Y., & Zhang, H. (2021). Enhanced physical and antimicrobial properties of alginate/chitosan composite aerogels based on electrostatic interactions and noncovalent crosslinking. *Carbohydrate Polymers*, *266*, 118102.

Panahi, Y., Gharekhani, A., Hamishehkar, H., Zakeri-Milani, P., & Gharekhani, H. (2019). Stomach-specific drug delivery of clarithromycin using a semi interpenetrating polymeric network hydrogel made of montmorillonite and chitosan: Synthesis, characterization and in vitro drug release study. *Advanced pharmaceutical bulletin*, *9*(1), 159.

Patil, U. S. (2012). Laboratory Methodologies for Bacterial Antimicrobial Susceptibility Testing. *OIE Terrestrial Manual*, 1–11.

Payne, C. (2018). *The Development of Hydrogels and Nanoparticles for Drug and Cell Delivery to the Distal Airways* (Doctoral dissertation, Royal College of Surgeons in Ireland).

Peers, S., Montembault, A., & Ladavière, C. (2020). Chitosan hydrogels for sustained drug delivery. *Journal of Controlled Release*, *326*, 150-163.

Pellá, M. C., Lima-Tenório, M. K., Tenório-Neto, E. T., Guilherme, M. R., Muniz, E. C., & Rubira, A. F. (2018). Chitosan-based hydrogels: From preparation to biomedical applications. *Carbohydrate polymers*, *196*, 233-245.

Perea, G. N., Pavinatto, A., Schneider, R., Munk, M., Brandão, H. M., & Correa, D. S. (2023). Electrospun nanofibers based on polyvinylpyrrolidone/chitosan and cloxacillin: investigation of morphological features, antibiotic release and antimicrobial properties. *Journal of Polymer Research*, *30*(5), 166.

Pereira, A. K. D. S., Reis, D. T., Barbosa, K. M., Scheidt, G. N., da Costa, L. S., & Santos, L. S. S. (2020). Antibacterial effects and ibuprofen release potential using chitosan microspheres loaded with silver nanoparticles. *Carbohydrate research*, *488*, 107891.

Qader, H. A., & Fakhre, N. A. (2015). Spectrophotometric determination of amoxicillin trihydrate in pure and pharmaceutical dosage forms. *Ibn AL-Haitham Journal for Pure and Applied Science*, *28*(3), 142-153.

Rade, P. P., Giram, P. S., Shitole, A. A., Sharma, N., & Garnaik, B. (2022). Physicochemical and in vitro antibacterial evaluation of metronidazole loaded Eudragit S-100 nanofibrous mats for the intestinal drug delivery. *Advanced Fiber Materials*, *4*(1), 76-88.

Radhakrishnan, A., Jose, G. M., & Kurup, M. (2015). PEG-penetrated chitosan–alginate co-polysaccharide-based partially and fully cross-linked hydrogels as ECM mimic for tissue engineering applications. *Progress in Biomaterials*, *4*, 101-112.

Rahimzadeh, G., Saeedi, M., Moosazadeh, M., Hashemi, S. M. H., Babaei, A., Rezai, M. S., & Nokhodchi, A. (2021). Encapsulation of bacteriophage cocktail into chitosan for the treatment of bacterial diarrhea. *Scientific Reports*, *11*(1), 15603.

Rahma, A., Munir, M. M., Prasetyo, A., Suendo, V., & Rachmawati, H. (2016). Intermolecular interactions and the release pattern of electrospun curcumin-polyvinyl (pyrrolidone) fiber. *Biological and Pharmaceutical Bulletin*, *39*(2), 163-173.

Rahman, M. M., Jahan, F. I., Fahim, N. F., Paul, N., Jahan, N., Harun-Or-Rashid, M., & Tanny, S. Z. (2020). In vitro comparative quality evaluation of leading brands of metronidazole tablets available in Bangladesh. *Vitro*, *2*, 63-72.

Rapp, T. L., & DeForest, C. A. (2021). Targeting drug delivery with light: A highly focused approach. *Advanced drug delivery reviews*, *171*, 94-107.

Rassu, G., Salis, A., Porcu, E. P., Giunchedi, P., Roldo, M., & Gavini, E. (2016). Composite chitosan/alginate hydrogel for controlled release of deferoxamine: A system to potentially treat iron dysregulation diseases. *Carbohydrate polymers*, *136*, 1338-1347.

Reddy, C. L. N., Swamy, B. Y., Prasad, C. V., Rao, K. M., Prabhakar, M. N., Aswini, C., Subha, M. C. S., & Rao, K. C. (2012). Development and characterization of Chitosan-Poly (vinyl pyrrolidone) Blend microspheres for controlled release of metformin hydrochloride. *International Journal of Polymeric Materials*, *61*(6), 424–436.

Ribeiro, D., Yuto, G., & Titotto, S. L. M. C. (2019). Analysis about the behavior and modeling of PH-sensitive hydrogels with different ratios of chitosan and polyvinylpyrrolidone. *Journal of Materials Science and Chemical Engineering*, *7*(8), 64-76.

Rodríguez-villodres, Á., Gil-Marqués, M. L., Álvarez-Marín, R., Bonnin, R. A., Pachón-Ibáñez, M. E., Aguilar-Guisado, M., ... & Smani, Y. (2020). Extended-spectrum resistance to β-lactams/β-lactamase inhibitors (ESRI) evolved from low-level resistant Escherichia coli. *Journal of Antimicrobial Chemotherapy*, *75*(1), 77-85.

Sabbagh, H. A. K., Abudayeh, Z., Abudoleh, S. M., Alkrad, J. A., Hussein, M. Z., & Hussein-Al-Ali, S. H. (2019). Application of multiple regression analysis in optimization of metronidazole-chitosan nanoparticles. *Journal of Polymer Research*, *26*, 1-14.

Saini, K. (2017). Preparation method, Properties and Crosslinking of hydrogel: a review. *PharmaTutor*, *5*(1), 27-36.

Segale, L., Giovannelli, L., Mannina, P., & Pattarino, F. (2016). Calcium alginate and calcium alginate-chitosan beads containing celecoxib solubilized in a self-emulsifying phase. *Scientifica*, *2016*.

Segura-Egea, J. J., Martín-González, J., del Carmen Jiménez-Sánchez, M., Crespo-Gallardo, I., Saúco-Márquez, J. J., & Velasco-Ortega, E. (2017). Worldwide pattern of antibiotic prescription in endodontic infections. *International dental journal*, *67*(4), 197-205.

Sharma, A. K., Kaith, B. S., Chandel, K., & Singh, A. (2020). Chemically modified chitosan-sodium alginate as chemo-sensor adsorbent for the detection of picric acid and removal of biebrich scarlet. *International journal of biological macromolecules*, *147*, 582-594.

Sharma, C., Dinda, A. K., Potdar, P. D., Chou, C. F., & Mishra, N. C. (2016). Fabrication and characterization of novel nano-biocomposite scaffold of chitosan–gelatin–alginate–hydroxyapatite for bone tissue engineering. *Materials Science and Engineering: C*, *64*, 416-427.

Sharma, S., Jain, P., & Tiwari, S. (2020). Dynamic imine bond based chitosan smart hydrogel with magnified mechanical strength for controlled drug delivery. *International Journal of Biological Macromolecules*, *160*, 489-495.

Shoukat, H., Pervaiz, F., Noreen, S., Nawaz, M., Qaiser, R., & Anwar, M. (2020). Fabrication and evaluation studies of novel polyvinylpyrrolidone and 2-acrylamido-2-methylpropane sulphonic acid-based crosslinked matrices for controlled release of acyclovir. *Polymer Bulletin*, *77*, 1869-1891.

Siboro, S. A., Anugrah, D. S., Ramesh, K., Park, S. H., Kim, H. R., & Lim, K. T. (2021). Tunable porosity of covalently crosslinked alginate-based hydrogels and its significance in drug release behavior. *Carbohydrate Polymers*, *260*, 117779.

Song, G., Zhao, Z., Peng, X., He, C., Weiss, R. A., & Wang, H. (2016). Rheological behavior of tough PVP-in situ-PAAm hydrogels physically cross-linked by cooperative hydrogen bonding. *Macromolecules*, *49*(21), 8265-8273.

Spizzirri, U. G., & Cirillo, G. (Eds.). (2017). *Functional hydrogels in drug delivery: key features and future perspectives*. CRC Press.

Suhail, M., Khan, A., Rosenholm, J. M., Minhas, M. U., & Wu, P. C. (2021). Fabrication and characterization of diclofenac sodium loaded hydrogels of sodium alginate as sustained release carrier. *Gels*, *7*(1), 10.

Su, T., Zhao, W., Wu, L., Dong, W., & Qi, X. (2020). Facile fabrication of functional hydrogels consisting of pullulan and polydopamine fibers for drug delivery. *International Journal of Biological Macromolecules*, *163*, 366–374.

Sun, C. K., Ke, C. J., Lin, Y. W., Lin, F. H., Tsai, T. H., & Sun, J. S. (2021). Transglutaminase cross-linked gelatin-alginate-antibacterial hydrogel as the drug delivery-coatings for implant-related infections. *Polymers*, *13*(3), 414.

Sun, Lingfeng, Xiangjiang Nie, Wenjie Lu, Qing Zhang, Wenyou Fang, Song Gao, Shengqi Chen, and Rongfeng Hu. "Mucus-penetrating alginate-chitosan nanoparticles loaded with berberine hydrochloride for oral delivery to the inflammation site of ulcerative colitis." *AAPS PharmSciTech* 23, no. 6 (2022): 179.

Tahtat, D., Mahlous, M., Benamer, S., Khodja, A. N., Oussedik-Oumehdi, H., & Laraba-Djebari, F. (2013). Oral delivery of insulin from alginate/chitosan crosslinked by glutaraldehyde. *International journal of biological macromolecules*, *58*, 160-168.

Tang, S., Yang, J., Lin, L., Peng, K., Chen, Y., Jin, S., & Yao, W. (2020). Construction of physically crosslinked chitosan/sodium alginate/calcium ion double-network hydrogel and its application to heavy metal ions removal. *Chemical Engineering Journal*, *393*, 124728.

Thakur, V. K., & Thakur, M. K. (Eds.). (2018). *Hydrogels: recent advances*. Springer, 87, 268–474.

Uzunoğlu, B., Wilson, C. G., Sağıroğlu, M., Yüksel, S., & Şenel, S. (2021). Mucoadhesive bilayered buccal platform for antifungal drug delivery into the oral cavity. *Drug Delivery and Translational Research*, *11*, 318-327.

Van Donge, T., Fuchs, A., Leroux, S., Pfister, M., Rodieux, F., Atkinson, A., & Bielicki, J. (2021). Amoxicillin dosing regimens for the treatment of neonatal sepsis: balancing efficacy and neurotoxicity. *Neonatology*, *117*(5), 619-627.

Veeraraghavan, B., Bakthavatchalam, Y. D., & Sahni, R. D. (2021). Orally administered amoxicillin/clavulanate: current role in outpatient therapy. *Infectious Diseases and Therapy*, *10*, 15-25.

Viswanathan, P., Muralidaran, Y., & Ragavan, G. (2017). Challenges in oral drug delivery: a nano-based strategy to oVercome. In *Nanostructures for oral medicine* (pp. 173-201). Elsevier.

Wang, G., Wang, X., & Huang, L. (2017). Feasibility of chitosan-alginate (Chi-Alg) hydrogel used as scaffold for neural tissue engineering: a pilot study in vitro. *Biotechnology & Biotechnological Equipment*, *31*(4), 766-773.

Wang, L., Sun, L., Gu, Z., Li, W., Guo, L., Ma, S., & Chang, J. (2022). N-carboxymethyl chitosan/sodium alginate composite hydrogel loading plasmid DNA as a promising gene activated matrix for in-situ burn wound treatment. *Bioactive Materials*, *15*, 330-342.

Wang, S., Liu, R., Fu, Y., & Kao, W. J. (2020). Release mechanisms and applications of drug delivery systems for extended-release. *Expert Opinion on Drug Delivery*, *17*(9), 1289-1304.

Wang, X., Li, S., Yu, H., Lv, J., Fan, M., Wang, X., ... & Zhao, Z. (2022). The biocompatibility of multi-source stem cells and gelatin-carboxymethyl chitosan-sodium alginate hybrid biomaterials. *Tissue Engineering and Regenerative Medicine*, *19*(3), 491-503.

Wathoni, N., Yuniarsih, N., Cahyanto, A., & Muhctaridi, M. (2019). α-Mangostin hydrogel film based chitosan–alginate for recurrent aphthous stomatitis. *Applied Sciences*, *9*(23), 5235.

Webber, M. J., & Pashuck, E. T. (2021). (Macro) molecular self-assembly for hydrogel drug delivery. *Advanced drug delivery reviews*, *172*, 275-295.

Wilson, A. N. (2014). *Drug delivery with feedback control in bioresponsive hydrogels* (Doctoral dissertation, Clemson University), *39*, 78-172.

Wong, R. S. H., Ashton, M., & Dodou, K. (2015). Effect of crosslinking agent concentration on the properties of unmedicated hydrogels. *Pharmaceutics*, *7*(3), 305-319.

Wu, T., Li, Y., Shen, N., Yuan, C., & Hu, Y. (2018). Preparation and characterization of calcium alginate-chitosan complexes loaded with lysozyme. *Journal of Food Engineering*, *233*, 109-116.

Wu, T., Yu, S., Lin, D., Wu, Z., Xu, J., Zhang, J., & Cai, X. (2020). Preparation, characterization, and release behavior of doxorubicin hydrochloride from dual cross-linked chitosan/alginate hydrogel beads. *ACS Applied Bio Materials*, *3*(5), 3057-3065.

Wu, X., Tang, Z., Liao, X., Wang, Z., & Liu, H. (2020). Fabrication of chitosan@ calcium alginate microspheres with porous core and compact shell, and application as a quick traumatic hemostat. *Carbohydrate polymers*, *247*, 116669.

Xiong, W., Zhang, Q., Yin, F., Yu, S., Ye, T., Pan, W., & Yang, X. (2016). Auricularia auricular polysaccharide-low molecular weight chitosan polyelectrolyte complex nanoparticles: Preparation and characterization. *Asian journal of pharmaceutical sciences*, *11*(3), 439-448.

Yang, J., Chen, J., Pan, D., Wan, Y., & Wang, Z. (2013). pH-sensitive interpenetrating network hydrogels based on chitosan derivatives and alginate for oral drug delivery. *Carbohydrate polymers*, *92*(1), 719-725.

Yang, S. J., Jeong, J. O., Lim, Y. M., & Park, J. S. (2021). Synthesis and characterization of PVP microneedle patch using metal bioelectrodes for novel drug delivery system. *Materials & Design*, *201*, 109485.

Zainal, S. H., Mohd, N. H., Suhaili, N., Anuar, F. H., Lazim, A. M., & Othaman, R. (2021). Preparation of cellulose-based hydrogel: A review. *Journal of Materials Research and Technology*, *10*, 935-952.

Zamani, M. H., Khatibi, A., Tavana, B., Zahedi, P., & Aghamohammadi, S. (2023). Characterization of drug-loaded alginate-chitosan polyelectrolyte nanoparticles synthesized by microfluidics. *Journal of Polymer Research*, *30*(2), 86.

Zhang, H., Wang, W., Ding, J., Lu, Y., Xu, J., & Wang, A. (2020). An upgraded and universal strategy to reinforce chitosan/polyvinylpyrrolidone film by incorporating active silica nanorods derived from natural palygorskite. *International Journal of Biological Macromolecules*, *165*, 1276-1285.

Zhang, S., Han, D., Ding, Z., Wang, X., Zhao, D., Hu, Y., & Xiao, X. (2019). Fabrication an characterization of one interpenetrating network hydrogel based on sodium alginate and polyvinyl alcohol. *Journal of Wuhan University of Technology-Mater. Sci. Ed.*, *34*(3), 744-751.

Zou, Z., Zhang, B., Nie, X., Cheng, Y., Hu, Z., Liao, M., & Li, S. (2020). A sodium alginate-based sustained-release IPN hydrogel and its applications. *RSC advances*, *10*(65), 39722-39730

APPENDIX I

a) Swelling ratios of hydrogels H1 to H5 in SGF (pH 1.2)

Time (min)	H1	SD	H2	SD	H3	SD	H4	SD	H5	SD
0	0.0825	0.0025	0.1125	0.0014	0.0955	0.0028	0.0996	0.00023	0.05726	0.00155
10	140.822	6.6473	142.48	2.2302	177.27	5.456	197.434	5.7452	203.102	7.942
30	213.438	9.1522	256.672	3.856	268.157	2.1903	312.785	8.7204	342.82	8.627
60	312.376	10.966	346.36	6.398	372.130	3.7511	392.95	11.155	432.03	9.28
90	386.734	14.878	407.43	3.648	414.522	14.277	439.976	10.722	488.080	12.391
120	429.2	15.306	447.445	6.554	460.011	10.736	478.311	14.276	509.057	7.8203
150	457.116	11.278	473.393	7.0838	476.28	16.015	497.710	14.053	518.856	7.294
180	474.249	15.270	486.371	2.494	492.127	7.496	507.539	11.479	531.686	14.875
210	475.817	14.842	495.93	2.830	501.065	6.4071	509.282	8.3103	532.490	5.0768
240	475.55	12.965	496.06	3.975	505.740	3.470	512.244	7.0876	535.471	8.875

b) Swelling ratios of hydrogels H1 to H5 in SIF (pH 6.8)

Time (min)	H1	SD	H2	SD	H3	SD	H4	SD	H5	SD
0	0.0812	0.0056	0.1145	0.0034	0.1055	0.0037	0.0966	0.00186	0.0342	0.00072
10	129.155	14.699	154.376	7.1608	175.39	9.260	184.761	4.531	204.145	13.161
30	190.970	17.613	245.395	8.1113	265.738	11.173	275.82	12.225	316.955	18.817
60	278.861	18.081	330.353	12.825	358.124	17.531	367.604	6.628	412.66	5.623
90	353.598	12.481	392.72	14.357	407.585	14.830	433.180	9.4038	469.826	7.823
120	399.50	19.848	427.058	14.626	444.829	17.224	477.410	10.976	494.072	15.178
150	425.563	16.777	452.857	16.878	466.683	10.465	482.99	12.525	501.27	16.527
180	447.89	19.034	470.26	14.055	482.35	10.675	496.716	9.768	511.758	12.811
210	451.324	18.093	475.476	12.624	487.66	12.934	502.34	16.675	520.185	13.915
240	452.987	21.843	474.25	13.621	487.28	10.281	509.84	10.473	522.22	9.451

c) Swelling ratios of hydrogels H1 to H5 in SCF (pH 7.4)

Time (min)	H1	SD	H2	SD	H3	SD	H4	SD	H5	SD
0	0.0771	0.00129	0.10123	0.00015	0.0990	0.00244	0.09723	0.00085	0.03483	0.00095
10	91.072	0.7146	143.6277	7.7703	151.787	5.2323	177.68	2.9973	202.22	17.05
30	158.702	8.6895	216.926	6.5541	241.98	7.5795	248.267	2.8059	279.54	11.636
60	226.407	2.0980	282.440	7.5303	305.742	9.8272	322.585	4.0327	344.002	20.374
90	274.591	3.8744	331.66	9.6903	361.577	9.4711	374.21	5.2989	396.772	12.608
120	305.700	3.9117	368.907	5.9003	394.59	11.517	410.32	4.4722	441.743	18.837
150	336.944	13.579	396.60	8.1064	416.194	11.960	436.575	7.102	462.83	21.328
180	351.192	8.5359	407.920	4.846	431.599	8.742	456.271	5.2464	472.435	26.060
210	367.43	6.1969	409.29	7.0775	440.58	9.538	461.71	6.091	480.60	17.500
240	368.82	6.527	410.88	3.648	448.86	10.562	471.00	6.7129	488.19	18.982

d) Swelling ratios of hydrogels H2-G1 to H2-G5 in SGF (pH 1.2)

Time (min)	H2-G1	SD	H2-G2	SD	H2-G3	SD	H2-G4	SD	H2-G5	SD
0	0.04956	0.00247	0.1062	0.0053	0.1119	0.0055	0.1938	0.0096	0.1349	0.0067
10	145.241	27.262	184.48	19.224	208.252	18.412	139.69	16.984	69.82	23.491
30	222.161	23.108	299.009	14.950	347.459	17.372	189.46	19.473	127.67	16.383
60	308.913	25.445	379.98	18.999	421.076	21.053	261.321	23.066	166.845	18.342
90	352.602	21.630	429.725	21.486	486.014	24.3007	303.894	15.194	206.017	20.3008
120	384.661	20.233	474.390	23.719	528.969	20.448	335.179	16.758	222.752	19.137
150	406.410	20.320	507.955	21.397	560.192	22.009	346.535	17.32	236.428	21.821
180	422.82	21.141	535.690	20.784	573.698	20.684	353.85	17.692	244.795	20.239
210	436.84	21.8422	547.407	17.3703	580.219	19.010	356.964	17.8482	249.835	21.4917
240	449.28	22.4644	548.683	17.4341	588.4101	18.420	360.524	18.0262	257.240	22.862

e) Swelling ratios of hydrogels H2-G1 to H2-G5 in SIF (pH 6.8)

Time (min)	H2-G1	SD	H2-G2	SD	H2-G3	SD	H2-G4	SD	H2-G5	SD
0	0.05293	0.00161	0.1022	0.00037	0.08903	0.00080	0.17253	0.00144	0.1548	0.00470
10	131.351	6.0365	173.945	3.6213	196.241	4.4083	119.555	2.6852	48.111	3.0585
30	193.686	4.542	277.408	4.200	310.728	4.0519	180.447	0.652	117.46	19.249
60	263.66	6.4741	358.679	9.9450	404.408	10.821	238.06	3.27	156.83	12.105
90	320.311	10.959	407.210	2.253	468.68	3.498	295.237	6.2392	194.26	10.466
120	358.695	19.346	454.057	0.6263	509.496	2.732	322.625	7.725	212.233	15.801
150	387.570	17.4003	487.922	7.925	544.677	8.515	337.024	1.376	217.96	12.482
180	398.613	18.803	507.472	2.376	563.342	12.566	348.434	3.949	225.054	12.691
210	407.927	15.158	513.86	1.730	562.011	15.105	352.943	4.792	231.881	16.136
240	412.16	15.83	516.30	2.980	557.447	16.726	355.63	5.641	235.541	14.179

f) Swelling ratios of hydrogels H2-G1 to H2-G5 in SCF (pH 7.4)

Time (min)	H2-G1	SD	H2-G2	SD	H2-G3	SD	H2-G4	SD	H2-G5	SD
0	0.0876	0.0003	0.1073	0.00158	0.0936	0.0028	0.1302	0.00627	0.2133	0.0045
10	88.1045	3.7930	164.273	11.811	170.481	12.246	72.876	9.6126	43.0406	2.6894
30	139.215	2.2272	273.770	6.8367	278.439	14.558	119.768	12.411	86.153	3.2892
60	217.626	0.1892	350.854	6.5057	371.121	11.598	180.528	15.188	122.768	3.2704
90	266.857	3.0531	413.712	8.4046	422.847	16.186	228.314	15.586	146.386	7.0137
120	310.166	4.3869	441.488	6.2357	454.848	10.860	264.671	18.739	158.073	6.0612
150	330.775	1.7164	460.932	15.166	478.189	18.783	288.861	16.517	167.825	4.660
180	348.396	5.2131	468.44	16.619	482.819	16.013	302.75	19.518	175.493	5.3357
210	356.409	5.737	474.65	16.498	494.247	10.331	316.086	18.85	176.895	5.0841
240	365.717	5.9647	483.496	20.527	502.960	7.3526	320.134	19.011	179.31	4.9702

APPENDIX II

a) Swelling ratios of hydrogels B1-B5 in SGF (pH 1.2)

Time(min)	B1	SD	B2	SD	B3	SD	B4	SD	B5	SD
0	0.34428	0	0.29376	0	0.57233	0	0.50606	0	0.46206	0
10	20.3970	4.11679	34.3356	4.83884	42.9120	0.94470	46.6078	4.04018	54.3067	2.06606
30	48.428	2.39961	59.7639	4.51593	66.0104	5.44518	74.8979	5.29193	80.1760	4.74923
60	61.790	5.15223	71.9391	4.13111	76.1502	2.74676	88.9672	3.27140	97.5184	5.64342
90	73.442	1.93821	80.1089	3.05140	86.9423	3.38879	99.5718	5.79919	104.249	4.29421
120	77.626	2.6535	86.1341	4.23328	97.1112	4.37096	107.047	4.87564	112.956	4.10420
150	82.299	2.4105	92.8060	3.96157	100.058	2.6324	111.098	4.70691	116.368	5.60979
180	80.612	2.3094	91.886	4.1000	102.556	3.24245	111.171	3.53338	117.457	4.02026
210	83.048	2.1864	93.997	3.88891	103.185	3.1927	111.665	4.63457	119.167	5.8683
240	84.136	2.7197	93.509	3.1170	106.70	2.3106	115.40	4.59379	121.2668	4.558666

b) Swelling ratios of hydrogels B1-B5 in SIF (pH 6.8)

Time(min)	B1	SD	B2	SD	B3	SD	B4	SD	B5	SD
0	0.586867	0	0.584933	0	0.3984	0	0.2362	0	0.331833	0
10	51.068	8.17600	50.3840	6.733	44.820	7.3249	24.238	8.044	20.803	9.4472
30	110.892	9.1480	96.432	8.0593	84.270	8.2582	77.088	12.799	63.154	10.294
60	156.842	7.752	126.901	9.3148	104.74	7.6627	95.936	14.079	79.045	8.1656
90	227.151	6.143	158.53	8.6106	130.44	9.1445	108.987	12.319	89.382	8.9867
120	280.450	6.0557	196.444	9.2521	147.64	8.644	126.044	12.683	105.524	11.937
150	314.311	9.6015	244.765	8.2079	173.46	7.5444	141.379	10.282	117.77	7.7323
180	327.553	11.731	287.109	6.2248	194.21	7.4314	141.873	7.9621	122.029	8.6483
210	332.454	5.6937	300.99	7.5527	200.21	6.859	150.931	9.1707	124.892	8.4601
240	334.206	5.5261	306.504	9.1743	205.86	8.2594	157.491	8.6343	126.770	10.311

c) Swelling ratios of hydrogels B1-B5 in SCF (pH 7.4)

Time(min)	B1	SD	B2	SD	B3	SD	B4	SD	B5	SD
0	0.3867	0	0.5381	0	0.2967	0	0.2316	0	0.2926	0
10	60.229	9.1605	46.021	7.6616	61.622	10.342	44.932	9.5106	46.059	7.6314
30	125.84	9.824	98.289	7.2444	99.079	8.1790	91.632	8.8857	78.929	9.4196
60	179.549	7.5404	134.703	8.4164	139.638	9.824	126.153	6.7941	102.744	8.6311
90	243.874	8.581	186.994	8.1622	157.646	8.2431	140.070	7.7632	121.287	7.2546
120	297.904	6.4424	240.122	9.7180	188.514	9.7456	158.688	10.078	143.963	6.94705
150	359.751	7.5546	278.667	11.156	234.980	10.810	170.619	7.466	152.767	7.4308
180	388.992	8.4236	299.148	10.767	246.739	8.7069	180.665	8.70461	162.437	8.0312
210	404.375	7.4599	308.693	8.0181	262.588	8.3909	193.691	7.633	168.929	9.6855
240	406.842	9.1212	311.79	7.5839	267.473	6.3187	197.619	9.5296	177.357	8.4382

d) Swelling ratios of hydrogels B1-C1 to B1-C5 in SGF (pH 1.2)

Time(Min)	B1-C1	SD	B1-C2	SD	B1-C3	SD	B1-C4	SD	B1-C5	SD
0	0.67566	5.4184	0.8013	0.8119	1.001	1.9293	0.7563	0.5343	0.4746	2.6002
10	60.335	1.7025	58.527	1.6988	47.086	1.1139	43.763	3.707	37.008	3.583
30	84.95	4.794	72.587	1.6508	61.205	1.940	56.280	2.0988	49.297	4.3192
60	92.945	1.778	81.821	1.533	74.69	3.569	67.43	3.749	54.28	2.829
90	99.65	2.956	88.602	3.179	80.153	1.363	71.74	2.53	59.33	3.2660
120	104.44	1.482	92.429	2.132	83.416	1.471	73.953	3.674	61.37	2.986
150	107.054	1.545	94.841	1.889	84.781	1.183	75.583	2.8140	63.132	2.6341
180	107.893	2.9203	95.133	1.2746	85.081	1.642	78.316	3.223	67.064	1.1729
210	108.238	1.5663	92.346	2.0173	86.313	1.7758	78.889	1.865	68.609	2.959
240	106.265	1.482	93.55	2.533	85.647	2.508	78.457	1.334	70.646	3.4809

e) Swelling ratios of hydrogels B1-C1 to B1-C5 in SIF (pH 6.8)

Time(min)	B1-C1	SD	B1-C2	SD	B1-C3	SD	B1-C4	SD	B1-C5	SD
0	0.53866	1.50987	0.24293	3.32056	0.5036	0.2582	0.7783	1.5132	1.0676	0.9574
10	52.787	9.5098	47.318	10.0008	47.263	8.7328	40.171	8.1413	38.526	7.8098
30	108.667	8.4808	78.863	8.1583	71.815	9.1299	61.156	7.0264	49.235	6.7039
60	172.43	6.6550	133.314	8.2392	104.69	1.8401	79.186	5.5688	59.662	5.4579
90	228.440	7.5551	172.062	7.6394	127.361	8.259	96.188	6.3704	62.784	5.561
120	264.329	7.8002	193.167	9.235	151.670	6.9047	116.402	4.8272	72.338	6.123
150	278.919	8.0905	231.86	7.2988	173.44	7.821	122.698	5.7416	74.24	5.770
180	300.784	7.1486	262.26	6.235	182.22	8.776	137.430	7.7987	79.987	7.0397
210	312.325	6.5098	274.074	5.1077	187.699	7.678	151.99	6.084	85.669	6.0198
240	310.235	7.3356	287.100	7.6585	197.578	8.4560	160.042	6.5417	89.291	5.373

f) Swelling ratios of hydrogels B1-C1 to B1-C5 in SCF (pH 7.4)

Time(min)	B1-C1	SD	B1-C2	SD	B1-C3	SD	B1-C4	SD	B1-C5	SD
0	0.4896	0.3689	0.286	1.66	0.4284	1.8550	0.507633	1.3685	1.069667	1.4523
10	83.235	14.121	85.117	14.174	72.05955	11.262	55.21045	9.2259	47.89654	6.4669
30	217.14	13.647	182.830	11.844	128.3499	14.512	97.97754	10.474	89.52945	8.8851
60	331.13	11.984	261.505	12.186	162.7792	13.589	114.1309	9.2718	96.07354	7.6906
90	382.19	10.170	315.353	9.0598	189.1439	14.297	132.7861	10.581	105.0795	6.6375
120	419.14	8.738	355.174	8.733	217.6179	12.041	145.8467	11.36	114.7398	7.8145
150	448.46	10.049	366.533	10.509	241.7494	8.595	161.9345	10.478	119.383	6.857
180	463.51	12.734	385.858	11.232	265.3226	10.637	188.1345	12.615	127.4852	8.728
210	491.32	11.813	396.769	10.122	273.6352	11.396	200.9718	11.148	123.2627	7.7498
240	512.65	9.417	418.795	11.501	295.3474	12.471	213.1525	9.5021	125.3973	9.5188

APPENDIX III

a) Porosity (%) of hydrogels H1 to H5

Hydrogel code	Porosity (%)	SD
H1	60.63862	1.15
H2	68.71148	1.2421
H3	74.06437	1.3121
H4	78.31797	1.1543
H5	83.06467	1.2134

b) Porosity (%) of hydrogels H2-G1 to H2-G5

Hydrogel code	porosity(%)	SD
H2-G1	77.27698	3.848193
H2-G2	80.13731	3.21666
H2-G3	94.62756	2.335367
H2-G4	72.98401	2.646677
H2-G5	63.83688	2.033537

c) Porosity (%) of hydrogels B1 to B5

Polymer ratio	Porosity (%)	SD
B1	91.95458	1.30061
B2	86.00161	1.390098
B3	82.43358	1.87988
B4	79.74657	2.142819
B5	74.61792	2.873545

d) Porosity (%) of hydrogels B1 to B5

hydrogel code	Porosity (%)	SD
B1-C1	86.82627	2.646677
B1-C2	82.93877	3.21666
B1-C3	77.64307	2.033537
B1-C4	74.78525	1.286158
B1-C5	68.65456	3.848193

APPENDIX IV

a) Gel fraction (%) of hydrogels H1 to H5

Hydrogel code	Gel fraction (%)	SD
H1	90.43923	0.494184
H2	86.66118	0.627119
H3	81.60887	0.48065
H4	79.02741	0.552005
H5	77.48461	0.535605

b) Gel fraction (%) of hydrogels H2-G1 to H2-G5

Hydrogel code	Gel fraction (%)	SD
H2-G1	79.33769	1.212687
H2-G2	81.04218	0.744417
H2-G3	86.09723	1.04498
H2-G4	93.73368	0.78329
H2-G5	96.28998	1.364606

c) Gel fraction (%) of hydrogels B1 to B2

Hydrogel code	Gel fraction (%)	SD
B1	77.48461	0.64184
B2	80.02741	0.992712
B3	84.60887	0.811488
B4	86.66118	0.69592
B5	90.43923	0.777536

d) Gel fraction (%) of hydrogels B1-C1 to B1-C5

Hydrogel code	Gel fraction (%)	SD
B1-C1	77.15	1.32
B1-C2	80.40	1.28
B1-C3	86.07	1.35
B1-C4	92.17	1.12
B1-C5	96.02	1.15

APPENDIX V

a) Cumulative AMX release from hydrogel AMX-H2-G3 in SGF, SIF, and SCF

Time(hour)	SGF(pH 1.2)	SD	SIF(pH6.8)	SD	SCF (pH7.4)	SD
0.5	7.502	1.375	6.680	1.670	5.470	1.870
1	12.975	1.488	10.274	1.299	8.512	1.233
2	18.502	1.251	14.960	1.425	12.450	1.330
3	21.490	1.451	17.798	1.625	14.129	1.476
4	26.572	1.862	19.624	1.129	16.801	1.590
5	31.062	2.153	23.960	1.503	18.450	1.273
6	37.623	1.281	26.005	1.481	21.026	1.751
7	39.358	1.268	29.798	1.868	24.129	2.064
8	42.281	2.014	33.291	1.764	26.996	1.850
9	45.316	2.066	35.103	2.066	29.439	1.872
10	47.453	2.073	37.212	1.966	31.629	1.966
11	49.256	2.063	41.333	2.173	33.635	2.073
12	51.391	1.570	43.234	1.362	34.985	1.362
13	52.467	2.023	46.131	1.467	36.763	1.467
14	53.341	1.667	47.413	2.130	39.754	1.680
15	54.145	1.726	48.234	1.430	41.452	1.340
24	60.398	1.199	53.322	2.030	46.754	1.680
25	61.256	1.163	54.245	1.540	47.524	2.020

b) Cumulative release of MTZ from the hydrogel MTZ-H2-G3 in SGF, SIF, and SCF

Time(hour)	SGF (pH 1.2)	SD	SIF (pH6.8)	SD	SCF (pH 7.4)	SD
0.5	6.973	1.349	5.557	1.124	4.475	0.349
1	12.635	1.582	9.847	1.387	5.742	0.582
2	16.713	1.357	11.981	1.511	7.223	0.736
3	24.858	1.793	18.401	1.177	9.354	0.793
4	30.441	1.922	23.776	1.798	13.354	1.092
5	34.673	1.334	28.593	1.823	17.462	1.134
6	41.051	2.025	31.811	1.882	21.480	1.253
7	48.253	1.349	36.253	1.349	25.253	1.349
8	51.961	1.582	39.961	1.582	29.161	1.582
9	56.565	1.566	44.565	1.736	35.565	1.757
10	59.239	1.793	48.239	1.929	38.239	1.793
11	63.127	1.392	50.127	2.092	42.127	1.922
12	65.728	1.937	52.728	2.034	44.728	1.367
13	67.876	1.203	54.876	1.283	46.876	1.203
14	68.263	1.865	55.263	1.349	48.263	1.349
15	69.329	1.582	56.329	1.582	49.329	1.582
24	70.842	1.357	57.942	1.736	51.842	1.357
25	71.025	1.793	58.225	1.793	52.125	1.729

APPENDIX VI

a) Correlation comparison of swelling ratio of hydrogel H2-G3 hydrogel and AMX release profile

	SW-SGF	SW-SIF	SW-SCF	DR-SGF	DR-SIF	DR-SCF
SW-SGF	1					
SW-SIF	0.99885	1				
SW-SCF	0.99742	0.99708	1			
DR-SGF	0.98369	0.98306	0.97279	1		
DR-SIF	0.98119	0.98264	0.97034	0.99657	1	
DR-SCF	0.97015	0.97471	0.95833	0.9905	0.99524	1

2-tailed test of significance is used ($p < 0.05$).
DR - Drug release
SW - Swelling ratio

b) Correlation comparison of swelling ratio of hydrogel H2-G3 and MTZ release profile

	SW-SGF	SW-SIF	SW-SCF	DR-SGF	DR-SIF	DR-SCF
SW-SGF	1					
SW-SIF	0.99885	1				
SW-SCF	0.99742	0.99708	1			
DR-SGF	0.97941	0.97923	0.96783	1		
DR-SIF	0.98106	0.98289	0.97126	0.99811	1	
DR-SCF	0.97155	0.9727	0.96027	0.99578	0.99687	1

2-tailed test of significance is used ($p < 0.05$).
DR -Drug release
SW - Swelling ratio

APPENDIX VII

a) Cumulative release of AMX from the hydrogel AMX-B1-C1 in SGF, SIF, and SCF

Time(hour)	SGF(pH 1.2)	SD	SIF(pH 6.8)	SD	SCF(pH 7.4)	SD
1	2.579	1.843	7.241	1.821	8.795	1.303
2	13.584	1.848	15.716	1.860	22.278	1.267
3	19.354	1.762	25.298	1.218	33.822	1.348
4	25.880	1.608	29.894	1.303	45.499	1.304
5	30.044	1.220	35.044	1.825	52.353	1.203
6	34.443	1.410	40.403	1.210	58.901	1.470
7	37.875	1.353	48.861	1.475	63.458	1.225
8	39.363	1.472	54.255	1.274	66.192	1.206
9	42.395	2.021	58.416	1.530	69.051	1.276
10	45.584	1.721	62.146	1.366	70.377	1.251
11	46.720	1.390	63.849	1.473	72.239	1.314
12	48.220	1.831	64.523	1.228	73.594	1.268
13	50.630	1.566	65.680	1.884	73.750	1.219
14	52.579	1.079	66.007	1.636	73.801	1.414
15	53.382	1.166	67.016	1.282	73.644	1.261
24	54.046	1.246	67.606	1.661	74.573	1.438
25	54.707	1.031	68.141	1.573	74.349	1.301

b) Cumulative release of MTZ from the hydrogel MTZ-H2-G3 in SGF, SIF, and SCF

Time(hour)	SGF (pH1.2)	SD	SIF (pH6.8)	SD	SCF (pH 7.4)	SD
0.5	6.351	1.778	8.117	2.513	10.002	2.930
1	8.549	1.370	12.798	2.272	16.814	1.010
2	13.023	1.590	19.361	2.463	25.871	2.981
3	19.907	2.901	26.275	2.611	32.125	2.825
4	25.974	1.477	32.811	2.086	42.142	2.133
5	28.832	1.400	38.332	3.035	50.055	2.401
6	33.409	2.877	45.003	2.677	59.683	2.218
7	37.720	2.248	48.211	2.425	62.162	2.823
8	40.443	2.063	51.310	1.027	66.929	2.514
9	43.479	2.147	54.228	2.554	68.699	2.886
10	45.710	2.987	57.621	2.234	71.698	2.598
11	48.698	1.329	61.059	2.061	75.030	1.873
12	51.790	1.369	63.154	1.381	76.943	2.491
13	54.690	1.189	65.016	3.130	78.236	2.705
14	56.732	3.021	66.329	1.614	79.157	1.941
15	58.701	1.378	68.302	2.603	80.590	1.793
24	62.812	2.621	73.638	2.746	81.252	2.954
25	63.996	1.441	73.944	3.132	81.964	3.070

APPENDIX VIII

a) AMX-B1-C1 Correlation

	SW-SGF	SW-SIF	SW-SCF	DR-SGF	DR-SIF	DR-SCF
SW-SGF	1					
SW-SGF	0.95378	1				
SW-SIF	0.97426	0.98833	1			
SW-SIF	0.84295	0.95606	0.92812	1		
SW-SCF	0.8631	0.96394	0.94051	0.99632	1	
SW-SCF	0.86084	0.95958	0.93742	0.97774	0.99088	1

2-tailed test of significance is used ($p < 0.05$).
DR -Drug release
SW - Swelling ratio

MTZ-B1-C1 Correlation

	SW-SGF	SW-SIF	SW-SCF	DR-SGF	DR-SIF	DR-SCF
SW-SGF	1					
SW-SGF	0.95378	1				
SW-SIF	0.97426	0.98833	1			
SW-SIF	0.94322	0.98977	0.9858	1		
SW-SCF	0.87347	0.95946	0.95084	0.98955	1	
SW-SCF	0.94176	0.99595	0.98607	0.97881	0.97557	1

2-tailed test of significance is used ($p < 0.05$).
DR -Drug release
SW - Swelling ratio

APPENDIX IX

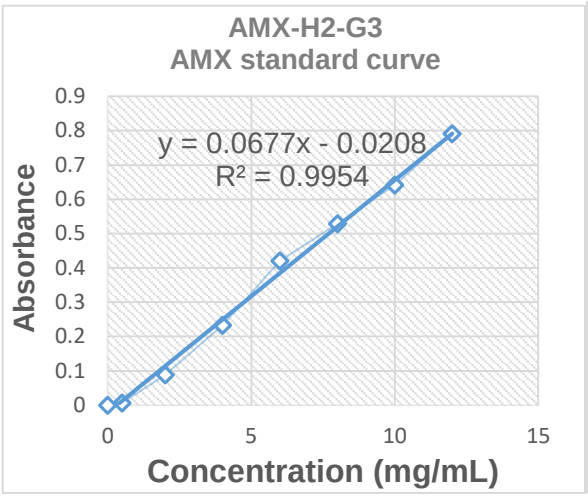
AMX-H2-G3
AMX standard curve
y = 0.0677x - 0.0208
R² = 0.9954
Absorbance
Concentration (mg/mL)

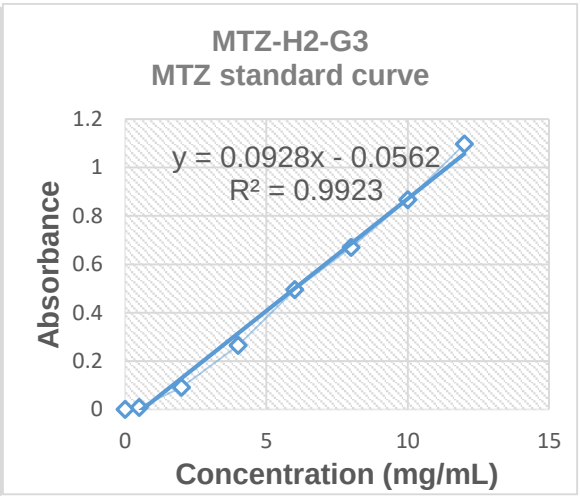
MTZ-H2-G3
MTZ standard curve
y = 0.0928x - 0.0562
R² = 0.9923
Absorbance
Concentration (mg/mL)

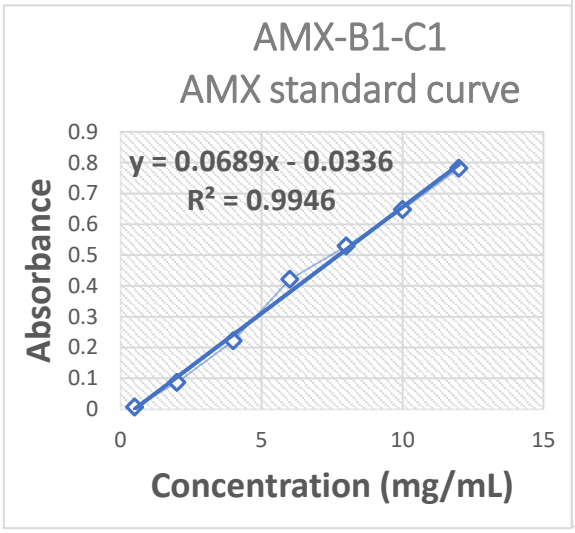
AMX-B1-C1
AMX standard curve
y = 0.0689x - 0.0336
R² = 0.9946
Absorbance
Concentration (mg/mL)

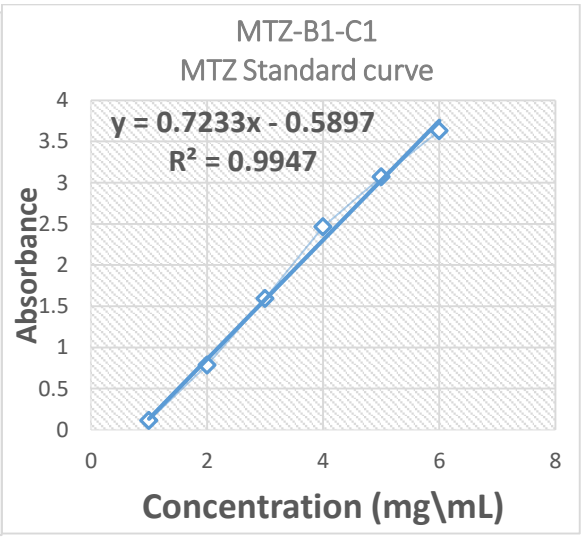
MTZ-B1-C1
MTZ Standard curve
y = 0.7233x - 0.5897
R² = 0.9947
Absorbance
Concentration (mg\mL)